PRODUCTION DATA INTEGRATION INTO HIGH RESOLUTION

GEOLOGIC MODELS WITH TRAJECTORY-BASED METHODS AND

A DUAL SCALE APPROACH

A Dissertation

by

JONG UK KIM

Submitted to the Office of Graduate Studies of
Texas A&M University
in partial fulfillment of the requirements for the degree of

DOCTOR OF PHILOSOPHY

August 2009

Major Subject: Petroleum Engineering

PRODUCTION DATA INTEGRATION INTO HIGH RESOLUTION

GEOLOGIC MODELS WITH TRAJECTORY-BASED METHODS AND

A DUAL SCALE APPROACH

A Dissertation

by

JONG UK KIM

Submitted to the Office of Graduate Studies of
Texas A&M University
in partial fulfillment of the requirements for the degree of

DOCTOR OF PHILOSOPHY

Approved by:

Chair of Committee,	Akhil Datta-Gupta
Committee Members,	William John Lee
	Christine Ehlig-Economides
	Yalchin Efendiev
Head of Department,	Stephen A. Holditch

August 2009

Major Subject: Petroleum Engineering

ABSTRACT

Production Data Integration into High Resolution Geologic Models with Trajectory-
based Methods and a Dual Scale Approach. (August 2009)
Jong Uk Kim, B.S., Seoul National University, Korea;
M.S., Seoul National University, Korea
Chair of Advisory Committee: Dr. Akhil Datta-Gupta

Inverse problems associated with reservoir characterization are typically under-determined and often have difficulties associated with stability and convergence of the solution. A common approach to address this issue is through the introduction of prior constraints, regularization or reparameterization to reduce the number of estimated parameters.

We propose a dual scale approach to production data integration that relies on a combination of coarse-scale and fine-scale inversions while preserving the essential features of the geologic model. To begin with, we sequentially coarsen the fine-scale geological model by grouping layers in such a way that the heterogeneity measure of an appropriately defined 'static' property is minimized within the layers and maximized between the layers. Our coarsening algorithm results in a non-uniform coarsening of the geologic model with minimal loss of heterogeneity and the 'optimal' number of layers is determined based on a bias-variance trade-off criterion. The coarse-scale model is then updated using production data via a generalized travel time inversion. The coarse-scale inversion proceeds much faster compared to a direct fine-scale inversion because of the significantly reduced parameter space. Furthermore, the iterative minimization is much more effective because at the larger scales there are fewer local minima and those tend to be farther apart. At the end of the coarse-scale inversion, a fine-scale inversion may be carried out, if needed. This constitutes the outer iteration in the overall algorithm. The fine-scale inversion is carried out only if the data misfit is deemed to be unsatisfactory.

We propose a fast and robust approach to calibrating geologic models by transient pressure data using a trajectory-based approach that based on a high frequency asymptotic expansion of the diffusivity equation. The trajectory or ray-based methods are routinely used in seismic tomography. In this work, we investigate seismic rays and compare them with streamlines. We then examine the applicability of streamline-based methods for transient pressure data inversion. Specifically, the high frequency asymptotic approach allows us to analytically compute the sensitivity of the pressure responses with respect to reservoir properties such as porosity and permeability. It facilitates a very efficient methodology for the integration of pressure data into geologic models.

DEDICATION

To beloved Kong Ju, Heesoo, Jeesoo and their endless patience and love

ACKNOWLEDGMENTS

I feel extremely privileged to have had the opportunity to pursue a PhD at Texas A&M. I am deeply indebted to Dr. Akhil Datta-Gupta for his invaluable help during these great four years. I would like to thank Dr. John Lee, Dr. Christine Ehlig-Economides, and Dr. Yalchin Efendiev for considering being part of my advisory committee.

I would like to thank Dr. William Milliken and Dr. Wen Chen at Chevron ETC for their encouragement and support during my summer internships at San Ramon. I acknowledge their helpful comments and suggestions in shaping career as well as research.

I would like to acknowledge my friends, Professor Deepak Devegowda, Dr. Eduardo Jimenez, Dr. Ichiro Osako, Dr. Adedayo Oyerinde, Dr. Ahmed Al-Huthali for the endless and supportive deliberations. They are all mentors for my graduate study.

Finally I would like to thank my friends: Han-young, Jichao, Alvaro, Eric, Jiang, Suksang, Song, Qing, Yip, Satyajit and all my fellow Aggies who made this doctorate an enjoyable journey. You are all in good shape.

Thank you very much.

TABLE OF CONTENTS

LIST OF FIGURES

Page

CHAPTER I

INTRODUCTION AND SIGNIFICANCE

1.1. Introduction

Geologic model calibration has received a great deal of attention in the oil and gas industries because production forecasting is based on integrated geologic models and accurate forecast is critical for prudent business decisions. Geologic models now routinely consist of several hundred thousands to millions of grid cells to represent the geological characteristics derived from static data such as seismic and logging data. A challenging task is the calibration of these models to dynamic data such as pressure and production response.

The integration of production data typically requires the solution of an inverse problem. It is well known that such inverse problems for subsurface flow are generally ill-posed and can result in non-unique and unstable solutions, often leading to a loss in geologic realism. A common approach to at least partially alleviate the problem is via incorporation of prior information or regularization such as 'norm' or 'roughness' constraints. However, there are additional outstanding challenges that have deterred the routine integration of production data into reservoir models using inverse modeling. First, the computational cost is still extremely high, in particular when the number of parameters is very large. Second, the relationship between the production response and reservoir properties such as permeability or porosity can be highly non-linear which often causes the solution to converge to a local minimum with an inadequate match to the data.

Our approach to address the ill-posed nature of the inverse problem and the difficulties with the existence of local minima is through decomposing the inverse

This dissertation follows the style of *SPE Journal.*

problem by scale and also use of efficient trajectory-based methods. Synthetic and field examples will be used to validate our approach.

1.2. Background

Several multiscale approaches have been proposed in the literature for the integration of production data via inverse modeling. These methods, however, rest on a recursive refinement based on the production data. No consideration of the prior model or static information is taken into account during reparameterization. We propose an approach to history matching that relies on sequential coarsening rather than sequential refinement. We adopt the technique called 'optimal coarsening' to coarsen the fine-scale geologic model. This technique is designed to preserve the features of the geologic model to the maximum extent.

Our scale-decomposition approach to inversion offers a number of advantages. First, computational efficiency is significantly enhanced compared to direct fine-scale inversion of production data because typical fine-scale models can consist of several hundred thousands to millions of parameters. Second, we can avoid over-parameterization and the subjectivity arising from introduction of artificial regularization terms. Finally, the iterative minimization is much more effective because at larger scales there are fewer local minima and those tend to be farther apart. Thus, the solution is more likely to reach the global minimum or at least a local minimum that in the close vicinity of the global solution. The coarse-scale solution can then be recursively refined by using it as the initial solution for the fine-scale inversion.

For the purpose of the geologic model calibration, pressure data provides several advantages. First, pressure transient tests are easier and less expensive to carry out in the field. Second, the pressure perturbations travel much faster compared to tracer or water front, resulting that pressure responses can be obtained early in the field life compared to other types of dynamic data. This makes interference tests much more appealing compared to tracer tests which may require months to see a field response. However, the

computation cost and localized nature of pressure sensitivities pose difficulties in history matching transient pressure data with a finite difference model. Also, pressure tests from multiple wells are difficult to analyze because of superposition of pressure responses.

1.3. Objectives

The main objective of this research is to develop a practical and efficient workflow to calibrate high-resolution geologic models using multi-phase production and pressure data. We propose two approaches to accomplish this objective. The first method involves a dual scale approach with an 'optimal' coarsening technique. The second method is aimed towards integrating transient pressure data into geologic models using efficient trajectory-based approach.

1.3.1. 'Optimal' Coarsening of Geologic Models

Our scale-decomposition approach requires a coarse-scale geologic model for inversion process. Because the inversion scheme rests on the coarse-scale grid system, it is important that the coarse-scale model preserves the dominant flow characteristics of the fine-scale geologic model. We adopt an 'optimal' coarsening algorithm proposed by King et al. and propose further improvements that better preserves the fine-scale permeability contrasts. The coarsening algorithm preserves the fine-scale heterogeneity to the maximal extent based on the static properties only such as permeabilities, porosities etc. and is independent of the flow boundary condition. It leads to a variable resolution of vertical layering and especially preserves the pay/non-pay juxtaposition

1.3.2. Dual Scale Inversion

History matching will be carried out primarily at the coarse-scale. Coarse-scale inversion is appropriate because of the resolution of production data. Typically, production

histories from well have low resolution of information. The coarse-scale geologic model, thus, is well-suited for production data integration. Inversion process at the coarse-scale also avoids artificial regularization or 'smoothness' constraints. Reduced number of model parameters in history matching process leads the faster convergence and less ill-posed behavior. The inversion will be more robust because of reduced tendencies to converge to local minimum.

1.3.3. Transient Pressure Data History Matching

In this work, we propose an approach to integrating transient pressure data using a trajectory based approach that relies on a high frequency asymptotic solution of the diffusivity equation. Specifically, the trajectory-based method such as the high frequency asymptotic approach allows us to analytically compute the sensitivity of the pressure data with respect to reservoir properties such as porosity and permeability. We validate the approximation of the pressure front trajectory using streamline which is easily available after single flow simulation. This results in a very efficient approach to integration of pressure data into geologic models.

1.4. Software Implementation

We have incorporated the algorithms proposed here into a general purpose software called 'DESTINY'. The software is very versatile because it works with commercial numerical reservoir simulators such as ECLIPSE and VIP. The field applications presented here have been carried out using DESTINY. A detailed manual of DESTINY is given in Appendix A.

CHAPTER II

A DUAL SCALE APPROACH TO PRODUCTION DATA INTEGRATION INTO HIGH RESOLUTION GEOLOGIC MODELS[*]

Inverse problems associated with reservoir characterization are typically under-determined and often have difficulties associated with stability and convergence of the solution. A common approach to address this issue is through the introduction of prior norm constraints, smoothness regularization or reparameterization to reduce the number of estimated parameters.

We propose a dual scale approach to production data integration that relies on a combination of coarse-scale and fine-scale inversions while preserving the essential features of the geologic model. To begin with, we sequentially coarsen the fine-scale geological model by grouping layers in such a way that the heterogeneity measure of an appropriately defined 'static' property is minimized within the layers and maximized between the layers. Our coarsening algorithm results in a non-uniform coarsening of the geologic model with minimal loss of heterogeneity and the 'optimal' number of layers is determined based on a bias-variance trade-off criterion. The coarse-scale model is then updated using production data via a generalized travel time inversion. The coarse-scale inversion proceeds much faster compared to a direct fine-scale inversion because of the significantly reduced parameter space. Furthermore, the iterative minimization is much more effective because at the larger scales there are fewer local minima and those tend to be farther apart. At the end of the coarse-scale inversion, a fine-scale inversion may be

---

[*] Part of this chapter is reprinted with permission from "A Dual Scale Approach to Production Data Integration into High Resolution Geologic Models" by Kim, J.U. and Datta-Gupta, A., 2009. paper SPE 118950 presented at the 2009 SPE Reservoir Simulation Symposium, The Woodlands, TX, February 2 – 4. Copyright 2009 by the Society of Petroleum Engineers.

carried out, if needed. This constitutes the outer iteration in the overall algorithm. The fine-scale inversion is carried out only if the data misfit is deemed to be unsatisfactory.

In this work, we demonstrate our approach using both synthetic and field examples. The field example involves waterflood history matching of a structurally complex and faulted offshore turbiditic oil reservoir. Permeability and fault transmissibilities are the main uncertainties. The geologic model consists of more than 800,000 cells and 10 years of production data from 8 producing wells. Using our dual scale approach, we are able to obtain a satisfactory history match with a finite-difference model in less than a day in a PC. Compared to a manual history matching, the dual scale approach is shown to better preserve the geological features and the pay/non-pay juxtapositions in the original geologic model.

2.1. Chapter Introduction

Geologic models now routinely consist of several hundred thousands to millions to grid cells. Reconciling such high- resolution geological models derived from static data to the field production history is critical for reliable reservoir performance forecasting. Several methods have been proposed in the literature for this purpose. These include gradient-based methods (Brun et al., 2004), stochastic approaches such as simulated annealing and genetic algorithms (Quenes et al., 1994) and more recently the Ensemble Kalman Filter (Devegowda et al., 2007). The integration of production data typically requires the solution of an inverse problem. It is well known that such inverse problems are typically ill-posed and can result in non-unique and unstable solutions. A common approach to at least partially alleviate the problem is through incorporation of prior information or regularization such as 'norm' or 'roughness' constraints. However, there are additional outstanding challenges that have deterred the routine integration of production data into reservoir models using inverse modeling. First, the computational cost is still extremely high, particularly when the number of parameters is very large. Second, the relationship between the production response and reservoir properties can be highly non-linear. This

often causes the solution to converge to a local minimum with an inadequate match to the data. Furthermore, the solution itself can be unstable, leading to a loss in geologic realism.

One approach to address the ill-posed nature of the inverse problem and the difficulties with the existence of local minima is through decomposing the inverse problem by scale. The scale-decomposition approach to inversion offers a number of advantages. First, computational efficiency is significantly enhanced compared to direct fine-scale inversion of production data because typical fine-scale models can consist of several hundred thousand to millions of parameters. Second, we can avoid over-parameterization and the subjectivity arising from introduction of artificial regularization terms as discussed before. Finally, the iterative minimization is much more effective because at larger scales there are fewer local minima and those tend to be farther apart. Thus, the solution is more likely to reach the global minimum or at least a local minimum that is in the close vicinity of the global solution. The coarse-scale solution can then be recursively refined by using it as the initial solution for the fine-scale.

Yoon et al. (2001) proposed a multiscale history matching method that starts with the largest scale and successively progresses to smaller scale. This approach explicitly accounts for the resolution of the production data by refining the parameterization only up to a level sufficient to match the data. However, the refinement was carried out uniformly throughout the domain without consideration of the available data. The approach was subsequently modified by Grimstad et al. (2004) through introduction of an adaptive multiscale inversion whereby the parameterization is introduced via local refinement rather than global refinement. Furthermore, the new degrees of freedom are introduced only in places where it is warranted by the data. Both of these methods rely on recursive refinement based on the production data. No consideration of the prior model or static information is taken into account during reparameterization. As a result these methods pose challenges in preserving prior geologic information which is typically incorporated using post-processing of the solution to the inverse problem.

In this chapter, we propose an approach to history matching that relies on sequential coarsening rather than sequential refinement. Starting with the fine-scale geologic model, first an 'optimal coarsening' of the model is carried out. The coarsening is designed to preserve the features of the geologic model to the maximum possible extent. It follows the approach proposed by King et al. (2005) and combines cells in the fine-scale model in such a manner that the variation of a 'properly defined' heterogeneity measure is minimized within the coarsened cells and maximized between the coarsened cells. A well defined statistical measure is used to determine the optimal level of coarsening. The history matching and model updating is carried out primarily at the coarse-scale and the updates are then mapped onto the fine-scale. When production data misfit is sufficiently reduced, an outer iteration allows for direct updating of the fine-scale model to further improve convergence, if necessary.

One important distinguishing feature of our approach is that the coarsening is primarily driven by the static model and thus, the method naturally preserves the important characteristics of the initial geologic model. Also, unlike the previous works, the coarsening is carried out in the vertical direction while taking into account property variations both in the areal and vertical directions. Our approach preserves all the advantages of the previously proposed multiscale methods in terms of computational efficiency, stability and convergence of the solution. In addition, because the parameterization is driven by the initial geologic model rather than production data, the approach naturally preserves geologic realism.

In this chapter, we outline major procedures of this approach followed by mathematical formulation of the coarsening scheme used and coarse-scale inversion including coarse-scale sensitivity coefficients computations. We demonstrate the effectiveness of our approach using water flooding history matching of synthetic and field cases.

2.2. Approach

Multiscale approaches are getting increasing attention both for the forward and inverse modeling applications of flow through porous media. For history matching applications, the previous works on multiscale methods (Yoon et al., 2001; Grimstad et al., 2004) mainly focused on dynamic parameterization of the permeability distribution based on the production data. More recently, Stenerud et al. (2008) presented an adaptive multiscale approach for history matching using streamline models. Their approach used a mixed multiscale finite element forward model to resolve the pressure and velocity variations and streamline-based sensitivities for inverse modeling. In our approach, we adopt many of the concepts from these previous works. However, the major difference is that our approach relies on a sequential coarsening of a fine-scale geologic model rather than a sequential refinement of a coarse-scale model. Thus, our approach is able to better preserve the geology embedded in the fine-scale model. The main steps of our approach are outlined below.

- **Optimal Coarsening of the Geologic Model**. The fine-scale geologic model is sequentially coarsened until an 'optimal' level of coarsening is achieved. We follow the approach of King et al. (2005) to coarsen the geologic model by grouping layers in such a way that the heterogeneity measure of an appropriately defined 'static' property is minimized within the layers and maximized between the layers. However, our approach differs from that of King et al. (2005) in the choice of the static parameter as discussed later. The optimal number of layers is then selected based on an analysis resulting in the minimum loss of heterogeneity because of the coarsening.

- **Flow Simulation and Sensitivity Computations**. We use a finite-difference or a streamline simulator for modeling multiphase flow in the reservoir. If a finite-difference simulator is used, then the cell fluxes are used to trace the streamlines and

the time of flight (Datta-Gupta and King, 2007). The streamline trajectories and time of flight are then used to analytically compute the sensitivity of the production data with respect to permeabilities (Oyerinde et al., 2007).

- **Coarse-scale Inversion**. History matching is carried out primarily at the coarse-scale. This constitutes our inner iteration in the overall inversion scheme. The coarse-scale permeabilities are updated via inverse modeling which proceeds in two steps: (i) a generalized travel time inversion that matches the production response based on an optimal travel time shift (Cheng et al., 2005), followed by (ii) an amplitude matching that further refines the match (Vasco et al., 1999). The coarse-scale inversion proceeds much faster compared to a direct fine-scale inversion because of the significantly reduced parameter space. Furthermore, the iterative minimization is much more effective because at the larger scales there are fewer local minima and those tend to be farther apart. (Bunks et al., 1995) The inversion is terminated when no further improvement in data misfit is observed. The permeability updates are then transferred to the fine-scale model. Because our 'optimal' coarsening method groups fine-scale cells with similar attributes, the coarse-scale updates are simply added back to the corresponding fine-scale cells.

- **Fine-scale Inversion**. At the end of the coarse-scale inversion, a fine-scale inversion may be carried out, if needed. This constitutes the outer iteration in the overall algorithm. The fine-scale inversion is carried out only if the data misfit is deemed to be unsatisfactory.

Fig. 2.1 shows overall workflow of the dual scale inversion. It is comprised of two major loops. The inner loop consists of a coarse-scale inversion and majority of the data misfit reduction is accomplished at this stage. The coarse-scale inversion can be carried out very efficiently because of the reduced parameterization. The optimal design of the coarse-scale preserves most of the initial heterogeneity and important geologic

continuity. Since the coarse-scale inversion has fewer tendencies to converge to a local minimum, it is more stable compared to the direct fine-scale inversion (Bunks et al., 1995), and does not require artificial regularization such as smoothness constraints. After convergence of the coarse-scale inversion, the updates to the geologic model are transferred to the fine-scale model. The outer loop consists of a direct fine-scale inversion on the updated model. This is carried out only if the data misfit is unsatisfactory and typically converges vary rapidly.
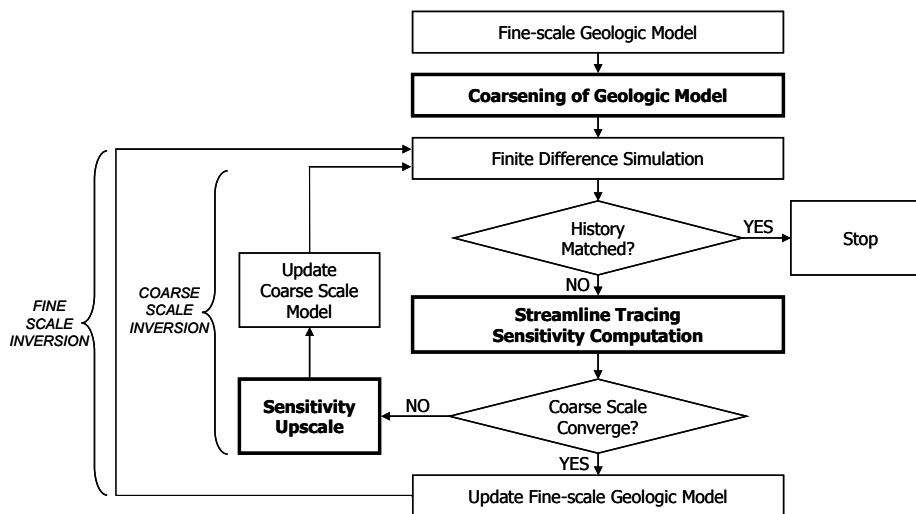
Fig. 2.1 Flow chart of dual scale inversion

2.3. Dual Scale Inversion: Mathematical Formulation

In this section we discuss the mathematical details related to our proposed dual scale inversion. We first discuss the optimal coarsening of the geologic model after King et al. (2005). We also point out the differences between our approach and that of King et al. (2005). Next, we discuss the details of the coarse-scale inversion. These include the sensitivity computations and the parameter estimation methods. The parameter sensitivities are computed along streamlines which can be obtained either from a finite-

difference or a streamline simulator. The parameter estimation is carried out using an iterative least squares method that is commonly used for large-scale geophysical inverse problems. (Paige and Saunders, 1982)

2.3.1. Optimal Coarsening of Geologic Models

Our approach relies on a sequential coarsening of the fine-scale geologic model as proposed by King et al. (2005). To start with, we determine which two adjacent layers in the geologic model may be merged. This is based on an analysis of the 'total variation' of a pre-defined static property denoted as p. King et al. (2005) chose the property, 'local velocity' given by $p = f'k/\phi$ where k/ϕ is the interstitial velocity and f' is the Buckley-Leverett speed. Instead of the 'local velocity', we have used the 'local slowness' which is simply the reciprocal of the local velocity as our static property that we want to preserve during the coarsening. The justification for our choice will be given later.

The 'total variation', as a measure of heterogeneity during coarsening, is decomposed into 'within cell variation (W)' and 'between cell variation (B)'. At any stage of coarsening, the quantity W is given by (King et al., 2005)

$$W = \sum_{i,j,k=1}^{NX,NY,NZ} n_{i,j,k}\left(p_{i,j,k} - p_{i,j,k}^{C}\right)^{2} \tag{2.1}$$

Eq. 2.1 is a summation over the entire reservoir model and quantifies the variation removed from the model after upgridding. The summation is weighted by $n_{i,j,k}$, which is the bulk rock volume of the cell. This ensures that W does not change under numerical refinement of the grid. Also, $p_{i,j,k}$ refers to the defined static property at the fine-scale and $p^{C}_{i,j,k}$ is the transitional static property that is calculated after every merging of adjacent layers as follows

$$p_{i,j,k}^{C} = \sum_{k} n_{i,j,k} \cdot p_{i,j,k} \left/ \sum_{k} n_{i,j,k} \right. \tag{2.2}$$

The quantity *B*, 'the between cell variation' quantifies the amount of heterogeneity preserved during upgridding. At any stage of coarsening it is given by

$$B = \sum_{i,j,k=1}^{NX,NY,NZ} n_{i,j,k} \left(p_{i,j,k}^{C} - \overline{p}_{i,j} \right)^2 \tag{2.3}$$

where $\overline{p}_{i,j}$ is the column-based average of our static property given by the following

$$\overline{p}_{i,j} = \sum_{k=1}^{NZ} n_{i,j,k} \cdot p_{i,j,k} \bigg/ \sum_{k=1}^{NZ} n_{i,j,k} \tag{2.4}$$

The goal of our algorithm is to minimize the amount of variation removed from our model and maximize the variation preserved while honoring geological markers during upgridding. The total variation of the model which is preserved during upgridding is given by the sum of 'within cell variation' and 'between cell variation' as follows

$$H = W + B \tag{2.5}$$

Detailed explanation of the preservation of *H* is described in Appendix C.
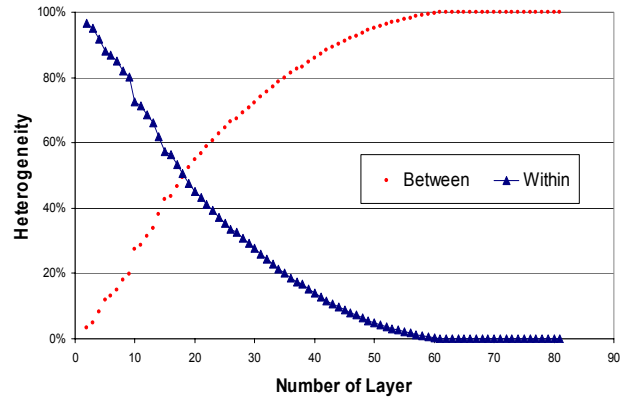
(a)
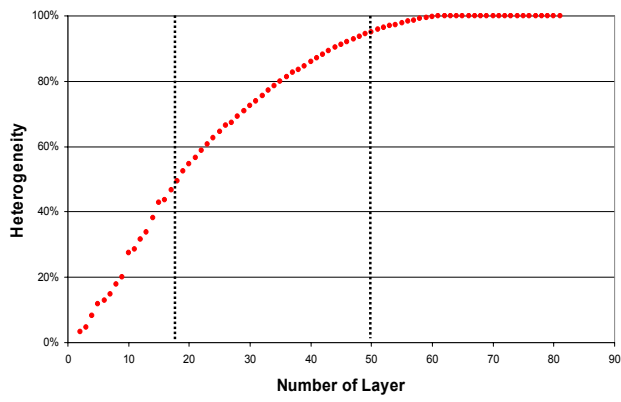
(b)
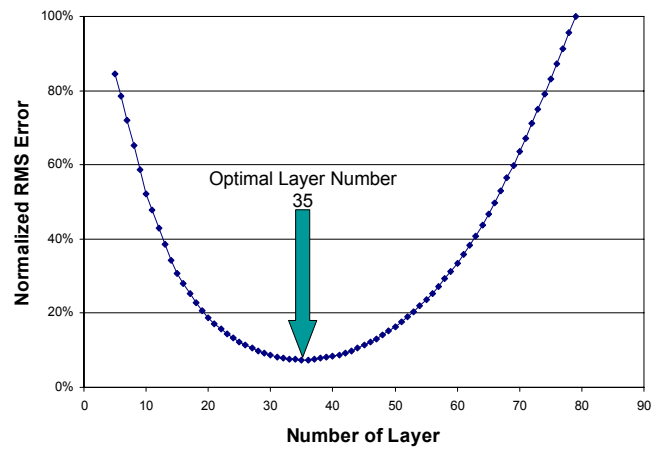
(c)

Fig. 2.2 Variation of heterogeneity during coarsening and determination of 'optimal' layer number

Fig. 2.2a shows the typical trends of W and B as a function of number of layers. The optimal number of layers will be decided by minimizing W (that is minimizing the loss of heterogeneity) or alternately maximizing B (that is preserving the geologic heterogeneity to the maximum possible extent). In Fig. 2.2b the between cell variation (B) shows three distinct heterogeneity regimes: a sharp increase for small number of layers, a slow increase for large number of layers, and a moderate increase between two. Intuitively, the optimal number of layers should be in the intermediate regime. In fact, the optimal number of layers is given by the point of maximum curvature in Fig. 2.2b. One approach to finding the optimal point is by calculating the RMSE (root mean square error) for a series of regression lines as discussed by Ma (2008) and shown in Fig. 2.2c.

Coarsening geologic models introduces smoothing which can cause biased estimation. This bias from the 'optimal' coarsening was examined by comparison with the fine-scale geologic model (King et al., 2005). This analysis shows that coarsened geologic model by this method is generally matched well with the fine-scale model although large bias might be introduced when model is coarsened extremely. King et al. validated also this method by comparing flow characteristics before and after coarsening with the inverse of the time of flight. These validations show that the effect of bias on the 'optimal' coarsening is minimal.

The major steps of the coarsening approach are as follows:

Step 1: Calculate the values of the property $p_{i,j,k}$ at each grid cell

Step 2: Group two adjacent layers sequentially and calculate the 'between the cell variation (B)' to quantify the amount of heterogeneity preserved after merging

Step 3: Merge those two layers that maximizes B based on the calculations in step 2

Step 4: Repeat steps 2 and 3 and continue merging layers until the model is reduced to a single layer

Step 5: Determine the optimal number of layers from the plot of '*B*' vs. number of layers as shown in Fig. 2.2c.

As mentioned before, the major difference between our approach and that of King et al. (2005) is the choice of 'slowness' instead of velocity for calculation of the heterogeneity measure. By preserving the 'slowness' distribution between the fine-scale and coarse-scale models, we are simply attempting to preserve the spatial variations of streamline time of flight which represents the water saturation front propagation. This becomes obvious if we recall the definition of the streamline time of flight (Datta-Gupta and King, 2007),

$$\tau(\psi) = \int_{\psi} s(\mathbf{x}) d\zeta , \tag{2.6}$$

where $s(\mathbf{x})$ is the slowness given by

$$s(\mathbf{x}) = \frac{\phi(\mathbf{x})}{|\mathbf{u}(\mathbf{x})|} \tag{2.7}$$

The water saturation velocity for a given saturation S_w along a streamline will be given by (Datta-Gupta and King, 2007),

$$\left.\frac{\partial \tau}{\partial t}\right|_{Sw} = \frac{df_w}{dS_w} = f' \tag{2.8}$$

and the travel time of the saturation front will be,

$$t_{S_w} = \frac{1}{f'} \int s(\mathbf{x}) d\zeta$$

$$= \frac{1}{f'} \int \frac{\phi(\mathbf{x})}{|\mathbf{u}(\mathbf{x})|} d\zeta$$

(2.9)

Thus, the water saturation distribution depends on the composite static quantity $\phi(\mathbf{x})$ /($f'_w k(\mathbf{x})$) which is used as the coarsening parameter in our calculations. The Buckley-Leverett speed, f', includes the facies and saturation dependent relative permeability terms. This coarsening parameter is simply the reciprocal of that used by King et al. (2005). In our experience our choice of the coarsening parameter leads to a more logical and conservative merging of layers. Similar observations have been reported by Hosseini et al. (2008).

2.4. Dual Scale Inversion

The production data integration is carried out in two stages: a coarse-scale inversion followed by a fine-scale inversion, if necessary. An integral part of the production data integration is the computation of sensitivity coefficients. The sensitivities relate the changes in the production response because of small perturbations in reservoir properties. These sensitivities are computed efficiently using streamlines. For our applications, we have used a commercial finite-difference simulator as our forward model. The streamlines and the time of flight are generated from the fluxes derived from the finite-difference simulator at each time step. Again, streamline and time of flight calculations involve analytic integration of the cell-fluxes and adds very little computational overhead (Jimenez et al., 2007). Detailed explanation regarding the streamline tracing is covered in Appendix A.

In the dual scale approach, we generally perform the forward simulation at the fine grid model and carry out the inverse modeling at both coarse and fine-scale. This considerably simplifies the workflow and allows us to preserve the well completions and perforations of the fine-scale model. However, further savings in computation time can

be achieved by performing the forward simulation of the coarse-scale inversion at the coarsened grid whenever possible. This is elaborated more in the application section.

The streamline-based parameter sensitivities are computed along with the forward simulation and involve one-dimensional integrals along streamline trajectories. The details of the streamline-based sensitivity computations can be found elsewhere (Vasco et al., 1999; Cheng et al., 2005). These sensitivity calculations have been extended to include gravity, changing field conditions and also three-phase flow (He et al., 2002; Oyerinde et al., 2007).

For coarse-scale inversion, we need to relate the fine grid sensitivities to the coarse-scale parameterization. It is important to point out that the coarsening algorithm will generally result in non-uniform coarsening of the fine-scale model. The sensitivity computations need to be able to address such non-uniform coarsening.

Let S_{iJ} denote the sensitivity coefficient that relates the change in the i-th production data because of a small perturbation in the J-th coarse-scale model parameter denoted by δm_J. Now the change in the i-th production response at the coarse-scale can be expressed as,

$$\delta d_i = \sum_{J=1}^{N} S_{iJ}\delta m_J \tag{2.10}$$

where N is the number of coarse-scale cells. Suppose $n(J)$ is the number of fine-scale cells embedded in the J-th coarse-scale cell. Now the quantity $S_{iJ}\delta m_J$ in Eq. 2.10 can be expressed in terms of fine-scale sensitivities S_{ij} as follows:

$$S_{iJ}\delta m_J = \sum_{j=1}^{n(J)} S_{ij}\delta m_j \ , \tag{2.11}$$

where δm_j is the change in the model parameter of the j-th fine-scale grid. We assume that the same changes apply to the coarse-scale cell and the embedded fine-scale cells, that is, $\delta m_j = \delta m_J$. This assumption is reasonable considering that the coarsening

algorithm is designed to minimize the variation in properties within the coarse-scale cells. From Eq. 2.11, we can now express the coarse-scale sensitivities in terms of the fine-scale sensitivities as follows:

$$S_{iJ} = \sum_{j=1}^{n(J)} S_{ij} \qquad (2.12)$$

Thus, the coarse-scale sensitivities are computed by simply integrating the fine-scale sensitivities embedded within each coarse-scale cell. Recall that the fine-scale sensitivities are already available from the forward simulation.

After sensitivity calculations, production data integration is carried out using an iterative minimization. We typically minimize a penalized objective function as follows,

$$\left\| \delta\mathbf{d} - \mathbf{S}\,\delta\mathbf{m} \right\| + \beta \left\| \delta\mathbf{m} \right\| \qquad (2.13)$$

$\delta\mathbf{d}$ is the vector of data misfit, $\mathbf{S}$ represents the parameter sensitivity matrix and $\delta\mathbf{m}$ is the vector of model parameter change. Note that the sizes of $\mathbf{S}$ and $\delta\mathbf{m}$ are different for the coarse-scale and the fine-scale inversion. In particular, the coarse-scale inversion will have much fewer parameters and can be carried out very efficiently compared to the fine-scale inversion. Because majority of the reduction in data misfit occurs at the coarse-scale, this leads to a substantial savings in computation time. After the coarse-scale inversion converges, we carry out the fine-scale inversion if the matches to the production data are not satisfactory. Typically, few iterations (<5) are needed at the fine-scale as we are already in the vicinity of the solution.

The minimization of Eq. 2.13 leads to an iterative least-squares solution (Paige and Saunders, 1982) to the augmented linear system given by

$$\begin{pmatrix} \mathbf{S} \\ \beta\mathbf{I} \end{pmatrix} \delta\mathbf{m} = \begin{pmatrix} \delta\mathbf{d} \\ 0 \end{pmatrix} \qquad (2.14)$$

where β is the weight determining the relative strengths of the production data and the prior model. It is to be noted that Eq. 2.13 does not contain any additional smoothness constraints unlike previous streamline-based history matching techniques. The reason the smoothness constraint is not included is that model parameters are smoothed implicitly during the coarsening of the fine-scale geologic model and with a significantly reduced parameter space, no additional regularization is necessary.

2.5. Applications

In this section, we discuss application of the dual scale approach to synthetic and field examples. The synthetic example is used to illustrate the detailed steps in our approach, its convergence characteristics with respect to direct fine-scale inversion and also some of its advantages. We then demonstrate the applicability of our approach to high resolution and geologically complex field cases using an example from offshore South America.

2.5.1. Synthetic Example

Our synthetic model is a 3D 9-spot case and involves matching of water-cut history at the producing wells. The geologic model consists of 21x21x10 grids and has a water injection well in the center and 8 producers in the perimeter of the model. Our reference permeability field and the observed water-cut data generated using this reference permeability are shown in **Figs. 2.3a** and 2.3b.

Our inversion starts with an initial geologic model which is typically the static model constructed using well and seismic data. The initial model for the synthetic example is shown in **Fig. 2.4a**. We have deliberately designed it to be quite distinct from the reference model to test the effectiveness of the dual scale inversion. The initial model has geological characteristic such as conspicuous directional heterogeneity that is different from reference model. This is also reflected in the water-cut mismatch with respect to the reference model, particularly for wells 3, 5, 6 and 7 (Fig. 2.3b)

(a)   (b)
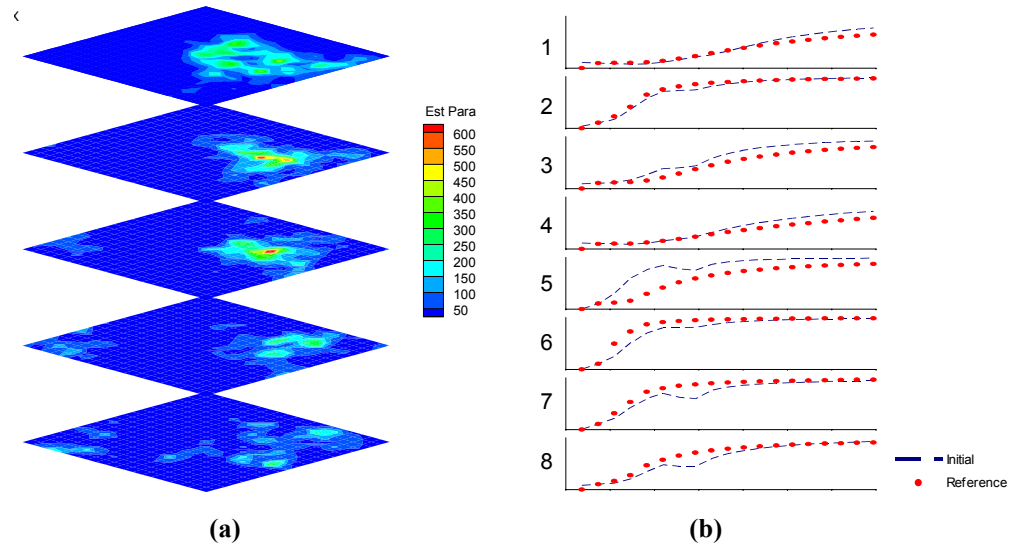
Fig. 2.3 Reference geological model (a) permeability and (b) its water-cut history and mismatch

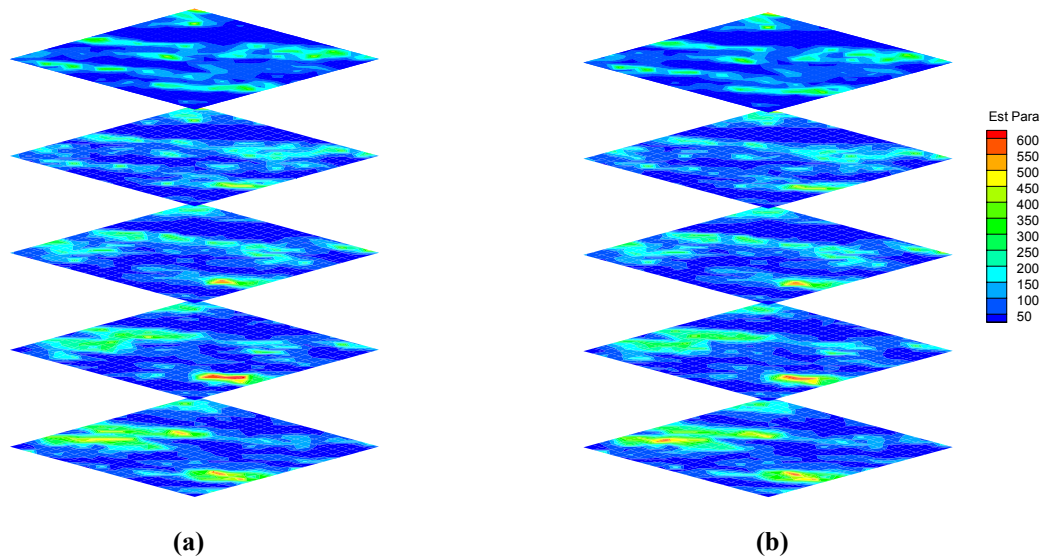(a)   (b)

Fig. 2.4 (a) Initial permeability field and (b) its coarsened model (i-j plane)

The first step in our approach is the 'optimal coarsening' of the geologic model. Using the method described earlier, the initial model is coarsened from 10 layers to 5 layers. Because of the coarsening, the initial number of grid cells 4,410 is reduced to 2,210, almost a two-fold reduction. Fig. 2.4a shows permeabilities for 5 layers from the initial fine-scale model. Fig. 2.4b shows the coarsened permeability field that is used for history matching. Just from visual observations, it is hard to discern any loss of heterogeneity because of coarsening. This is a critical feature of the 'optimal' coarsening algorithm that allows us to perform the history matching at the coarse-scale while preserving the major features of the fine-scale model. The subtle differences between the fine-scale and the coarse-scale models can be seen in their cross-sections (**Fig. 2.5**).
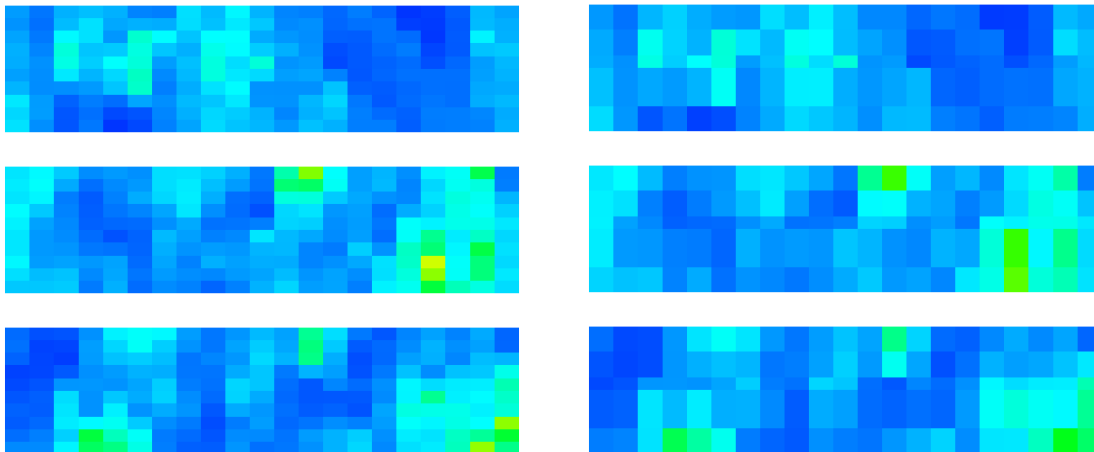
Fig. 2.5 (a) Initial permeability field (b) its coarsened model (i-k plane)

After coarsening we perform a coarse-scale history matching of the production data. This corresponds to the inner iteration in Fig. 2.1. The convergence behavior of the coarse-scale inversion is shown in **Fig. 2.6** in terms of the RMS of the water-cut misfit. As can be seen, the coarse-scale inversion converges rapidly and majority of the misfit reduction for the production data occurs at this stage. In other words, about 80% of the initial water-cut data misfit is reduced after 9 iterations in the coarse-scale inversion

while same amount of data misfit is reduced after 20 iterations in the direct fine-scale inversion. In this specific case, the coarse-scale approach is more than twice faster than the direct fine-scale inversion. The fast and smooth convergence behavior also underscores the fact that the misfit surface is generally better behaved at the coarse-scale with fewer local minima.

At the end of the coarse-scale inversion, the updated model properties from the coarse-scale are mapped onto the initial fine-scale geologic model. The updates from the coarse-scale inversion are simply added to the corresponding fine-scale cells embedded in each coarse-scale cell. Recall the 'optimal' coarsening was designed to merge fine-scale cells with 'similar' properties. Thus, when the updates from the coarse-scale inversion are added to the initial fine-scale geologic model, we expect that the matches to the production data will be preserved. This is typically the case for most of our examples. If the production data misfit deteriorates, we carry out a fine-scale inversion which is the outer iteration in Fig. 2.1.

From Fig. 2.6, we can see that the fine-scale inversion provides very little improvement to the data misfit. It is also computationally expensive because of the large number of parameters. It is obvious that the coarse-scale parameterization is more effective during the inversion and majority of the history matching can be accomplished at this stage. For comparison purposes, we have also shown the convergence behavior of a direct fine-scale inversion without any coarsening step. Not only the fine-scale inversion is computationally expensive, it also converges much slower. This clearly demonstrates the advantage of the dual scale approach.
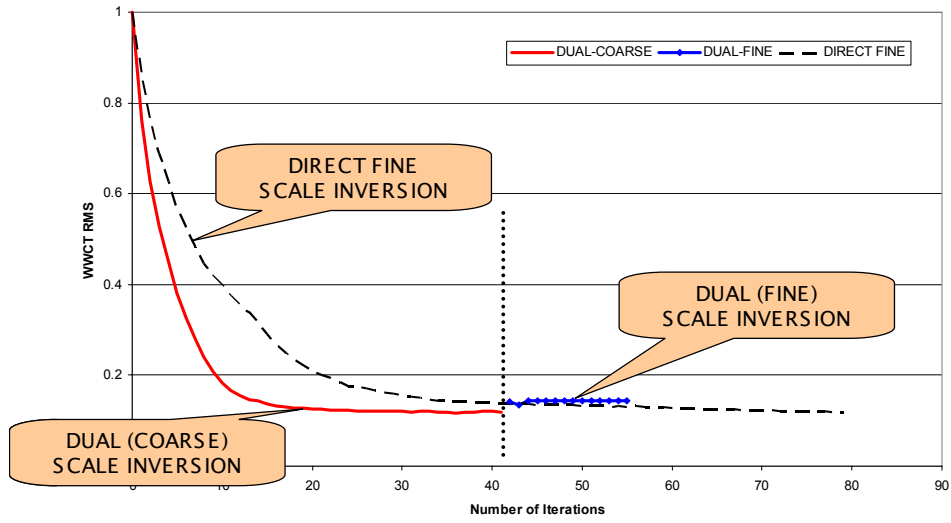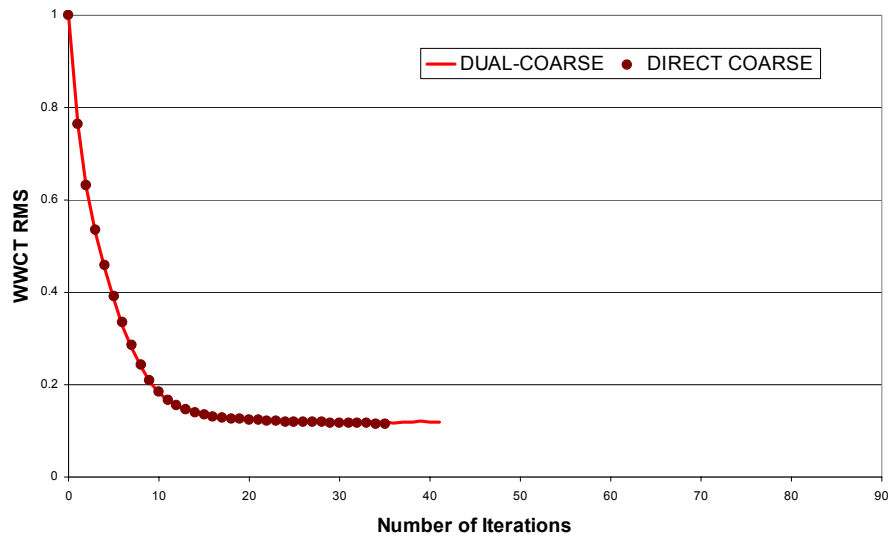
Fig. 2.6 Convergence of water-cut misfit

Fig. 2.7 Comparison of dual (coarse) scale inversion and direct coarse-scale inversion

As mentioned before, in our current implementation of the dual scale approach, while carrying out the coarse-scale inversion we perform the flow simulation and sensitivity computations at the fine-scale grid with coarsened model properties. Only the inversion is carried on the coarsened grid. Thus, majority of the computational savings is gained at the inversion stage in terms of fewer parameters and faster convergence. Although this simplifies the workflow and allows us to preserve the well completions and perforations of the fine-scale model, we can gain further computational efficiency by carrying out the forward simulation at the coarse-scale during the coarse-scale inversion. We can easily illustrate this for the synthetic example as the wells are perforated at all layers in the fine-scale model and thus, the well completions will not be affected by the coarsening. **Fig. 2.7** compares the convergence behavior for the coarse-scale inversion where the flow simulations are also carried out at the coarsened grid leading to significant time savings. As expected, the convergence behavior is not altered. However, we just emphasize that for practical field applications with partial perforations, recompletions and other changing field conditions, it is often difficult to maintain consistency between the coarse-scale and fine-scale simulation.

The history matching results and the updated permeability field from the dual scale approach are summarized in **Fig. 2.8**. For comparison purposes, the same results are also shown for a direct fine-scale inversion in **Fig. 2.9**. Both the methods are able to obtain a satisfactory match to the water-cut history. However, there are major differences in the updated permeability field derived from these two approaches. The updated model from the dual scale approach is able to retain features in initial permeability field much better compared to the direct fine-scale approach. This becomes clear in **Fig. 2.10** which shows the deviations from the initial model for both the approaches. The reason we are able to preserve geological characteristic is, again, because of the 'optimal' coarsening algorithm and the better convergence behavior of the coarse-scale inversion. It is well-recognized that preserving geologic realism during history matching is critical for improved performance forecasting and the dual scale approach appears to be able to accomplish that effectively.
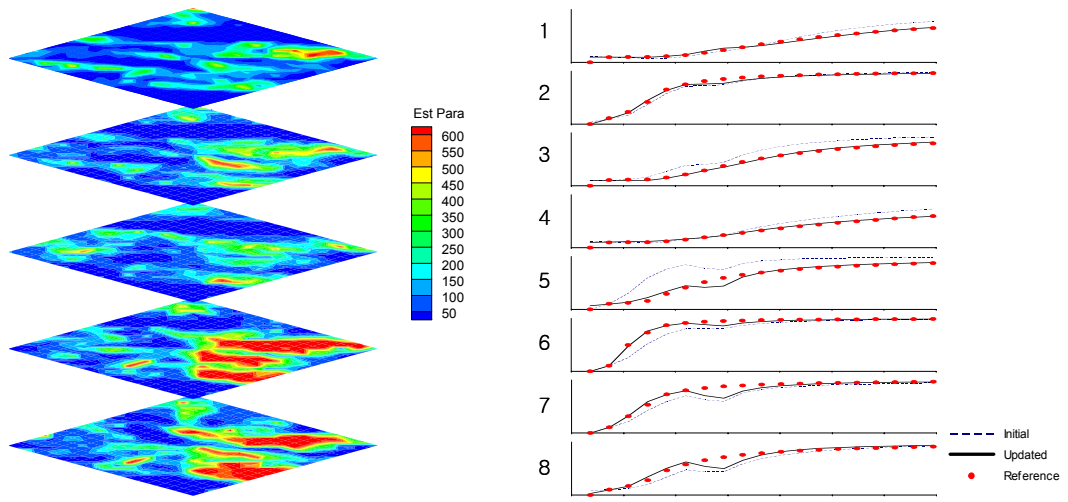
(a) Calibrated permeability field   **(b) Water-cut performance**

Fig. 2.8 Water-cut history match result from dual scale approach

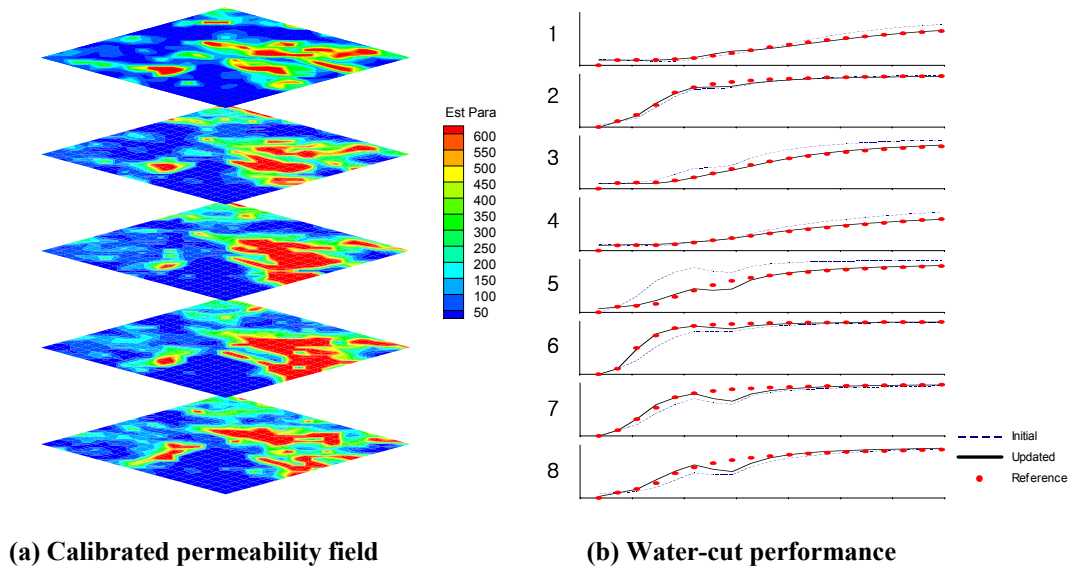(a) Calibrated permeability field   (b) Water-cut performance

Fig. 2.9 Water-cut history match result from direct fine-scale approach
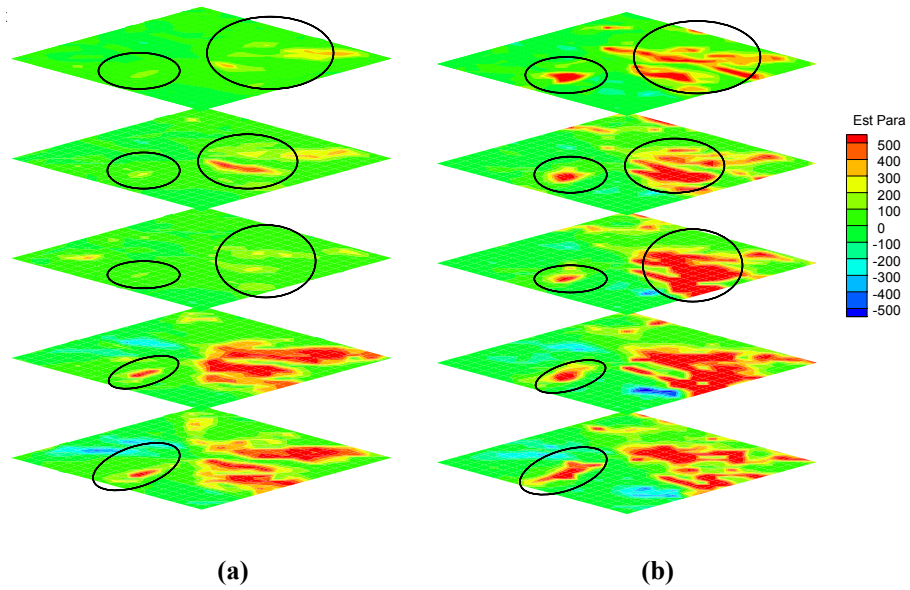

(a)   (b)

Fig. 2.10 Deviation from initial simulation model (a) Dual scale result vs. initial model and (b) Direct fine-scale inversion vs. initial model

2.5.2. Field Example

In this section we discuss the application of the dual scale history matching approach to a structurally complex offshore turbiditic reservoir. The field under consideration here is located offshore South America in water depths of 400 to 800 m. It consists of three partially connected Eocene deep-marine reservoirs (organized in sheet and channel sands) at a depth of approximately 3,000 m (**Fig. 2.11**). The sands are divided into 3 distinctive regions, Sand A, Sand B and the Main Sand, all with a k_v/k_h ratio of 0.01. The field was initially produced under primary depletion with 2 producers using well productivity and water-cut as the tools for monitoring. Subsequently, the field was converted to a waterflood after 3 years of field workovers adding 6 producers and 4 injectors. The field has a total 8 producer and 4 injector wells for use in history matching and forecasting in our simulation. The reservoir model was developed an 81 layer structurally complex and faulted turbiditic oil reservoir with excellent quality sands with high permeability, excellent porosity and distinctive transitions between low and high quality sands. Several normal faults span the field, and fault transmissibilities and permeability are the main uncertainties (Hohl et al. 2006).
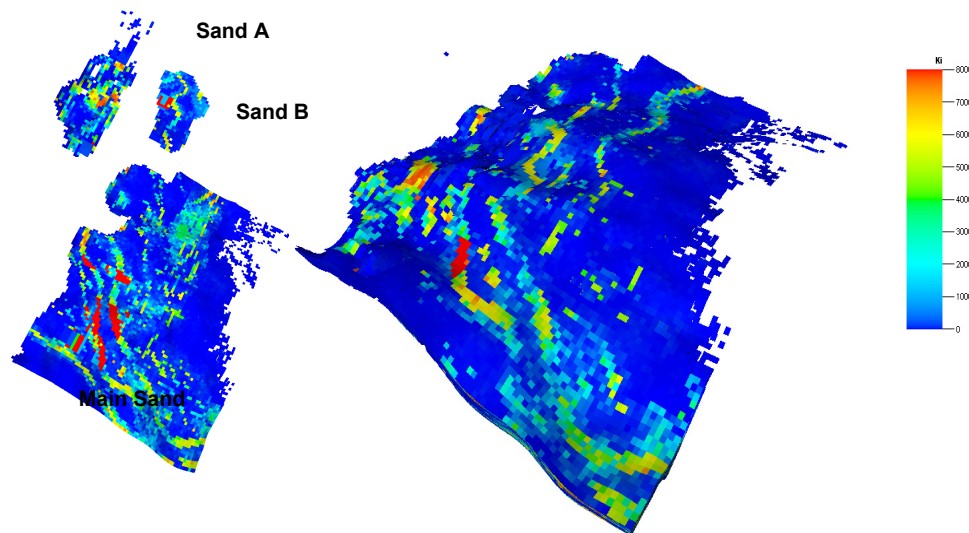
Fig. 2.11 Initial permeability distribution for field example
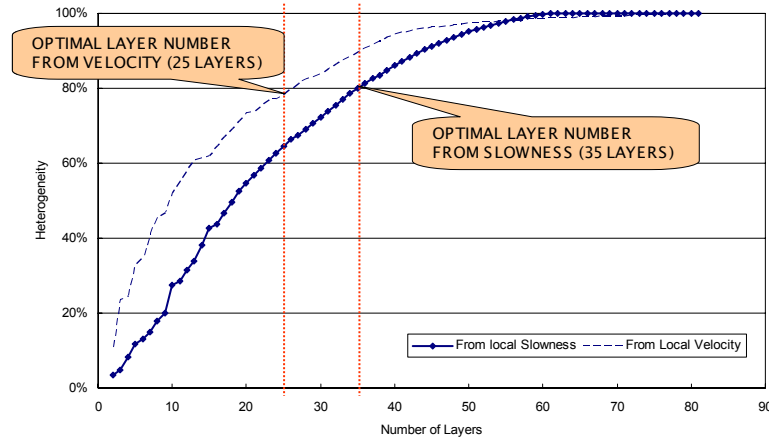
Fig. 2.12 Determination of 'optimal' layer number based on local slowness vs. local velocity

We apply the dual scale approach to this field case to update the permeability distribution in the initial geologic model using the water-cut history. The highly detailed initial geologic model consisted of more than 850,000 grid cells (about 200,000 of active cells). The first step in our approach is to coarsen the detailed geologic model using the 'optimal' coarsening approach. **Fig. 2.12** shows the behavior of 'between cell variation' (*B* in Eq. 2.3) during sequential coarsening of the fine-scale model. The results compare the behavior when we use 'velocity' vs. 'slowness' as the heterogeneity parameter. Clearly, the use of 'slowness' results in a more conservative grouping of layers with 35 layers as the 'optimal' as opposed to 25 layers when 'velocity' is used as the heterogeneity parameter. Our results appear to be consistent with the findings of Talbert et al. (2008) which suggest that the King et al. (2005) 'optimal coarsening' may lead to too much coarsening and the loss of initial geologic feature such as distinctive sands and barrier.

Figs. 2.13 through **2.15** compare the initial geologic model with the 'optimally' coarsened model. After coarsening, the number of grid cells is reduced from 850,000 to

370,000. In Fig. 2.13 we can see that the fine-scale model for Sand A has no distinctive channels and the coarsened model is able to preserve the low and high permeability regions. Sand B in **Fig. 2.14** shows a little smearing of the high permeability channels after coarsening. However, the general shape and distribution of the channels are still quite apparent. Fig. 2.15 shows selected layers from the Main Sand. It contains numerous channels and our coarsening algorithm results in very few merging of layers in the Main Sand. The algorithm leaves the Main Sand almost intact as can be seen in Fig. 2.15.
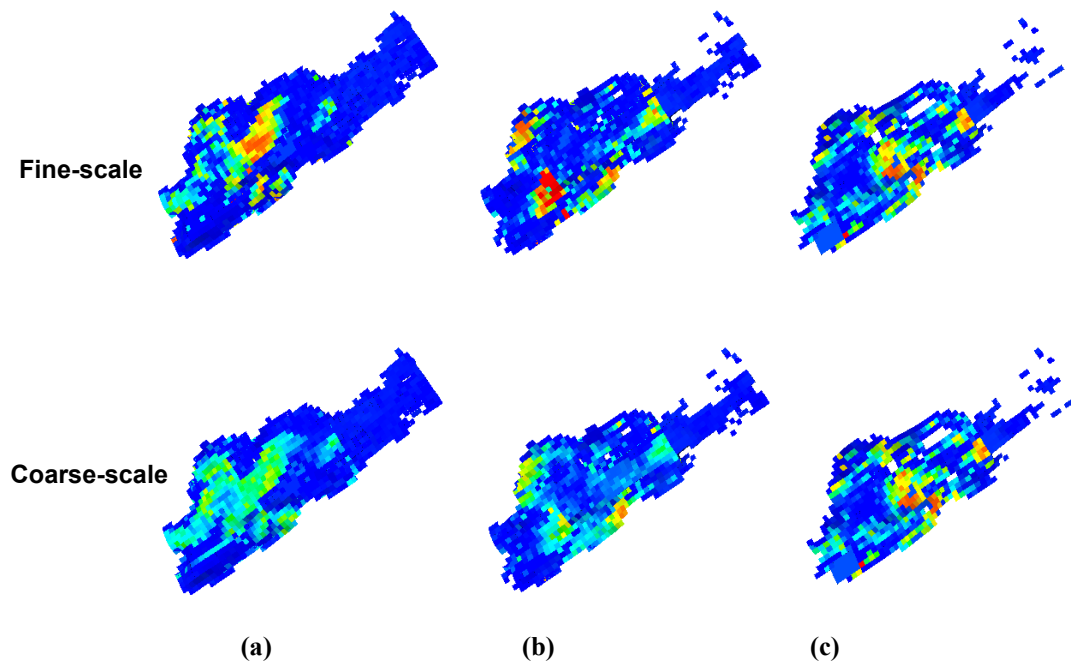
Fig. 2.13 Initial permeability field of Sand A (a) Layer 1 (b) Layer 16 and (c) Layer 27
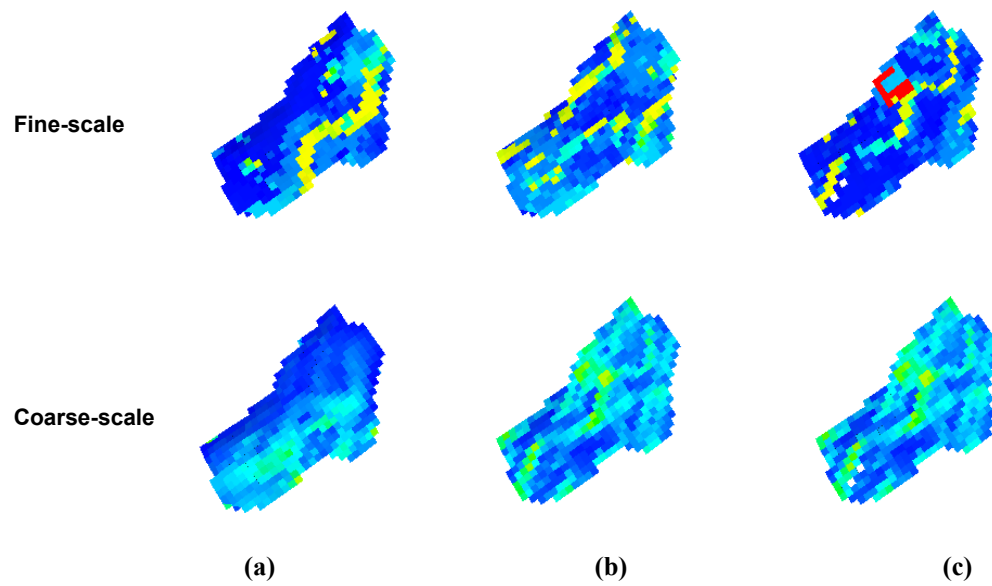
Fig. 2.14 Initial permeability field of Sand B (a) Layer 32 (b) Layer 40 and (c) Layer 49
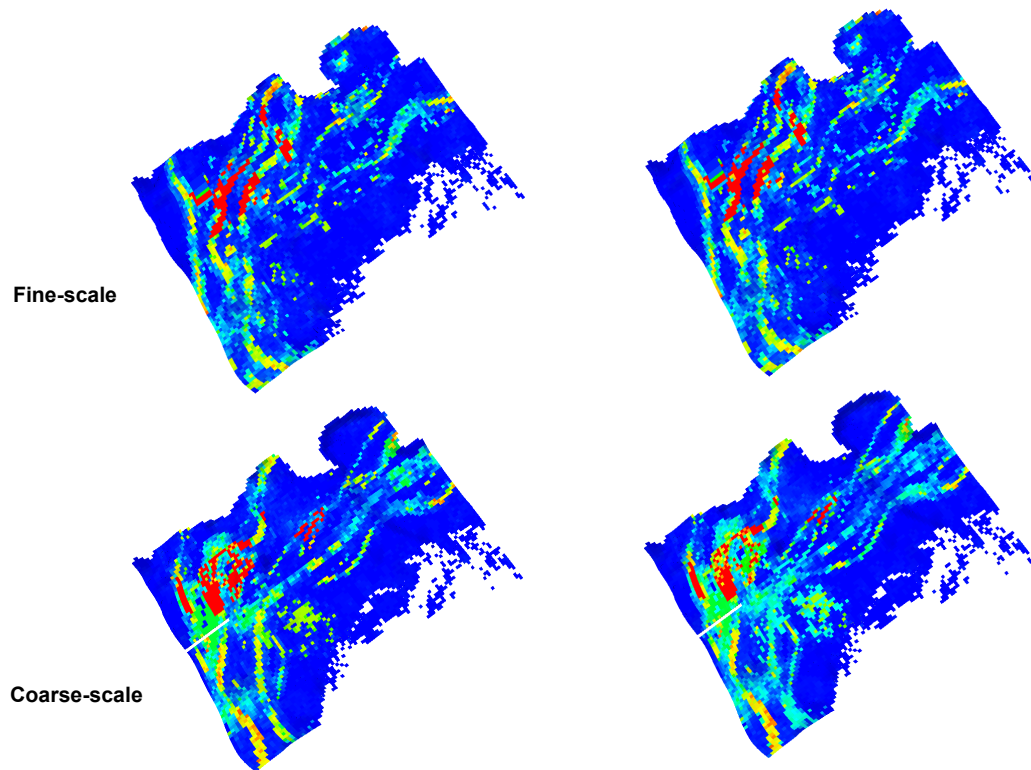
Fig. 2.15 Initial permeability field of Main Sand (a) Layer 53 and (b) Layer 72

(a)

(b)
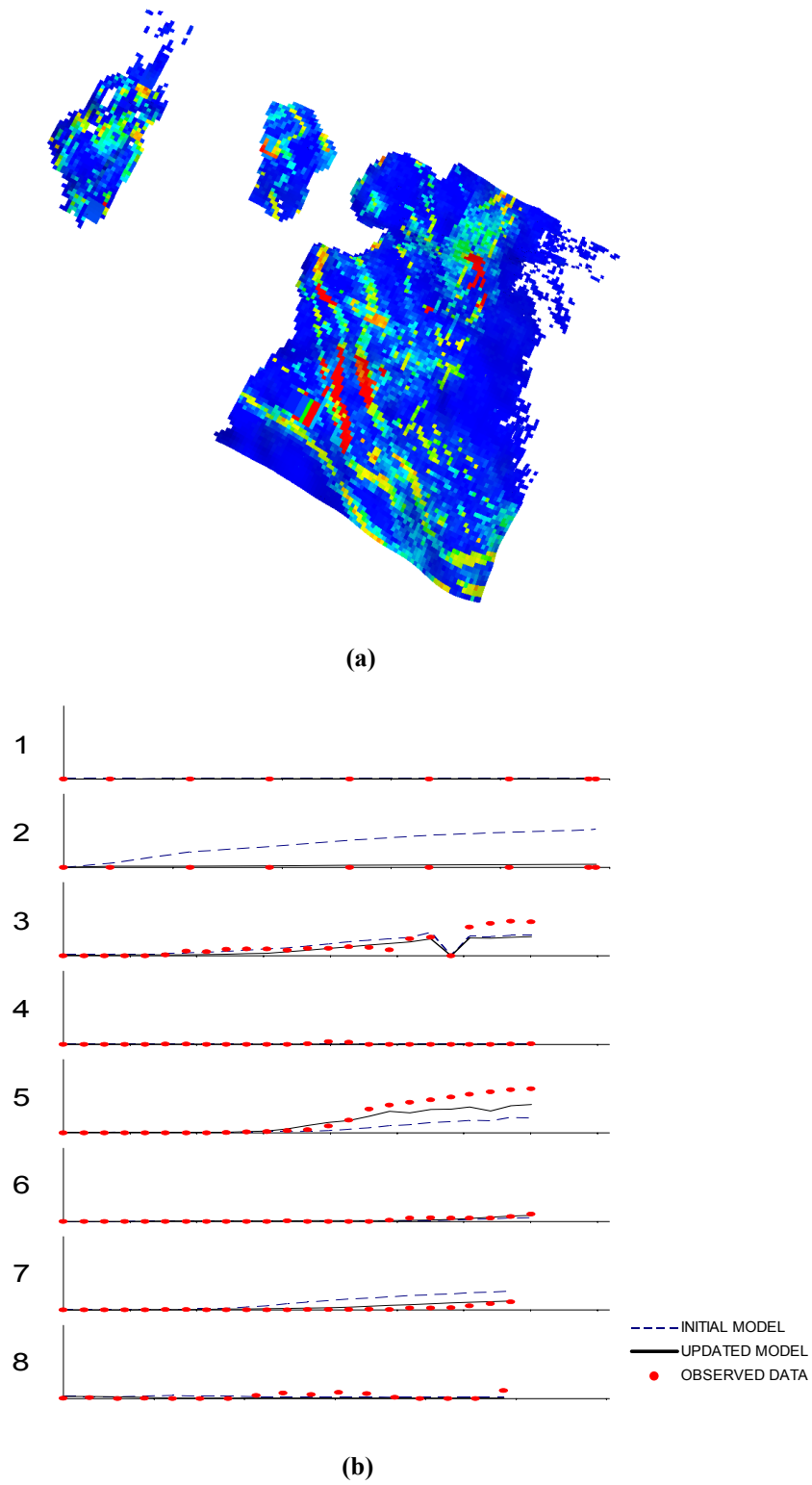
Fig. 2.16 (a) Calibrated permeability field and (b) water-cut history match result via dual scale inversion

(a) **(b)**
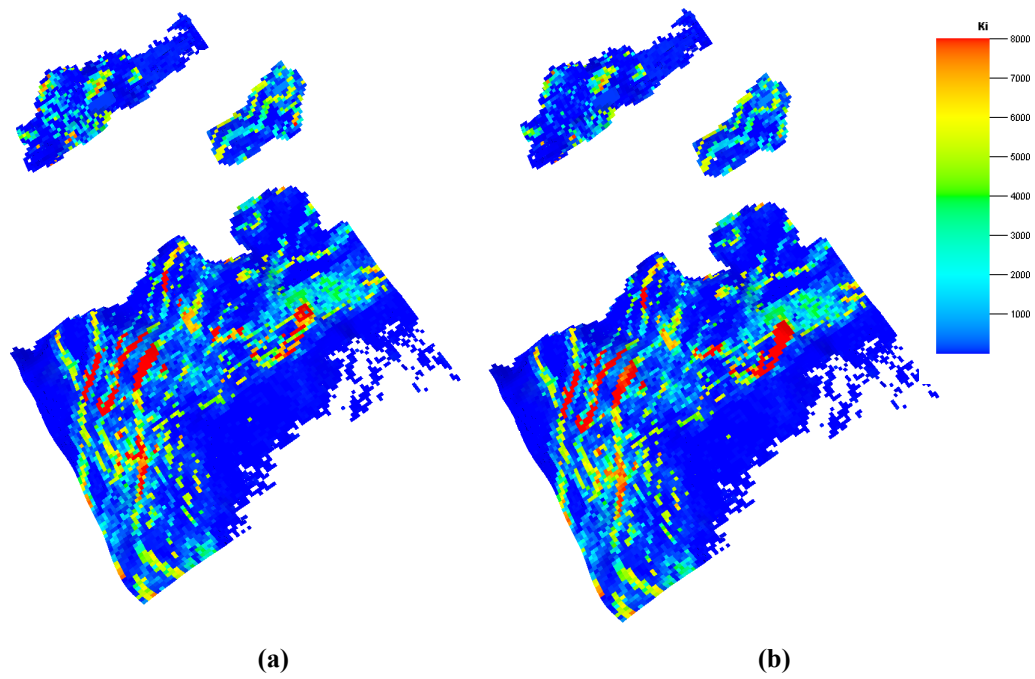
Fig. 2.17 Updated permeability field (a) after dual-coarse-scale inversion and (b) after dual-fine-scale inversion

(a) **(b)**
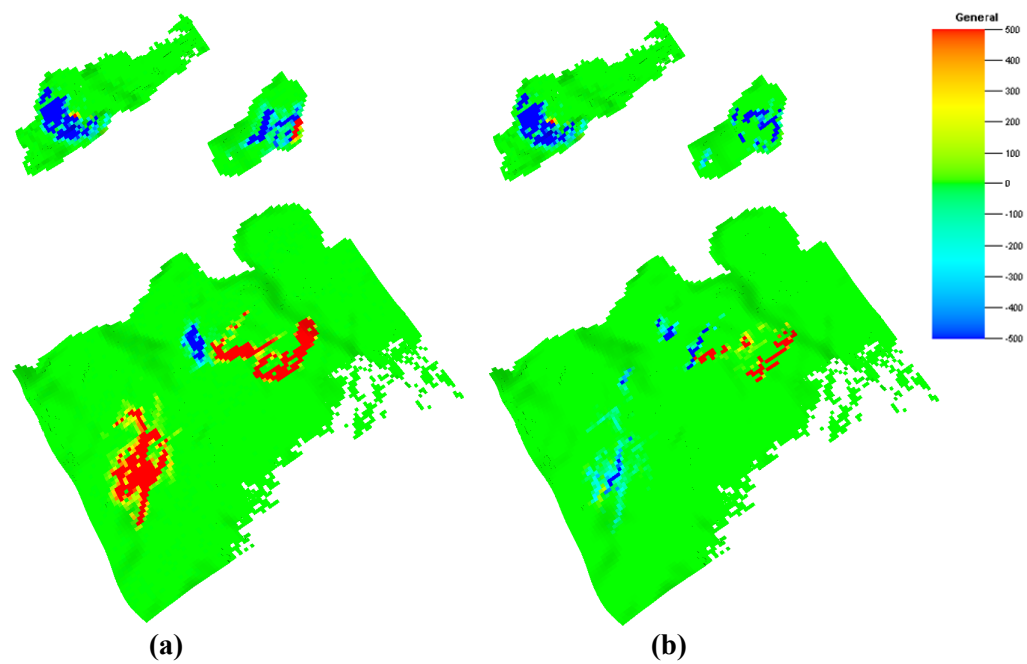
Fig. 2.18 Permeability change made (a) during dual-coarse-scale inversion and (b) during dual-fine-scale inversion
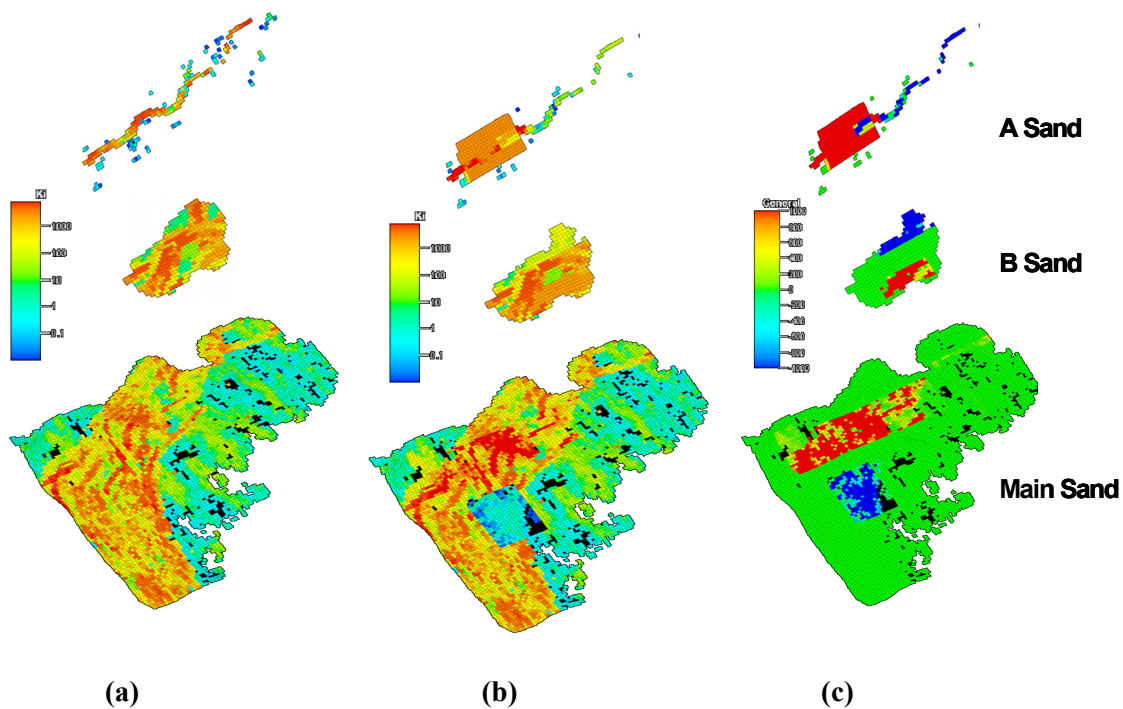
Fig. 2.19 Manual history matching (a) Initial model (b) Updated by manual history matching (c) Change made by manual history matching (Hohl et al., 2006)

The same procedure of dual scale inversion as in the synthetic example is followed. Coarse-scale inversion was carried out with coarsened model and the permeability updates are added to the initial fine-scale model. Finally, the fine-scale inversion is carried out. The matches to the water-cut responses are shown in **Fig. 2.16**. The overall water-cut history matching is improved. **Fig. 2.17** compares the permeability field after the coarse-scale and fine-scale inversion for 3 selected layers. The corresponding changes to the model are shown in **Fig. 2.18**. Again, as expected, majority of the changes occur during the coarse-scale history matching. Finally, in **Fig. 2.19** we show the permeability changes resulting from a manual history matching presented in Hohl et al. (2006). On comparing Fig. 2.19 with Figs. 2.17 and 2.18, the dual scale approach is able to preserve the pay and non-pay juxtaposition in the original geologic

model because the changes are mostly aligned along the channels. This is not the case for the manual history matching. Each of dual scale iteration took less than an hour in PC (Intel Core2 6600 @2.4/2.39GHz).

2.6. Chapter Summary

1. A dual scale approach to history matching high resolution geologic models is proposed. In this approach the majority of the history matching is performed on an 'optimally' coarsened model with further refinement, if needed, via a fine-scale inversion.

2. The 'optimal' coarsening using 'slowness' instead of 'velocity' is shown to result in a more conservative coarsening compared to previous works and is able to better preserve the features of the initial geologic model.

3. The coarse-scale history matching is computationally efficient because of the significantly reduced number of unknowns during inversion. Furthermore, the scale-decomposition of the inverse problem reduces the ill-posedness and makes the inversion more stable without the need for artificial regularization. At the coarse-scale the inversion encounters fewer local minima and thus converges faster.

4. We have demonstrated the power and applicability of the dual scale approach using both synthetic and field examples. The field application in a structurally complex turbiditic reservoir shows the ability of the dual scale inversion to preserve important geologic features during history matching.

CHAPTER III

**CALIBRATION OF HIGH-RESOLUTION RESERVOIR MODELS USING
TRANSIENT PRESSURE DATA**

Integrating dynamic data into high resolution reservoir models is a crucial aspect of any optimal reservoir development and management strategy. In this regard, pressure data provides several advantages. First, pressure transient tests are easier and less expensive to carry out in the field. Second, pressure responses can be obtained early in the field life compared to water-cut or tracer data. Finally, the pressure perturbations travel much faster compared to tracer or water front, resulting in quicker response in the field. This makes interference tests much more appealing compared to tracer tests which may require months to see a field response. However, the computation cost and localized nature of pressure sensitivities pose difficulties in history matching transient pressure data with a finite difference model. Also, pressure tests from multiple wells are difficult to analyze because of superposition of pressure responses.

We propose a fast and robust approach to integrating transient pressure data using a trajectory-based approach that relies on a high frequency asymptotic solution of the diffusivity equation. The trajectory or ray-based methods are routinely used in seismic tomography. In this chapter, we make a detailed comparison of streamlines and seismic rays and examine the applicability of streamline-based methods for transient pressure data inversion. Specifically, the high frequency asymptotic approach allows us to analytically compute the sensitivity of the pressure data with respect to reservoir properties such as porosity and permeability. This results in a very efficient approach for the integration of pressure data into geologic models.

We apply our proposed method to transient pressure data from both single well test and multi-well interference tests. Our results demonstrate the advantage of performing interference tests compared to performing tracer tests in terms of identifying

heterogeneities early in the field life. Finally, we apply this approach to data from a multiwell interference test in a Middle Eastern reservoir. Specifically, the pressure data obtained from permanent downhole gauges (PDG) in multiple wells are utilized to determine communications in the reservoir and to derive quantitative information about the permeability distribution in the reservoir for potential aid in the design and optimization of a miscible gas flood.

3.1. Chapter Introduction

Calibration of high-resolution reservoir models using dynamic field response such as transient pressure or tracer data typically requires the solution of an inverse problem. Such inverse modeling entails forward flow simulation of large three-dimensional models, either to compute the sensitivity of model parameters for a linearized inversion problem (Tarantola, 2005; Oliver et al., 2008) or to apply stochastic approaches such as genetic algorithms and the Ensemble Kalman Filter (Quenes et al., 1994; Devegowda et al., 2007). Gradient-based inverse methods require the computation of sensitivity coefficients which quantify the change in production response because of small perturbations in the reservoir parameters. These sensitivities constitute an essential and often time-consuming part of the inverse modeling. Trajectory-based methods, such as streamline simulation, have shown significant potential in this regard (Vasco and Datta-Gupta, 1999; Cheng et al., 2005; Oyerinde et al., 2007). With the trajectory methods, the sensitivities of the production response with respect to reservoir parameters can be computed analytically using a single flow simulation (Datta-Gupta and King, 2007).

Pressure data provides several advantages to facilitate high-resolution reservoir characterization. Pressure transient tests are easier to carry out and can be performed in a shorter time compared to performing tracer tests. Pressure responses are directly related to the permeability and porosity field and can be obtained much quicker than other production history such as water-cut data and tracer responses. The localized nature of pressure sensitivities, however, introduces some difficulties in the inversion approach.

That is, pressure responses are much more sensitive to model parameters near the wells than model parameters away from the wells (Vasco et al., 2000). Pressure tests from multiple wells can be more difficult to analyze because of the superposition of pressure responses.

Asymptotic ray theory has been widely applied to both electromagnetic (Kline and Kay, 1965; Luneburg, 1966) and seismic wave front propagation (Cerveny et al., 1978). In fact, the approach has proved very appealing in the examination of front propagation in general (Sethian, 1996). Asymptotic methods have also been applied to represent the solution for flow and transport, relating the orders of the expansion to attributes such as breakthrough or front arrival time (Vasco and Datta-Gupta, 1999; Vasco et al., 2000). The asymptotic approach has several advantageous features especially with regard to the inverse modeling. The asymptotic solutions are defined along the trajectories which are ray paths of the wave equation (Vasco and Finsterle, 2004). The 1-D nature of the solution along these trajectories scales favorably with model size. Thus, the technique is particularly well-suited for high-resolution simulation models. Also, a trajectory-based inversion algorithm offers significant advantages over traditional gradient-based methods because the parameter sensitivities are easily computed after a single flow simulation. In traditional gradient-based inverse methods, the sensitivity computations can be very time consuming, requiring multiple flow simulations or adjoint solutions.

In this chapter, we present a trajectory-based inversion approach for pressure transient tests and examine its basic mathematical formulation using high frequency asymptotic expansion. We then show that under several practical situations, the trajectories for transient pressure solutions can be approximated by the streamlines generated using the underlying velocity field. We validate our approach first with a two dimensional synthetic case and then, with a three dimensional field example. In the field example, permanent downhole gauges (PDG) with surface read-out are applied to obtain the downhole pressure data. Pressure transient data and pressure monitoring data during

the testing of other wells are available for pressure history matching from the PDG. We perform history matching of pressure peak arrival times to update the geologic model.

3.2. Approach

In this section we first discuss the asymptotic solution for the transient flow followed by the methodology for computing the trajectory for the propagation of the pressure wave front.

3.2.1. Asymptotic Approach to Transient Pressure Responses

Asymptotic approaches to inversion have been applied in several other disciplines such as medical, optical and geophysical imaging (Gordon and Herman, 1974; Iyer and Hirahara, 1993; Arridge, 1999). It provides the mathematical foundations with which we can relate the streamlines and ray methods from geophysics (Vasco and Finsterle, 2004; Datta-Gupta and King, 2007). It has also been applied to tracer tests, transient pressure inversion and two-phase flow data (Vasco and Datta-Gupta, 1999; Vasco et al., 2000; Vasco and Datta-Gupta, 2001). Here, we revisit the asymptotic approach to analyze the transient pressure data from well tests.

The transient pressure response from a heterogeneous permeable medium can be described by the diffusivity equation,

$$\phi(\mathbf{x})\mu c_t \frac{\partial P(\mathbf{x},t)}{\partial t} - \nabla \cdot \left(k(\mathbf{x})\nabla P(\mathbf{x},t)\right) = 0 \tag{3.1}$$

Using Fourier transform of Eq. 3.1, we obtain the following equation in the frequency domain.

$$\frac{\phi(\mathbf{x})\mu c_t}{k(\mathbf{x})}(-i\omega)\widetilde{P}(\mathbf{x},\omega) = \nabla^2 \widetilde{P}(\mathbf{x},\omega) + \frac{\nabla k(\mathbf{x})}{k(\mathbf{x})} \cdot \nabla^2 \widetilde{P}(\mathbf{x},\omega) \tag{3.2}$$

The goal of the asymptotic approach is to find a solution of the diffusive pressure equation that mimics the one found in wave propagation. The asymptotic solution for a transient pressure response assumes the following form (Fatemi et al., 1995; Vasco et al., 2000; Datta-Gupta et al., 2001)

$$\widetilde{P}(\mathbf{x},\omega)=e^{-\sqrt{-i\omega}\tau(\mathbf{x})}\sum_{k=0}^{\infty}\frac{A_k(\mathbf{x})}{\left(\sqrt{-i\omega}\right)^k}.$$ (3.3)

Eq. 3.3 is the summation of an infinite number of terms with coefficients $A_n(\mathbf{x})$. We generally consider only the first few terms which correspond to high frequency (large ω) in the series and these high frequency terms describe the physical propagation of a 'pressure front' (Vasco et al., 2000; Datta-Gupta et al., 2001). If we only consider the first term in Eq. 3.3, then

$$\widetilde{P}(\mathbf{x},\omega)=e^{-\sqrt{-i\omega}\tau(\mathbf{x})}A_0(\mathbf{x})$$ (3.4)

After inserting Eq. 3.4 into Eq. 3.2 and collecting terms with the highest order of $\sqrt{-i\omega}$, that is, $\left(\sqrt{-i\omega}\right)^2$, we obtain the equation for the front propagation in an isotropic permeable media,

$$\nabla\tau(\mathbf{x})\cdot\nabla\tau(\mathbf{x})=\frac{1}{\alpha(\mathbf{x})}$$ (3.5)

where $\alpha(\mathbf{x})$ is the diffusivity given by

$$\alpha(\mathbf{x})=\frac{k(\mathbf{x})}{\phi(\mathbf{x})\mu c_t}$$ (3.6)

Eq. 3.5 is actually a form of the eikonal equation which explains a variety of propagation behaviors (Kline and Kay, 1965; Kravtsov and Orlov, 1990). It is interesting and important to note that Eq. 3.5 has a form similar to that of the streamline time of flight equation which describes the propagation of a neutral tracer (Datta-Gupta and King, 2007).

$$v \cdot \nabla \hat{\tau}(\mathbf{x}) = 1 \qquad (3.7)$$

where $\hat{\tau}(\mathbf{x})$ is the streamline time of flight and v is the interstitial velocity of a neutral tracer. By analogy with the time of flight formulation, we can see that the pressure wave fronts travel with a velocity given by $(\alpha(\mathbf{x}))^{1/2}$. In fact, we can define a diffusive time of flight for the propagation of a pressure front as follows (Kulkarni et al., 2000; Datta-Gupta et al., 2001),

$$\tau(\mathbf{x}) = \int_\psi \frac{d\zeta}{\sqrt{\alpha(\mathbf{x})}}, \qquad (3.8)$$

However, the diffusive time of flight is defined along the trajectories of a 'pressure wave front' ψ, which are given by the ray paths of the wave equation. These trajectories are not necessarily the streamlines (Vasco and Finsterle, 2004). We will discuss this issue in detail later and exploit the analogy between streamlines and pressure trajectories for interpretation of the field pressure response. Also, note that the unit of diffusive time of flight in Eq. 3.8 is the square root of time which is consistent with the scaling behavior of diffusive flow.

3.2.2. Computation of Pressure Front Trajectory

In this section we first describe the computation of trajectories for asymptotic solution of the transient pressure equation. We also relate the diffusive time of flight to the actual

arrival time of the pressure wave front at the wells. The physical relationship between the diffusive time of flight and the propagation of the pressure wave front can be obtained by examining the time domain solution to the zeroth order asymptotic expansion in Eq. 3.4. The solution is given by the inverse Fourier transform,

$$P(\mathbf{x},t) = A_0(\mathbf{x}) \frac{\tau(\mathbf{x})}{2\sqrt{\pi t^3}} e^{-\frac{\tau^2(\mathbf{x})}{4t}} \qquad (3.9)$$

The above equation actually corresponds to the pressure response for an impulse (Dirac delta function) source or sink in the flow domain. This pressure response will be maximized at a fixed position $\mathbf{x}$, when the following time derivative vanishes

$$\frac{\partial P(t)}{\partial t} = A_0(\mathbf{x}) \frac{\tau(\mathbf{x})}{2\sqrt{\pi}} e^{-\frac{\tau^2(\mathbf{x})}{4t}} \left(-\frac{3}{2} t^{-\frac{5}{2}} + t^{-\frac{3}{2}} \frac{\tau^2(\mathbf{x})}{4t^2} \right) = 0 \qquad (3.10)$$

Eq. 3.10, after solving for the time t, provides us with a relationship between the physical time when the pressure response (drawdown or build up) reaches a maximum at the position $\mathbf{x}$ and the diffusive time of flight.

$$t_{max}(\mathbf{x}) = \frac{\tau^2(\mathbf{x})}{6} \qquad (3.11)$$

Thus, the arrival of the pressure wave front at a location can be interpreted as the time when the pressure reaches a maximum or minimum for a perturbation introduced by an impulse source or sink. We call this 'the peak arrival time'. In practical field applications, however, we do not have an impulse source or sink. Instead, we have a step change in rate (shut-in or start-up) which can be approximated by a 'Heaviside' function. Noting the fact that the impulse or the Dirac delta function is the derivative of the Heaviside

function, for practical applications we will compute the peak time corresponding to the derivative of the pressure data rather than the pressure data itself (Kulkarni et al., 2001).

Fig. 3.1 illustrates the computation of peak arrival time or 'the pressure wave front' arrival time. Fig. 3.1a shows the permeability field for the example case. This example case is a two dimensional example with nine wells. The producer at the center of the model is active. The eight wells at the perimeter of the model are not producing but are used for monitoring the pressure responses. We performed a flow simulation and obtained the time derivatives of pressure at each observation well location. Next, we determined the peak arrival time of the pressure front from the time corresponding to the maximum of the time derivative of the pressure responses. Fig. 3.1b is the time derivative of the pressure response at each monitoring well. Thus, the peak arrival time at each monitoring well location can be obtained as shown, for example producer 'P1' has 24,839 seconds (about 7 hours). Note that we take the absolute value of the time derivative of pressure for these calculations. In the same manner, peak arrival time at any spatial location in the flow domain can be computed from flow simulation. During flow simulation, we keep track of the pressure response at each cell of the model at each time step. The peak arrival time at any location is then computed corresponding to the time when the pressure derivative reaches a maximum. **Fig. 3.2a** is the contour of the peak arrival time, t_{max} of the pressure front as given by Eq. 3.11. The diffusive time of flight, $\tau(\mathbf{x})$ which is the primary information required for computation of the pressure front trajectories can now be calculated from Eq. 3.11. The pressure trajectories are now defined by integration along the direction of $\nabla\tau(\mathbf{x})$ as given in Eq. 3.8. We perform the trajectory calculations using the following steps.
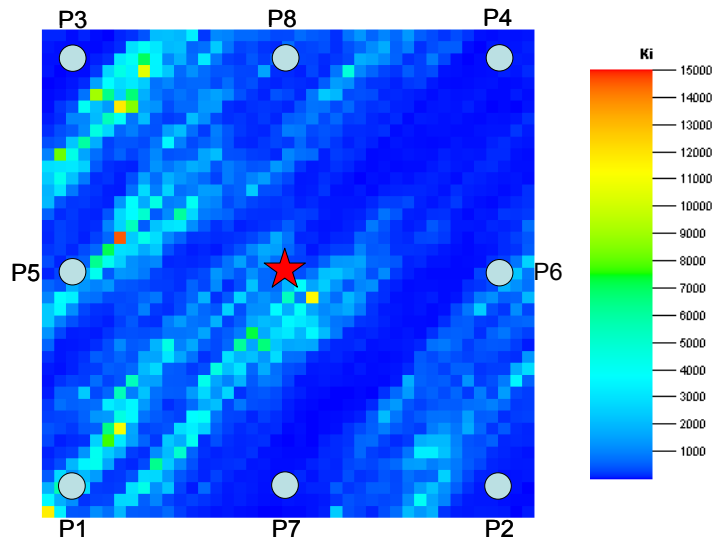
(a)
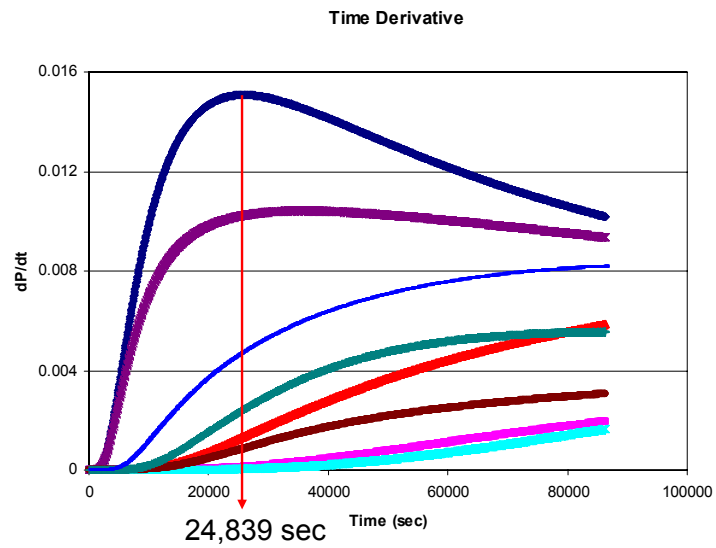
(b)

Fig. 3.1 Synthetic case (a) Permeability field (b) Time derivatives of well pressure of each monitoring well

- **Flow Simulation.** Given a geological model and well configuration, we first perform a flow simulation. The simulation results give us pressure response with time at each grid block in the flow domain. This information is saved for subsequent calculations.

- **Peak Arrival Time Computation.** As discussed in Eqs. 3.9 through 3.11, the pressure front arrival time can be calculated from the maximum of the time derivative of the pressure response at each grid block location. First, we scan the pressure history at each grid block and then compute its time derivatives. The time when the derivative reaches a maximum or minimum indicates the pressure front arrival time, t_{max}. The diffusive time of flight $\tau(\mathbf{x})$ is now easily obtained from Eq. 3.11.

- **Tracing the Trajectory Based on the Gradient of the Diffusive Time of flight.** We calculate the numerical gradients of diffusive time of flight for each grid block location. Pressure front trajectories are simply curves along these gradients of the diffusive time of flight. For trajectory calculations we make use of the Heun's method (Kreyszig, 1993) which is explained below.

From Eq. 3.8, the pressure front trajectories are defined along $\psi(\zeta)$. The trajectory ψ is computed by integrating the differential equation (Vasco and Finsterle, 2004),

$$\frac{d\psi}{d\zeta} = \nabla \tau(\mathbf{x})$$

(3.12)

where the term ζ indicates the distance along the trajectory ψ. The gradient of diffusive time of flight, $\nabla \tau$ can be obtained from numerical simulation results as shown in Fig. 3.2a. The Heun's method, also known as the second-order Runge-Kutta method, is

applied to determine the trajectories. These results are more accurate than those of the Euler-Cauchy method (Kreyszig, 1993) in that we compute first an auxiliary value to improve the solution of the differential equation. In other words, we first estimate the gradient in each step using the current location to obtain the $(i+1)$-th step point (predictor step),

$$\psi_{i+1}^* = \psi_i - \nabla \tau(\psi_i)\delta\zeta \tag{3.13}$$

Next, the $(i+1)$-th step point is further refined using the gradient at ψ_{i+1}^* (corrector step)

$$\psi_{i+1} = \psi_i - \frac{\delta\zeta}{2}\left(\nabla \tau(\psi_i) + \nabla \tau(\psi_{i+1}^*)\right) \tag{3.14}$$

Detailed explanation and procedure is described in Appendix B.

For our example case, Fig. 3.2a shows the peak arrival time at each location. The diffusive time of flight at each location is then calculated from Eq. 3.11. The output of the trajectory computation based on the numerical gradient of the diffusive time of flight is shown in Fig. 3.2b. These are the trajectories along which the asymptotic solution for the transient pressure equation is defined. One of our goals in this chapter is to examine whether it is possible to approximate these pressure trajectories using the streamlines which are much easier to compute. We address this issue in the next section.
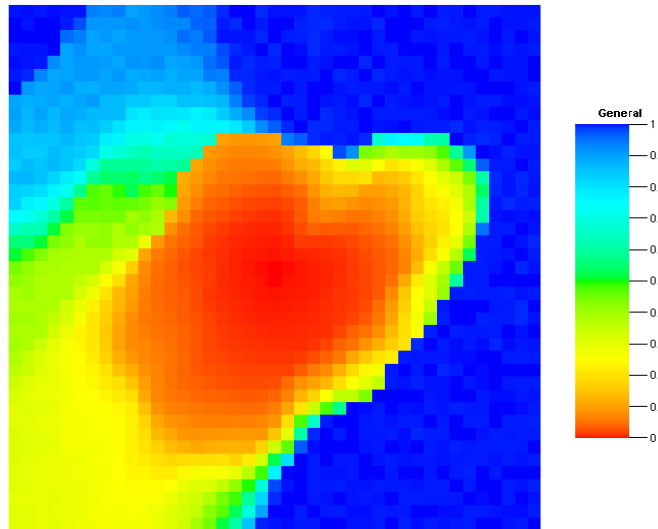
3.2.3. Pressure Front Trajectory vs. Streamline Trajectory

We now compare the pressure front trajectory with the streamlines. Note that the diffusive time of flight and pressure front trajectories are invariant with time for a given geological model and boundary conditions while streamlines will depend on the instantaneous pressure at each location and are a function of time. However, after the very early times, the streamline profile becomes stable rather quickly. **Fig. 3.3** shows the

streamlines corresponding to the pressure trajectories in Fig. 3.2b after this stabilization. Note that the general characteristics of both the pressure front trajectories and the streamlines are quite similar.

Fig. 3.4 shows the pressure wave front locations at various times for the synthetic example case. The left panel shows the 'true' pressure front locations rigorously computed based on the peak arrival time as discussed above. The right panel shows the approximate pressure front locations based on the integration of the diffusive time of flight equation (Eq. 3.8) along the streamline trajectories. Although the front locations are different in detail characters, especially later time, the general shapes are quite similar. Previous investigations by Kulkarni et al. (2001) using an analytical solution of drainage area during single well tests arrived at similar conclusions. These results indicate that the streamlines can be reasonable approximations for the pressure front trajectories at least for the purpose of production history matching with which we intend to calibrate large scale geologic features. This is the main feature that we will exploit for the efficient interpretation of the pressure interference test data as discussed in the next section.
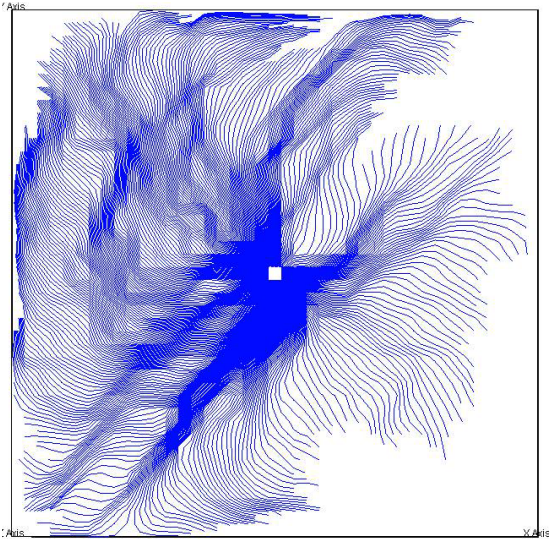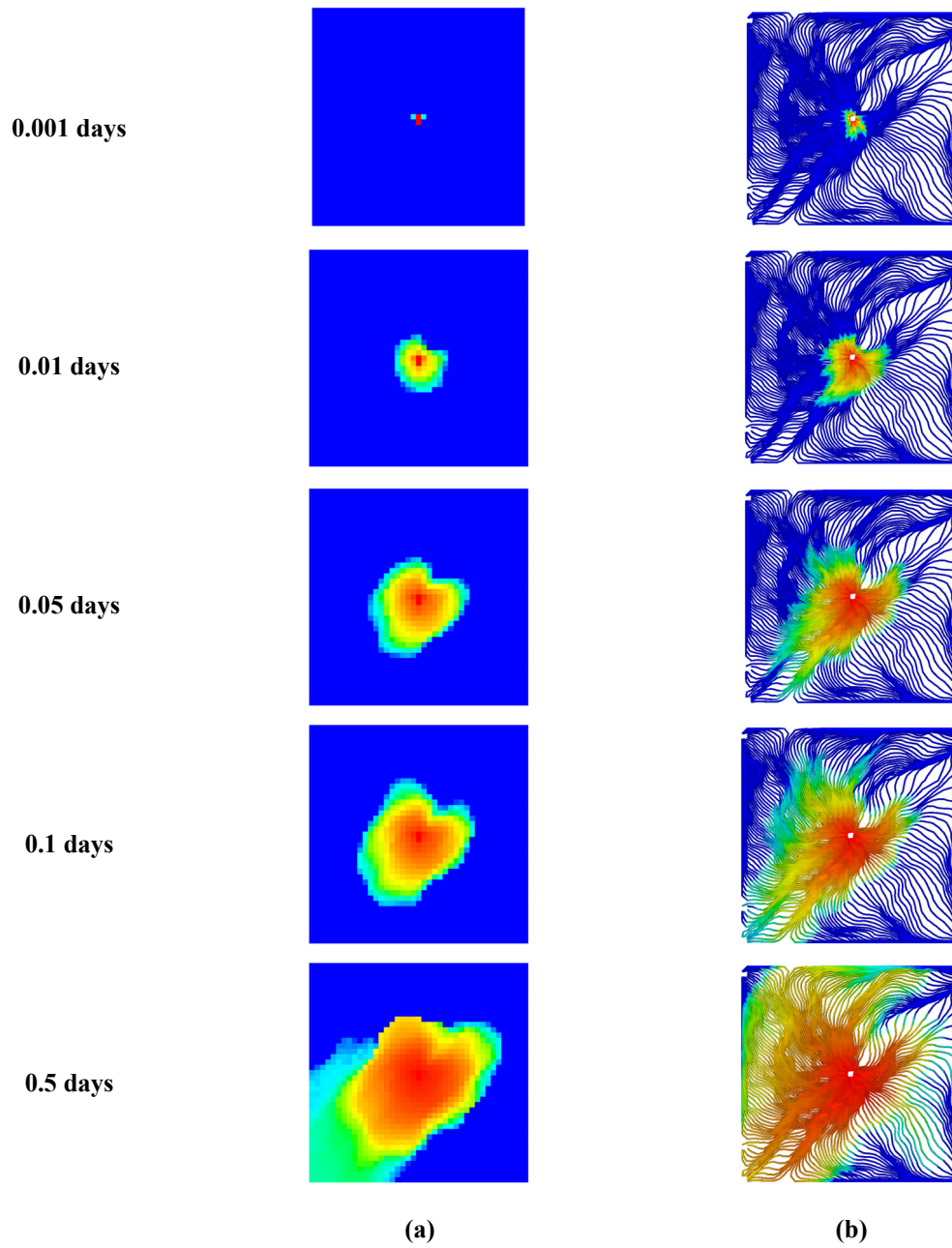
(a)
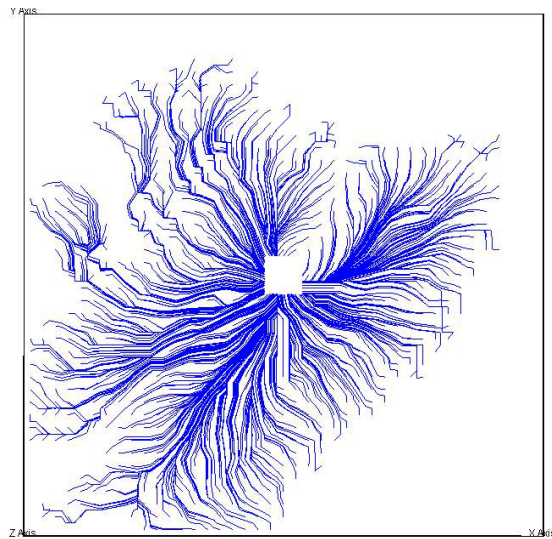
(b)

Fig. 3.2 Single test from producer P9
(a) Peak arrival time of the pressure front (b) The pressure front trajectory from the gradient of diffusive time of flight

Fig. 3.3 Streamline of synthetic case

0.001 days

0.01 days

0.05 days

**0.1 days**

0.5 days

(a)

(b)

Fig. 3.4 Pressure front arrival time.
(a) Computed from pressure response from finite difference simulation
**(b) Computed from diffusive time of flight along streamline**

3.2.4. Multiple Pressure Transient Tests

So far, we have discussed the diffusive time of flight and trajectory computations for a single active well. We now examine the situation when multiple wells are tested in a sequence. This is often the case in field applications as we will see later for the field example. The main purpose of this section is to investigate the difference between the diffusive time of flight and pressure trajectories from a single well test and those from multiple well tests. Specifically, we examine the possibility of replacing the pressure trajectory calculations from multiple tests with those from a sequence of single tests and their correspondence to streamlines.

For illustration purposes, we use the same well configuration as the single well test discussed before. The main difference is the testing schedule. To begin with, the producer 'P1' in Fig. 3.1a is produced for one day at a constant rate and then shut-in. This is followed by a build-up of one day when all the wells are shut-in. Next, the producer 'P5' is produced for one day. **Fig. 3.5a** shows the time derivatives of pressure during the test at the observation wells. Figs. 3.5b and 3.5c show the pressure wave front based on the peak arrival time and the corresponding pressure trajectories for well 'P5'. It is important to distinguish the response from the well 'P1' and 'P5' while calculating the peak arrival time. For example, in this case, the well 'P5' pressure front arrival time shown in Fig. 3.5b will correspond to the second peak in the time derivative of the pressure history at each grid cell. In a manner similar to the single active well case, we calculate the trajectory of the pressure front based on the numerical gradient of the diffusive time of flight. This result is shown in Fig. 3.5c. Thus, for multiple tests we expect to have multiple peaks in the pressure derivative response corresponding to each testing well. The trajectories related to testing at well 'P1' are shown in Fig. 3.5d. Although for this example case, the peaks were easily identifiable, it may not be the case in general. Hence, we examine the possibility of computing the pressure front and trajectories for multiple tests using sequence of single tests.
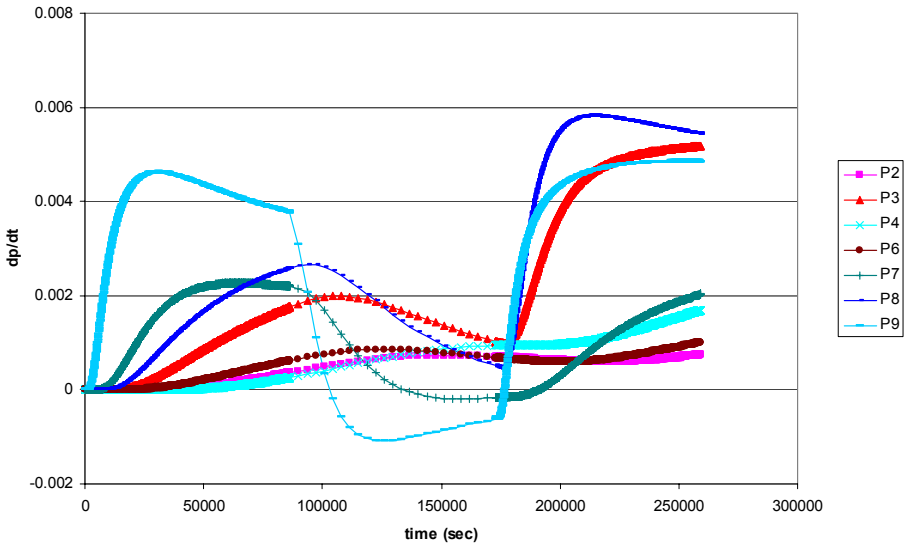
(a) Time derivatives of well pressure
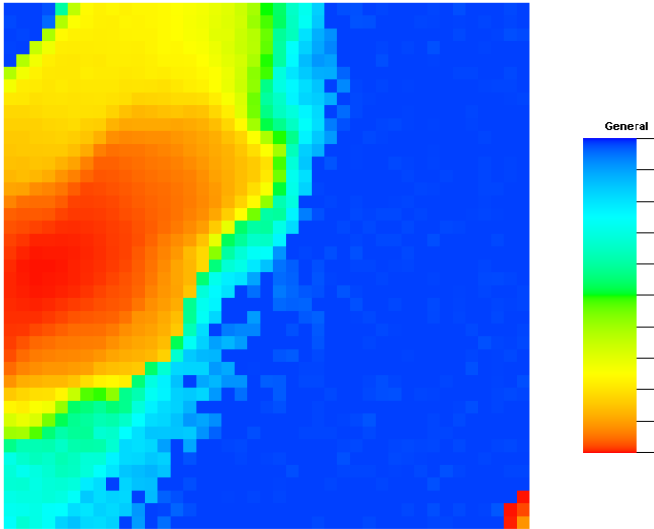
(b) Peak arrival time of the pressure front

Fig. 3.5 Multiple tests (P5 after P1)
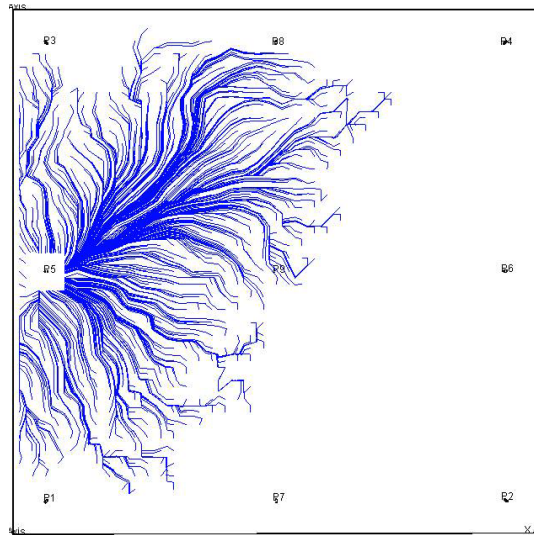
(c) Pressure front trajectory from the gradient of diffusive time of flight (P5)
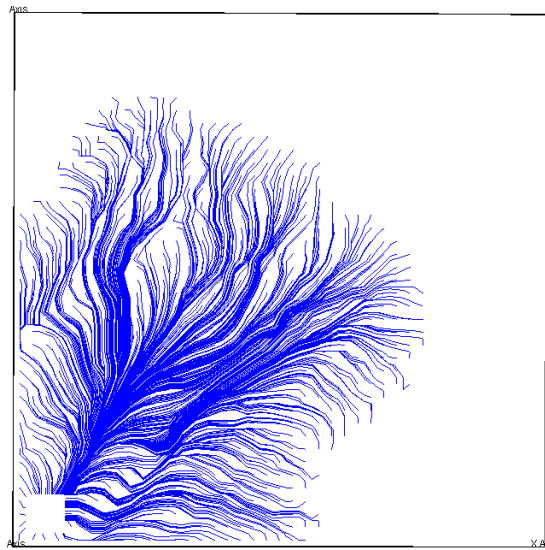
(d) Pressure front trajectory from the gradient of diffusive time of flight (P1)

Fig. 3.5 Continued

(a) Peak arrival time of the pressure front

(b) Pressure front trajectory from the gradient of diffusive time of flight

Fig. 3.6 Single tests from P5

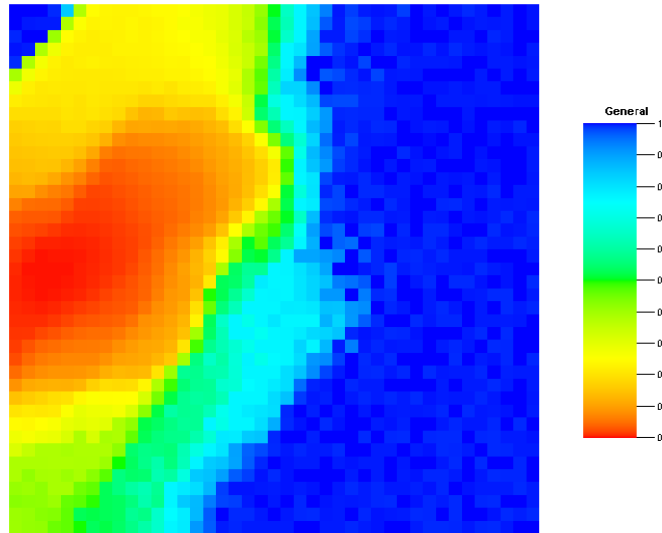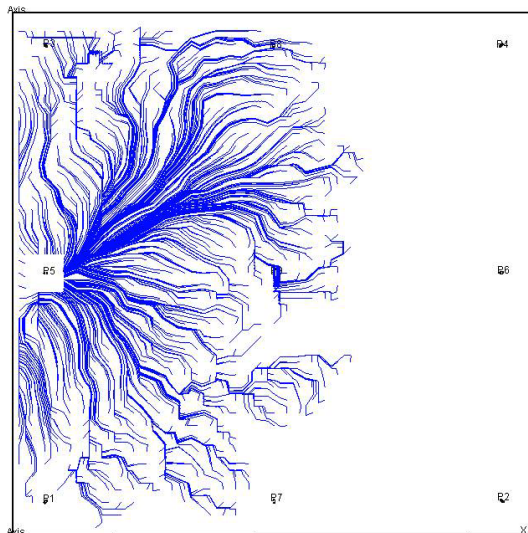For comparison purposes, we perform a single test from producer 'P5' without prior testing at producer 'P1' and compute the peak arrival time and the pressure front trajectories. The results are shown in **Fig. 3.6a** and 3.6b. Note that the contours of peak arrival time in Fig. 3.6a are nearly identical to those in Fig. 3.5b. This is because the peak arrival time or the diffusive time of flight is primarily a function of the reservoir properties, the geometry of the flow model and the boundary conditions. Thus, the fact that well 'P1' was produced before well 'P5' has minimal impact in the diffusive time of flight calculations as seen here. Fig. 3.6b shows the pressure trajectories for this case. On comparison with Fig. 3.5c, again we can see that the trajectories are almost identical. As before, in our applications we will approximate these trajectories using streamlines after stabilization of the pressure distribution.

3.2.5. Sensitivity Coefficients and Geologic Model Calibration

Simulation model calibration with pressure data typically requires the solution of an inverse problem. The mathematical formulation for such inverse models has been discussed in previous literature (Tarantola, 2005; Oliver et al., 2008). In our application, we minimize a penalized objective function as follows,

$$\|\delta \mathbf{d} - \mathbf{S}\,\delta \mathbf{m}\| + \beta_1\|\delta \mathbf{m}\| + \beta_2\|\mathbf{L}\,\delta \mathbf{m}\| \qquad (3.15)$$

where $\delta \mathbf{d}$ is the vector of the data misfit, that is, the difference between the observed and calculated pressure response, and $\mathbf{S}$ represents the parameter sensitivity matrix whose elements consist of the sensitivities which are partial derivative of the pressure response with respect to reservoir parameters. Also, $\delta \mathbf{m}$ is the vector of model parameter change and $\mathbf{L}$ is a second spatial difference operator. The first term quantifies the misfit between the observed and calculated pressure response. The second term ensures that the calibrated geologic model is not significantly different from the initial model which contains static data such as geologic input, petrophysical data and seismic information.

This is intended to preserve the geologic realism during history matching. Finally, the third term allows the smooth and large scale change of model parameters since pressure history data has low resolution information.

In general, one of the most time consuming aspects of the inverse modeling is construction of the sensitivity matrix, $\mathbf{S}$. That is, we need to quantify the relationship between the changes or perturbations in model parameters and corresponding variations in the predicted responses. From Eqs. 3.6 and 3.8, the sensitivity coefficient of diffusive time of flight can be obtained analytically as follows.

$$\frac{\partial \tau(\mathbf{x})}{\partial k(\mathbf{x})} = -\frac{1}{2} \int_{\psi} \frac{\sqrt{\phi(\mathbf{x})\mu c_t}}{k(\mathbf{x})\sqrt{k(\mathbf{x})}} d\zeta$$

$$\frac{\partial \tau(\mathbf{x})}{\partial \phi(\mathbf{x})} = \frac{1}{2} \int_{\psi} \frac{\sqrt{\phi(\mathbf{x})\mu c_t}}{\phi(\mathbf{x})\sqrt{k(\mathbf{x})}} d\zeta$$

(3.16)

Note that the sensitivities are defined along the pressure trajectories and are available after a single flow simulation. As discussed before, in our applications, the pressure front trajectories are approximated by streamlines which are easily calculated.

After sensitivity calculations, pressure data integration is carried out using an iterative minimization technique. The minimization of Eq. 3.15 leads to an iterative least-squares solution (Paige and Saunders, 1982) of the augmented linear system given by

$$\begin{pmatrix} \mathbf{S} \\ \beta_1 \mathbf{I} \\ \beta_2 \mathbf{L} \end{pmatrix} \delta \mathbf{m} = \begin{pmatrix} \delta \mathbf{d} \\ 0 \\ 0 \end{pmatrix}$$

(3.17)

where the terms β_1 and β_2 are the weights determining the relative strengths between the pressure data, the prior model and the smoothness penalty term.

3.3. Applications

In this section, we discuss application of the pressure transient data integration approach to synthetic and field examples. The synthetic example is used to illustrate the detailed procedure in our approach. It is followed by a demonstration of the applicability of our approach to a high resolution and geologically complex field case using an example from the Middle East.

3.3.1. Synthetic Example

Our synthetic model is a two dimensional example and the well configuration is a nine-spot pattern as shown in **Fig. 3.7a**. The geologic model is a 2-D model with the dimensions of 21x21x1. Multiple sequential interference testing was performed at eight wells from well 'P1' to well 'P8' in the perimeter of the model. The well pressure at well 'I1' has been monitored during the sequential multiple testing. Fig. 3.7a shows the reference permeability field and the location of the nine wells. The sequential well testing schedule is shown in Fig. 3.7b. We assume that only the pressure in well 'I1' is available for this example. **Figs. 3.8a** and 3.8b show observed pressure history from the reference model and its time derivative. As shown in Fig. 3.8b, the time derivative of pressure has eight peak arrival times of pressure corresponding to the testing of each well. The peak arrival times of pressure are treated as observed data for history matching and are used for the inversion process. The initial geologic model for this synthetic example is a homogeneous model and has a permeability of 500 md. **Figs. 3.9a** and 3.9b show the well pressure of well 'I1' and its time derivative. There are clear discrepancies (Fig. 3.9a) between the history and calculated response for the peak arrival times of pressure (Fig. 3.9b).
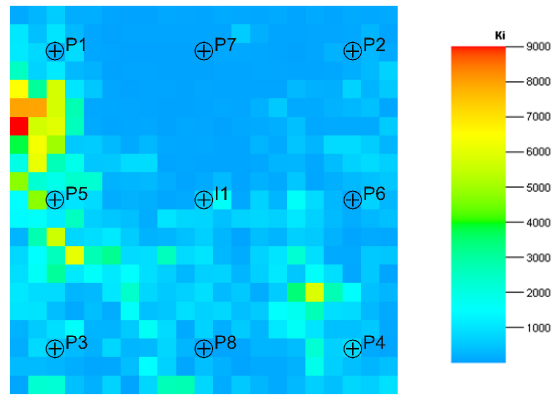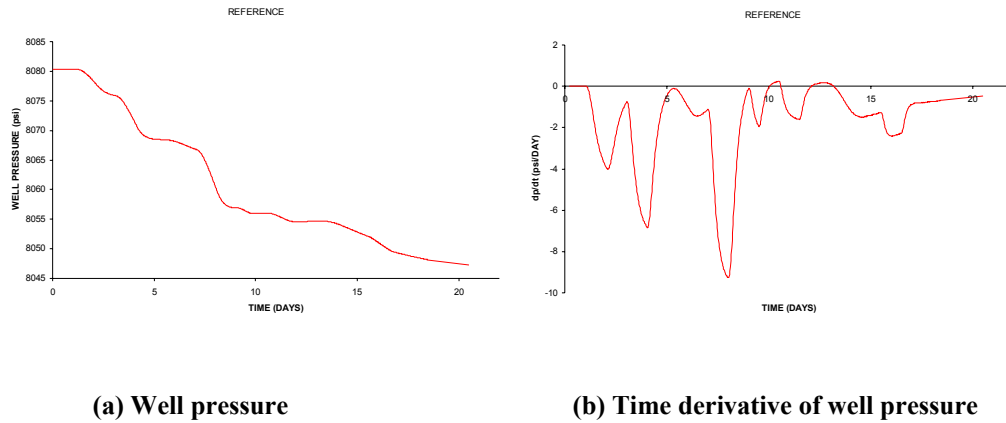
(a) Permeability field
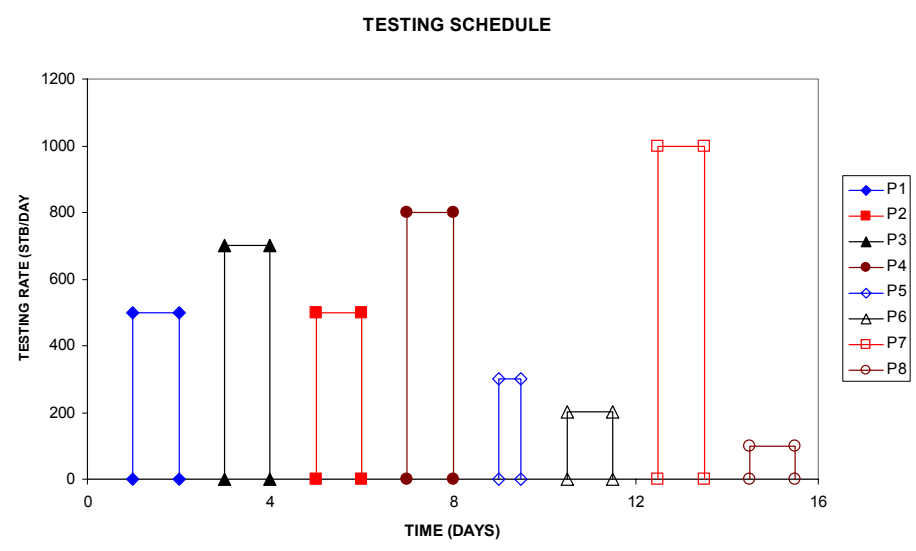
(b) Testing schedule

**Fig. 3.7 Reference geologic model and testing schedule**

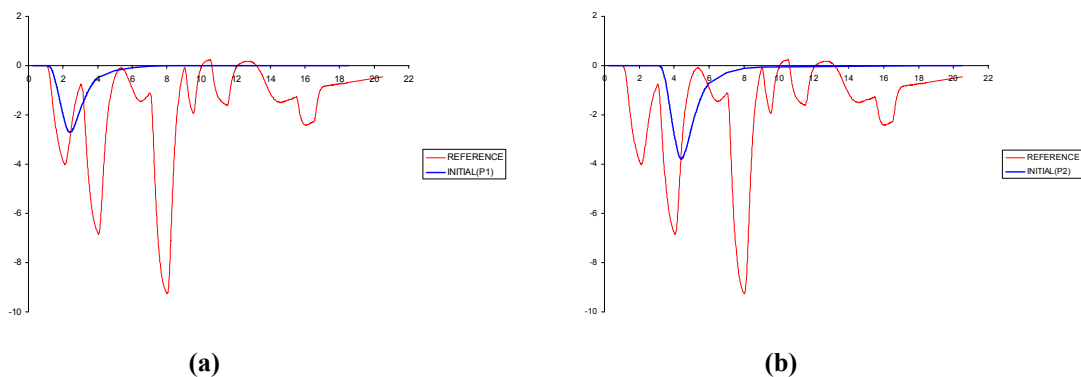(a) Well pressure   (b) Time derivative of well pressure

Fig. 3.8 Reference model pressure response from monitoring well (I1)

The history matching approach starts with the decomposition of multiple well tests into single tests. In other words, we deal with eight separate single well tests instead of multiple well tests in the same flow simulation. This decomposition of the pressure responses provides several advantages. First, it is convenient to investigate each pressure response without any interference from the other well tests because it is difficult to detect and distinguish peak arrival time of each test when multiple test responses are observed from a single flow simulation. The other advantage is that we can approximate the trajectory of the pressure front with streamlines in the case of single well testing only as discussed in previous sections. **Figs. 3.10a** through 3.10h show the time derivatives of pressure for the decomposed single well tests. Differences in the peak arrival time of each decomposed tests and the reference peak arrival times are data misfits for the inversion as described in Eq. 3.15.

(a) Well pressure   (b) Time derivative of well pressure
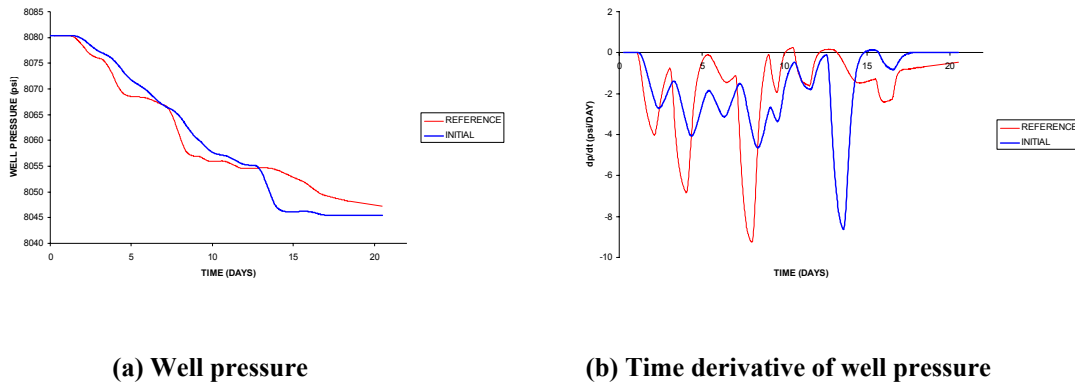
Fig. 3.9 Initial model pressure response from monitoring well (I1)

In order to obtain sensitivity coefficients of the local parameters such as permeability, the computation of the pressure front trajectory is essential. Because multiple test responses are decomposed into separate single tests, we approximate the pressure front trajectory with streamlines which can be easily calculated with little computational expense after the finite difference simulation. Thus, sensitivity coefficients are computed from Eq. 3.16 with streamlines at the last time step to make sure that the streamline profile is stabilized (Kulkani et al., 2001).

(a)   (b)

Fig. 3.10 Time derivative of pressure response decomposed by separate well testing (Initial model)
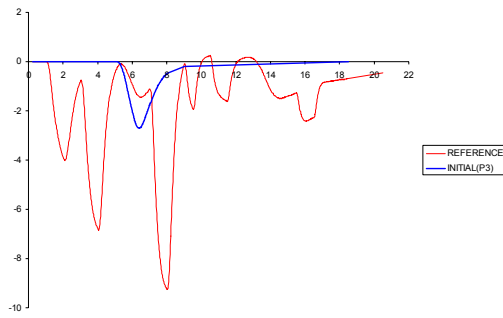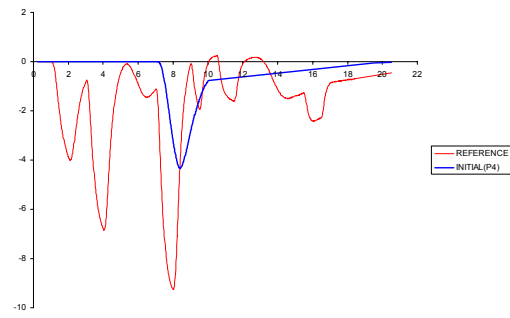
(c)   (d)
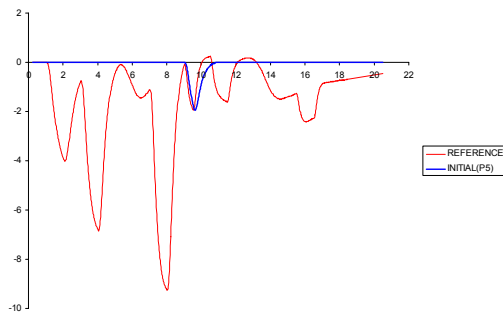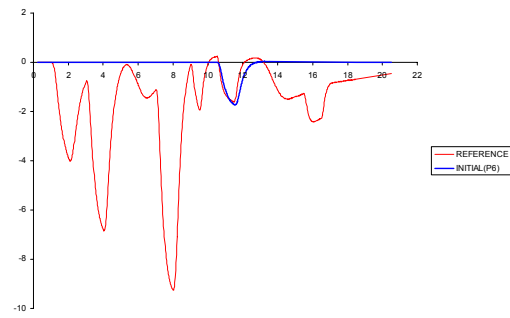
(e)   (f)
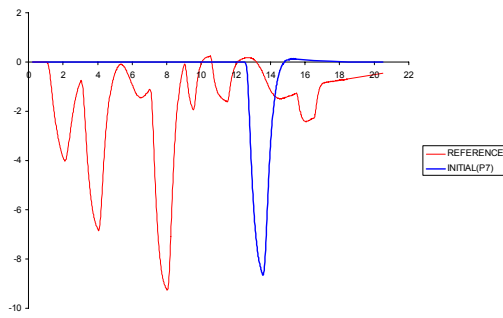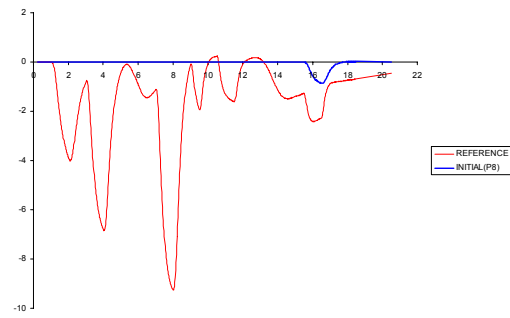
(g)   (h)

Fig. 3.10 Continued

The calibrated permeability field is able to capture large scale characteristics of
the reference model as shown in **Fig. 3.11a**. Monitoring well pressure and its time
derivative is shown in Figs. 3.11b and 3.11c. Basically, our history matching approach is

carried out using the time derivative of the monitoring well pressure. In other words, inversion scheme works to align the peak arrival time of the monitoring pressure rather than matching directly monitoring pressure itself in Fig. 3.11b. Matching the peak arrival time of pressure (Fig. 3.11c), however, results in a considerable improvement of well monitoring pressure.
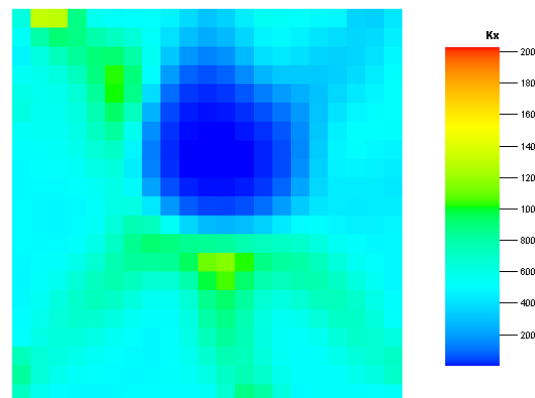
(a) Updated permeability field
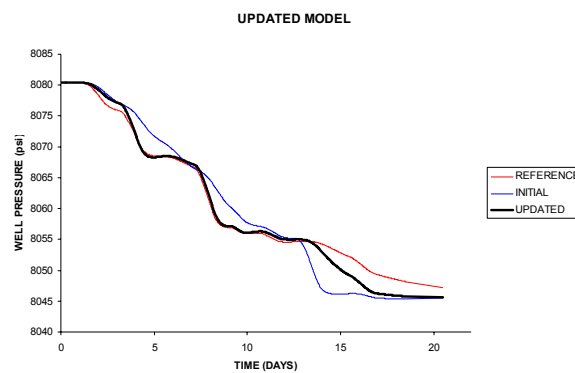
(b) Well pressure

Fig. 3.11 Updated permeability field and its pressure response

UPDATED MODEL

(c) Time derivative of well pressure
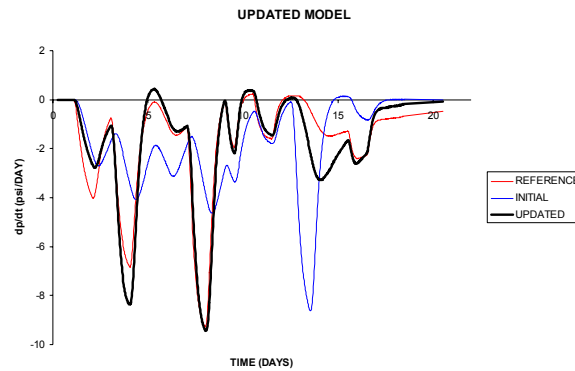
Fig. 3.11 Continued

3.3.2. Field Example

In this section, the application of this technique to field measured pressure transient data is described. The data comes from a multiwell interference test performed in a field in the Middle East. Pressure data from permanent downhole gauges (PDG) in multiple wells are utilized to determine the communication between wells in the reservoir and to derive quantitative information about the permeability distribution to potentially optimize the design of a miscible gas flood.
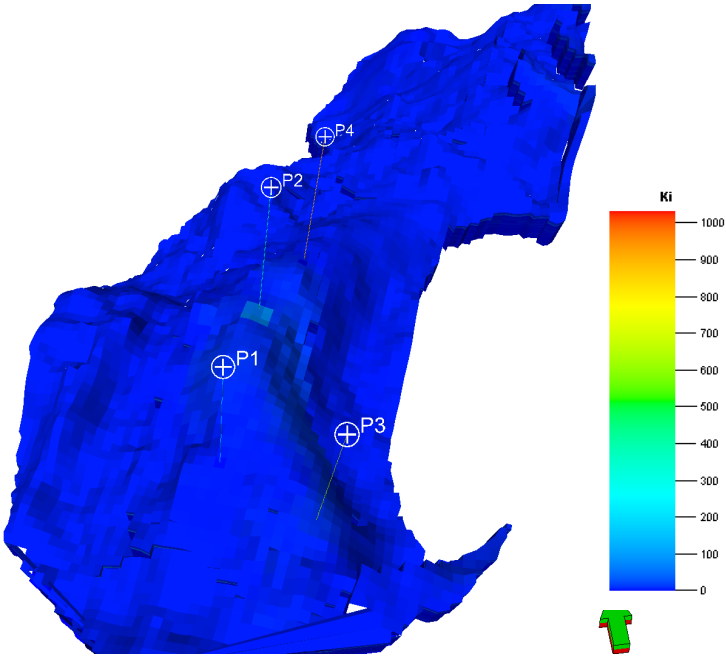
Fig. 3.12 Overview of field example geologic model and well location

A map of the geologic model permeability field and well locations are shown in **Fig. 3.12**. The geologic model consists of about 170,000 grid blocks and has 26 layers. This example has four producing wells and each well has undergone transient pressure testing as shown in **Fig. 3.13**. Pressure data is monitored from PDG during multiwell testing. Note that interference pressure data was monitored continuously only for well 'P2' (Fig. 3.13b) and this is the data that will be used for geologic model calibration.
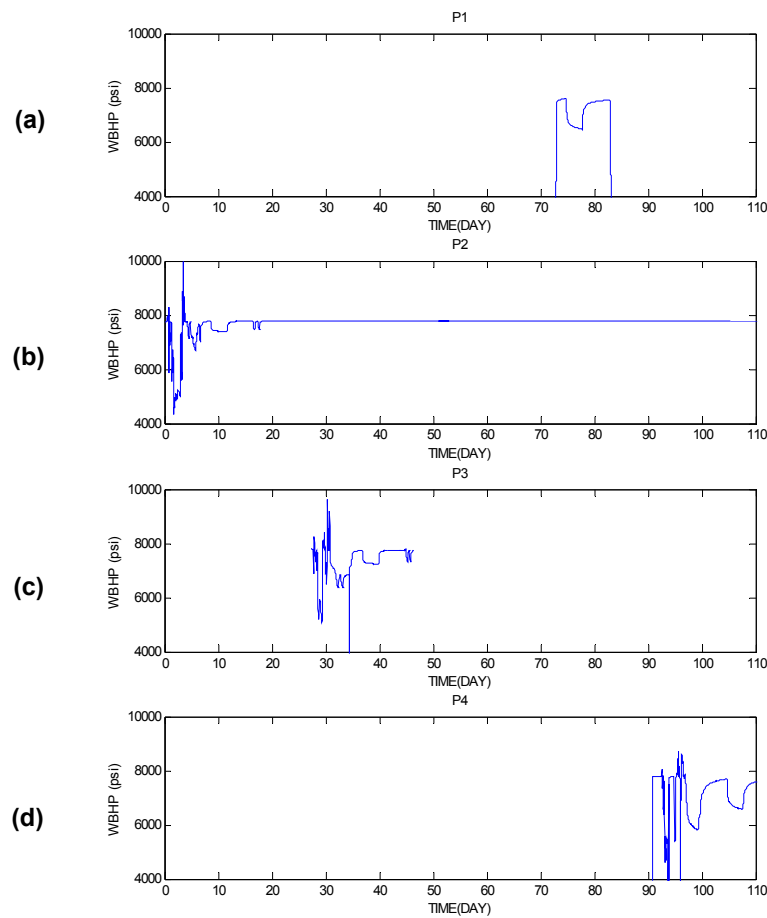
Fig. 3.13 Observed well pressure
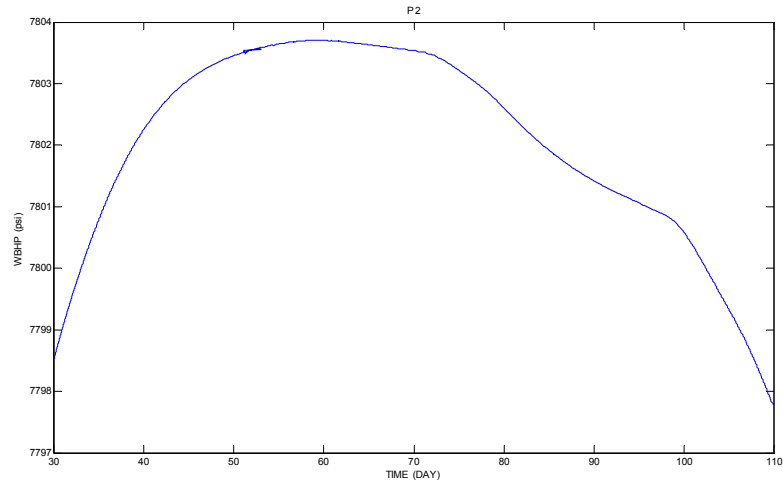
(a) Well pressure (P2)

(b) Time derivative of well pressure (P2)

Fig. 3.14 Detailed observed well pressure (P2)

MONITORING WELL PRESSURE (P2)

(a) Well pressure (P2)

TIME DERIVATIVE OF PRESSURE
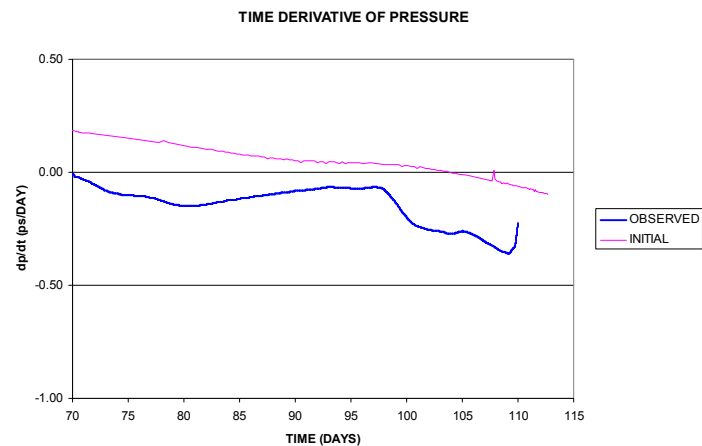
(b) Time derivative of well pressure (P2)

Fig. 3.15 Initial model response (P2)

Fig. 3.14a shows the detailed pressure response from well 'P2' and Fig. 3.14b shows the time derivative of the well pressure response. From the pressure derivative plot, we could not detect the arrival time corresponding to the test in well 'P3' which is the farthest well from the observation well (Fig. 3.12). Arrival times of pressure

corresponding to the testing of well 'P1' and two of testing well 'P4' can be detected in the pressure derivative as shown in Fig. 3.14b. Of these three times, the first arrival time corresponds to well 'P1' testing and the second and third arrival time corresponds to testing of well 'P4'. None of these arrivals can be attributed to well 'P3' because of the very large time lag (over 40 days) from the testing.

Figs. 3.15a and 3.15b show the pressure response and its time derivative for well 'P2' using the initial permeability field as shown in Fig. 3.12. The simulated and observed histories show significant differences in both monitoring well pressure and its time derivative. We follow the same procedures as in the synthetic example. For our applications, the multiple-testing schedule is decomposed into three of separate single testing events; in other words, the first test is performed in well 'P1' and the second and third tests are conducted in well 'P4'. Then, differences in the diffusive time of flight between the observed and the predicted response and sensitivity coefficients of each well testing data are computed as discussed before.

The initial permeability, the updated permeability field via inversion and the permeability difference obtained after history matching are shown as maps in **Fig. 3.16**. As expected, the permeability changes are located in between interference test wells. Pressure responses and their time derivatives are shown in **Figs. 3.17a** and 3.17b. The well pressure responses from the observed history and those from calculated results show a good match (Fig. 3.17a). Also, the pressure front arrival time of observed history and simulated result are aligned (Fig. 3.17b) after inversion. It is worth pointing out that even though the history matching process has been conducted in only part of the simulation time because of the availability of the observed peak arrival time of pressure (70 ~ 110 days), the pressure history match for the entire simulation, especially at the early times shows significant improvement as shown in **Fig. 3.18**.

LAYER

LAYER

LAYER

LAYER

LAYER

Figure

(a) Initial model   **(b) Updated model**   **(c) Difference between (a) and (b)**

LAYER 1
LAYER 3
LAYER 5
LAYER 7
LAYER 14
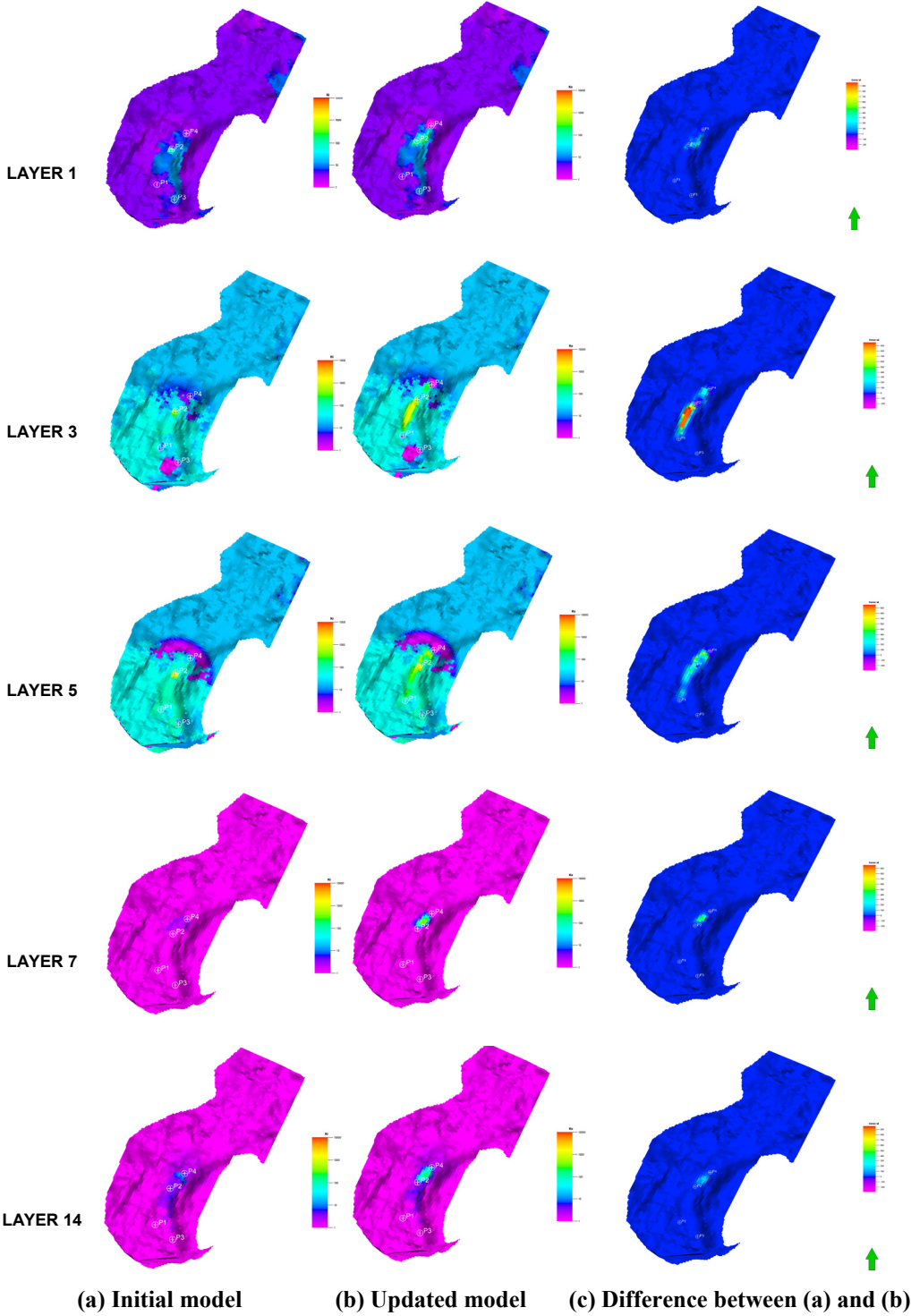
Fig. 3.16 Permeability field of selected layers

MONITORING WELL PRESSURE (P2)

(a) Well pressure (P2)

TIME DERIVATIVE OF PRESSURE

(b) Time derivative of well pressure (P2)
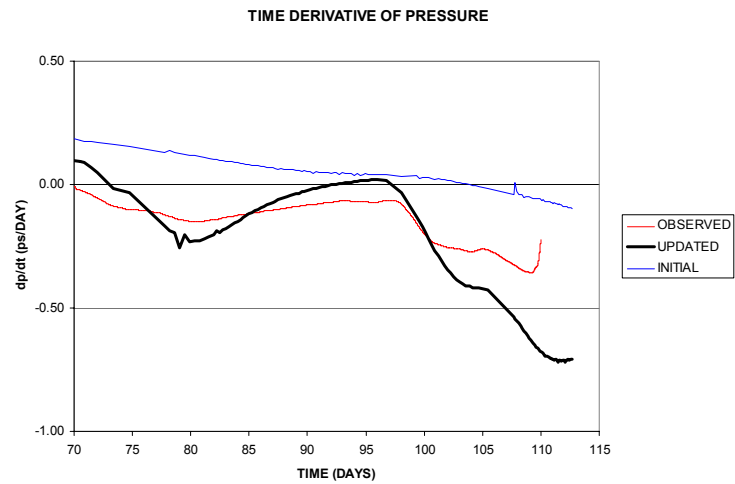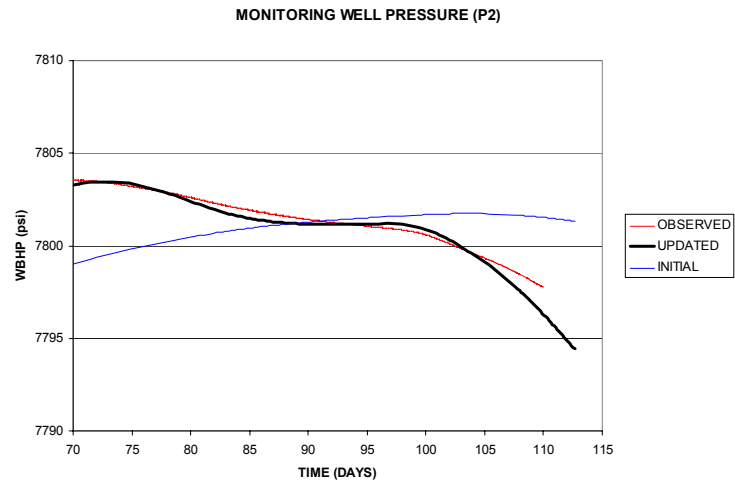
Fig. 3.17 Updated model response (P2)
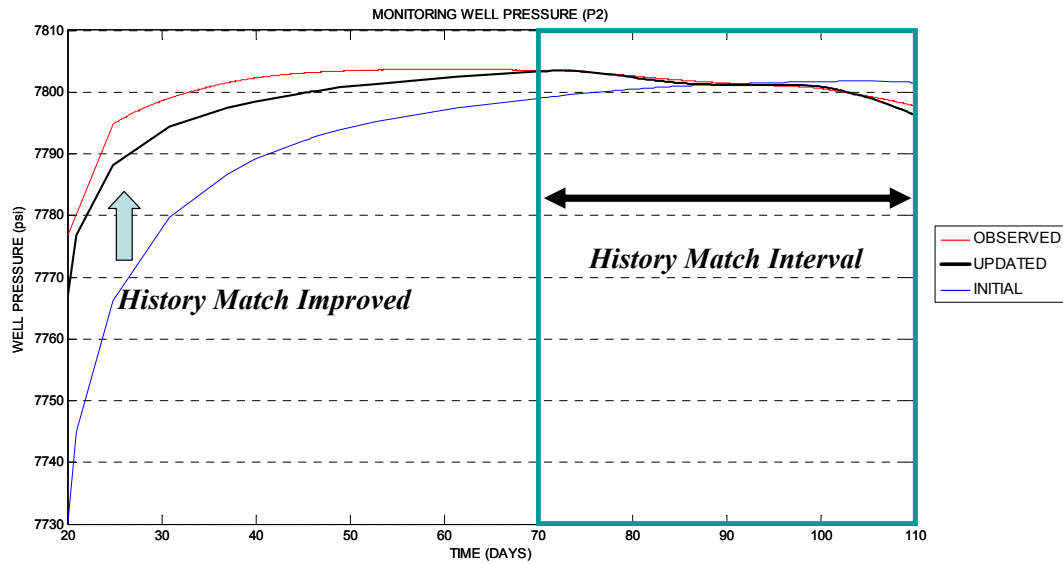
Fig. 3.18 Updated model overall response (P2)

3.4. Chapter Summary

1. We have presented the application of an approach for calibration of geologic models using transient well pressure behavior via high frequency asymptotic solution of the transient pressure equation and an arrival time inversion of the pressure wave front. The approach is computationally efficient because the arrival time sensitivities can be computed analytically using a single flow simulation.

2. The asymptotic solution of the transient pressure equation is defined along trajectories which are ray paths of the wave equation. We have made a comparison of the pressure trajectories and streamlines and showed that for practical applications, these trajectories can be approximated by streamlines after stabilization of the pressure field. This is important because streamlines can be computed much more efficiently compared to pressure trajectories. The sensitivities are then approximated as 1-D integral along streamlines.

3. We have showed that for model calibration purposes, a sequence of multiwell pressure interference tests can be decomposed a series of individual tests with single active well. This significantly facilitates the trajectory computations and the identification of the pressure wave front arrival times.

4. We have demonstrated the power and applicability of the model calibration approach using both synthetic and field examples. The field application with monitoring pressure data from permanent downhole gauges (PDG) shows the ability of the algorithm to analyze complex field tests and the role of interference tests in updating geologic models. Because pressure interference response is likely to be much faster compared to tracer tests, it is a very valuable tool for geologic model updating, particularly early in the field life.

CHAPTER IV

CONCLUSIONS AND RECOMMENDATIONS

In this work, we have investigated approaches to the dynamic data integration. It mainly consists of two parts; dual scale inversion approach and transient pressure data history matching. In chapter 2, we built the overall work flow of the dual scale inversion technique with 'optimal' coarsening algorithm and validated it with synthetic and field examples. Since less number of model parameters is involved in the coarse-scale inversion process, local minima and ill-posedness issues problem can be resolved easier than the direct fine-scale approach. As a result, the objective function of inversion problem will reduce quickly.

In chapter 3, we examined the behavior of transient pressure data with an asymptotic approach to the diffusivity formulation. We, then, investigated the methodology for computation of the pressure front trajectory and suggested the decomposition of multiple-testing condition to separate single testing condition for model calibration purpose. Finally, we demonstrated the transient pressure history matching examples in the synthetic and field cases.

Streamline can be calculated easily with a rigorous streamline tracing algorithm (DESTINY) developed by Texas A&M University even in case that the geometry of geologic model is complex, in other words, corner point geometry system, and has non-neighbor connection to represent faulted system. Detailed description of DESTINY will be covered in Appendix A. On balance, availability of streamline makes the trajectory-based history matching technique more appealing.

4.1 Conclusions

Several specific conclusions can be made from this work:

1. A dual scale approach to history matching high resolution geologic models is proposed. In this approach the majority of the history matching is performed on an 'optimally' coarsened model with further refinement, if needed, via a fine-scale inversion.

2. The 'optimal' coarsening using 'slowness' instead of 'velocity' is shown to result in a more conservative coarsening compared to previous works using 'velocity' and is able to honor the features of the initial geologic model.

3. The coarse-scale history matching is computationally efficient because of the significantly reduced number of unknowns during inversion. Furthermore, the scale-decomposition of the inverse problem reduces the ill-posedness and makes the inversion more stable without the need for artificial regularization. At the coarse-scale the inversion encounters fewer local minima and thus it converges faster.

4. We have demonstrated the power and applicability of the dual scale approach using both synthetic and field examples. The synthetic example shows the detailed procedures and benefit of this approach. The field application in a structurally complex turbiditic reservoir shows the ability of the dual scale inversion to preserve important geologic features during history matching.

5. We have presented the application of an approach for calibration of geologic models using transient well pressure behavior via high frequency asymptotic solution of the transient pressure equation and an arrival time inversion of the pressure wave front. The approach is computationally efficient because the arrival time sensitivities can be computed analytically using a single flow simulation.

6. The asymptotic solution of the transient pressure equation is defined along trajectories which are ray paths of the wave equation. We have made a comparison of the pressure trajectories and streamlines and showed that for practical applications, these trajectories can be approximated by streamlines after stabilization of the pressure field. This is important because streamlines can be computed much more efficiently compared to pressure trajectories. The sensitivities are then approximated as 1-D integral along streamlines.

7. We have showed that for model calibration purposes, a sequence of multiwell pressure interference tests can be decomposed a series of individual tests with single active well. This significantly facilitates the trajectory computations and the identification of the pressure wave front arrival times.

8. We have demonstrated the power and applicability of the model calibration approach using both synthetic and field examples. The field application with monitoring pressure data from permanent downhole gauges (PDG) shows the ability of the algorithm to analyze complex field tests and the role of interference tests in updating geologic models. Because pressure interference response is likely to be much faster compared to tracer tests, it is a very valuable tool for geologic model updating, particularly early in the field life.

4.2 Recommendations

In this work, we described the dual scale inversion approach to well production history matching. The coarse-scale inversion process showed the power and applicability in inversion process. Since the coarsening algorithm coarsens geologic model based on the given static geologic model only, the coarse-scale inversion scheme can be applied to other type of reservoir calibration approaches such as the Ensemble Kalman Filter and Markov Chain Monte Carlo simulation. With the coarse-scale approach, given geologic feature, which has significant information from other type of data such as geologic input, petrophysical data and seismic information, can be honored implicitly. In addition, coarse-scale is suit for production data integration because dynamic data from geologic model has low resolution.

NOMENCLATURE

B = between cell variation

d_i = data misfit for i-th dynamic data, i.e. well index

f' = Buckley-Leverett frontal speed

H = total heterogeneity

m_j = model parameter, i.e. permeability, for j-th cell in fine-scale system

m_J = model parameter, i.e. permeability, for J-th cell in coarse-scale system

$n_{i,j,k}$ = weight, bulk volume of cell i, j, k

NX, NY, NZ = dimension of flow simulation model

$p_{i,j,k}$ = upscaling parameter, local slowness, for cell i, j, k

$p^C_{i,j,k}$ = upscaled average of $p_{i,j,k}$

$\bar{p}_{i,j}$ = column average of $p_{i,j,k}$

s = slowness

S_{ij} = sensitivity coefficient regarding i-th dynamic data and j-th cell in fine-scale system

S_{iJ} = sensitivity coefficient regarding i-th dynamic data and J-th cell in coarse-scale system

W = within cell variation

τ = diffusive time of flight

$\hat{\tau}$ = neutral tracer time of flight

v = interstitial velocity

ζ = distance along trajectory

ψ = trajectory

t_{max} = peak arrival time of pressure

α = diffusivity coefficient

REFERENCES

Arridge, S. 1999. Optical tomography in medical imaging. *Inverse Problems* **15** (2): R41-R93.

Brun,B., Gosselin, O., and Barker, J.W. 2004. Use of Prior Information in Gradient-Based History Matching. *SPEJ* **9** (1): 67-78. SPE 66353-PA.

Bunks, C., Saleck, F.M., Zaleski, S. and Chavent, G. 1995. Multiscale seismic waveform inversion. *Geophysics* **60** (5): 1457-1473

Cerveny, V., Molotkov, I.A. and Psensik, I. 1978. *The Ray Method in Seismology.* Prague, Charles University Press.

Cheng, H., Datta-Gupta, A. and He, Z. 2003. A Comparison of Travel-Time and Amplitude Matching for Field-Scale Production Data Integration: Sensitivity, Non-Linearity and Practical Implications. Paper SPE 84570 presented at the SPE Annual Technical Conference and Exhibition, Denver, Colorado, 5-8 October.

Cheng, H., Dehghani, K., and Billiter, T. 2008. A Structured Approach for Probabilistic-Assisted History Matching Using Evolutionary Algorithms: Tengiz Field Applications. Paper SPE 116212 presented at the SPE Annual Technical Conference and Exhibition, Denver, Colorado, 21-24 September.

Cheng, H., Kharghoria, A. and Datta-Gupta, A. 2005. Fast History Matching of Finite-Difference Models Using Streamline-Derived Sensitivities. *SPEREE* **8** (5): 426-436. SPE 89447-PA.

Datta-Gupta, A. and King, M.J. 2007. *Streamline Simulation: Theory and Practice.* Richardson, Texas, Textbook Series, SPE.

Datta-Gupta, A., Kulkarni, K.N., Yoon, S., and Vasco, D.W. 2001. Streamlines, ray tracing and production tomography: generalization to compressible flow. *Pet. Geoscience* **7**: S75-S86.

Devegowda, D., Arroyo-Negrete, E., Datta-Gupta, A. and Douma, S.G. 2007. Efficient and Robust Reservoir Model Updating Using Ensemble Kalman Filter With

Sensitivity-Based Covariance Localization. Paper SPE 106144 presented at the SPE Reservoir Simulation Symposium, The Woodlands, Texas, 26-28 February.

Fatemi, E., Enguist, B. And Osher, S. 1995. Numerical Solution of the High Frequency Asymptotic Expansion of the Scalar Wave Equation. *J. of Computational Physics* **120**: 145-155.

Gordon, R. and Herman, G.T. 1974. Three Dimensional Reconstruction from Projections: A Review of Algorithms. *Intl. Review of Cytology* **36** (12): 3447-3465.

Grimstad, A., Mannseth, T., Aanonsen, S.I., Aavatsmark, I., Cominelli, A. and Mantica, S. 2004. Identification of Unknown Permeability Trends From History Matching of Production Data. *SPEJ* **9** (4): 419-428. SPE 77485-PA.

He, Z., Yoon, S. and Datta-Gupta, A. 2002. Streamline-Based Production Data Integration with Gravity and Changing Field Conditions. *SPEJ* **7** (4): 423-436. SPE 81208-PA.

Hohl, D., Jimenez, E.A. and Datta-Gupta, A. 2006. Field Experiences with History Matching an Offshore Turbiditic Reservoir Using Inverse Modeling. Paper SPE 101983 presented at the SPE Annual Technical Conference and Exhibition, San Antonio, Texas, 24-27 September.

Hosseini, S.A. and Kelkar, M. 2008. Analytical Upgridding Method to Preserve Dynamic Flow Behavior. Paper SPE 116113, presented at the SPE Annual Technical Conference and Exhibition, Denver, Colorado, 21-24 September.

Iyer, H.M. and Hirahara, K. 1993. *Seismic Tomography: Theory and Practice.* New York, Chapman and Hall.

Jimenez, E., Sabir, K. and Datta-Gupta, A. 2007. Spatial Error and Convergence in Streamline Simulation. *SPEREE* **10** (3): 221-232. SPE 92873-PA.

Kim, J.U. and Datta-Gupta, A. 2009. A Dual Scale Approach to Production Data Integration into High Resolution Geologic Models. Paper SPE 118950 presented at the SPE Reservoir Simulation Symposium, The Woodlands, Texas, 2-4 February.

King, M.J., Burn, K.S., Wang, P., Muralidharan, V., Alvardo, F., Ma, X. and Datta-Gupta, A. 2005. Optimal Coarsening of 3D Reservoir Models for Flow Simulation. Paper SPE 95759 presented at the SPE Annual Technical Conference and Exhibition, Dallas, Texas, 9-12 October.

Kline, M. and Kay, I.W. 1965. *Electromagnetic Theory and Geometrical Optics.* New York, John Wiley and Sons.

Kravtsov, Y.A. and Orlov, Y.I. 1990. *Geometrical Optics of Inhomogeneous Media.* New York, Springer-Verlag.

Kreyszig Erwin 1993. *Advanced Engineering Mathematics.7th Edition*, New York, John Wiley & Sons, Inc.

Kulkarni, K.N., Datta-Gupta, A. and Vasco, D.W. 2001. A Streamline Approach for Integrating Transient Pressure Data Into High-Resolution Reservoir Models. *SPEJ* **6** (3): 273-282. SPE 74135-PA.

Luneburg, R.K. 1966. *Mathematical Theory of Optics.* Berkeley, California, University of California Press.

Ma, X. 2008. History Matching and Uncertainty Quantification Using Sampling Method. PhD dissertation, Texas A&M U. College Station, Texas.

Oliver, D.S., Reynolds, A.C. and Liu, Ning. 2008. *Inverse Theory for Petroleum Reservoir Characterization and History Matching.* New York, Cambridge U. Press.

Oyerinde, A., Datta-Gupta, A. and Milliken, W. 2007. Experiences With Streamline-Based Three-phase History Matching. Paper SPE 109964, presented at the SPE Annual Technical Conference and Exhibition, Anaheim, California, 11-14 November.

Paige, C.C. and Saunders, M.A. 1982. LSQR: An Algorithm for Sparse Linear Equations and Sparse Least Squares. *ACM Trans. Math. Software* **8** (1): 43-71

Quenes, A., Bhagavan, S., Bunge, P.H. and Travis, B.J. 1994. Application of Simulated Annealing and Other Global Optimization Methods to Reservoir Description:

Myth and Realities. Paper SPE 28415, presented at the SPE Annual Technical Conference and Exhibition, New Orleans, Louisiana, 25-28 September.

Sethian, J.A. 1996. *Level Set Method.* New York, Cambridge University Press.

Stenerud, V.R., Kippe, V., Lie, K. and Datta-Gupta, A. 2008. Adaptive Multiscale Streamline Simulation and Inversion for High-Resolution Geomodels. *SPEJ* **13** (1): 99-111. SPE 106228-PA.

Talbert, M., Ma, X. and Datta-Gupta, A. 2008. Upgridding 3-D Geologic Models in a Channel-type Environment. Paper SPE 113245 presented at the 2008 Indian Oil and Gas Technical Conference and Exhibition, Mumbai, India, 4-6 March.

Tarantola, A. 2005. *Inverse Problem Theory and Methods for Model Parameter Estimation.* Philadelphia, Pennsylvania, The Soc. for Industrial and Applied Mathematics.

Vasco, D.W. and Datta-Gupta, A. 1999. Asymptotic Solutions for Solute Transport. *Water Resources Research* **35** (1): 1-16.

Vasco, D.W. and Datta-Gupta, A. 2001. Asymptotics, Saturation Fronts and High Resolution Reservoir Characterization. *Transport in Porous Media* **42**: 315-350.

Vasco, D.W. and Finsterle, S. 2004. Numerical Trajectory Calculations for the Efficient Inversion of Transient Flow and Tracer Observations. *Water Resources Research* **40** W01507, DOI:10.1029/2003WR002362.

Vasco, D.W., Keer, H. and Karasaki, K. 2000. Estimation of Reservoir Properties Using Transient Pressure Data: An Asymptotic Approach. *Water Resources Research* **36** (12): 3447-3465.

Vasco, D.W., Yoon, S. and Datta-Gupta, A. 1999. Integrating Dynamic Data into High-Resolution Reservoir Models Using Streamline-Based Analytic Sensitivity Coefficients. *SPEJ* **4** (4): 389-399. SPE 59253-PA.

Yoon, S., Malallah, A.H., Datta-Gupta, A., Vasco, D.W. and Behrens, R.A. 2001. A Multiscale Approach to Production-data Integration Using Streamline Models. *SPEJ* **6** (2): 182-192. SPE 71313-PA.

APPENDIX A

RIGOROUS STREAMLINE TRACING AND ASSISTED PRODUCTION HISTORY MATCHING ALGORITHM (DESTINY)

Robust streamline tracing and assisted production history matching algorithm (DESTINY) has been developed. In this appendix, we will investigate the overview, objectives and key new features of DESTINY. They are, then, followed by procedure of installation, how to set the interface file and finally example of streamline tracing and generalized travel time (GTT) inversion.

A.1. Overview of DESTINY

The key component of the dual scale inversion technique and the transient pressure history matching which are covered in chapter 2 and 3 is the computation of streamline trajectory and the time of flight. DESTINY is designed to compute the streamline trajectory and the time of flight from finite difference simulator. **Fig. A.1** shows the overall work flow of streamline tracing and production history matching. Note that the description in this appendix is based on only ECLIPSE100 developed by Schlumberger for the simplicity of documentation although DESTINY has been interfaced to several commercial and in-house simulators such as VIP, E300 (black oil mode), MORES etc.

A.1.1. Objectives

The streamline provides several benefits in reservoir engineering section. First, it is a useful tool to check reservoir management. It can visualize the connectivity and the communication among wells or between well and aquifer. Second, sensitivity coefficient of local parameter can be computed easily from the streamline trajectory and the time of

flight. This point is quite obvious when it is compared with other inversion techniques, for instance, perturbation or adjoint state method (Cheng et al., 2008). Finally, it can be incorporated in stochastic history matching approach such as the covariance localization in the Ensemble Kalman Filter approach (Devegowda et al., 2007) or 2-stage Markov Chain Monte Carlo (MCMC) technique (Ma, 2008).

The main objectives of DESTINY are to trace streamline even in complex corner point and faulted (non-neighbor connection) geometry as well as the sensitivity coefficient computation of generalized travel time inversion (He et al., 2002; Cheng et al., 2005; Oyerinde et al., 2007).
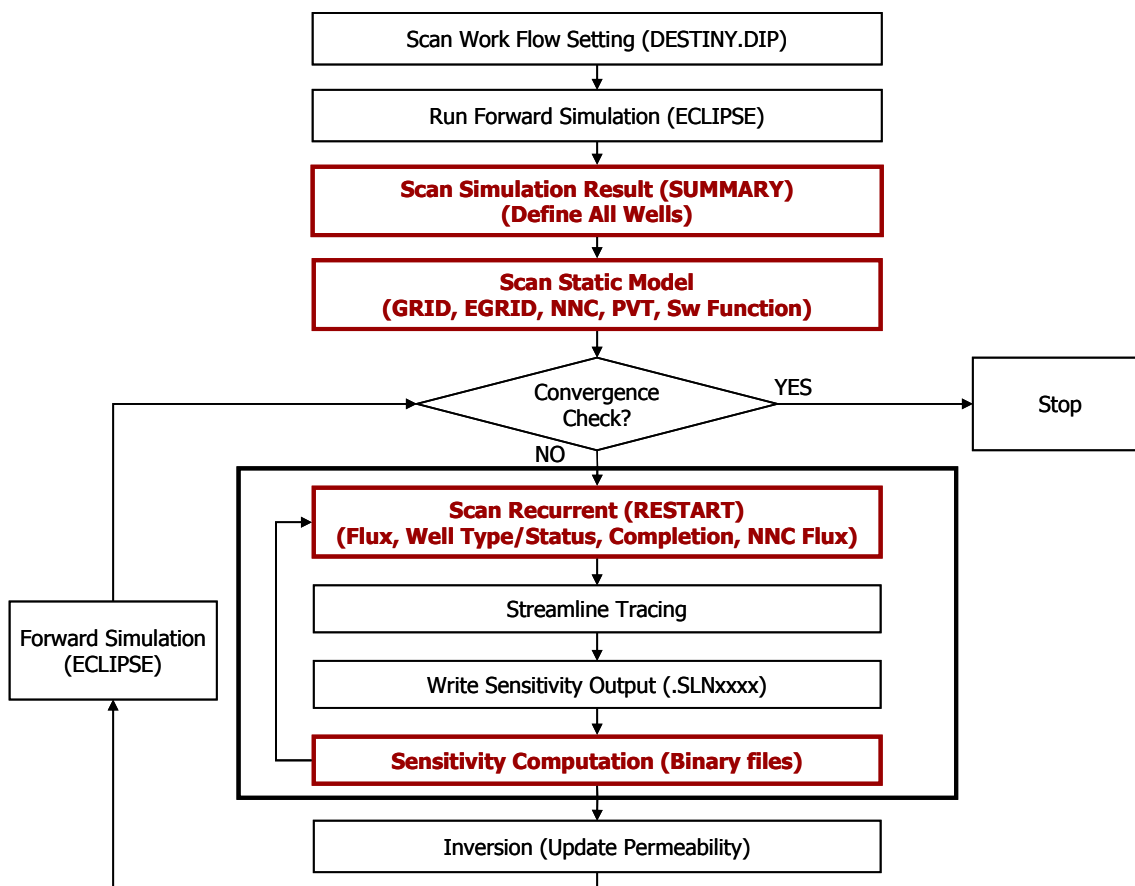

Fig. A.1 Overall of flow chart of DESTINY

A.1.2. Key New Features

The previous version (Jimenez et al., 2007) was designed to obtain input information from files made by user. User needed to prepare the geometry data, the schedule data for completion and observed history data. Commercial simulator such as ECLIPSE, however, has much of flexibility to describe the flow simulation model. It requires huge amount of coding to catch up with all of flexibility. Instead of scanning input information made by user, DESTINY scans necessary data to trace streamline from output files from simulator. It enables user to utilize full of flexibility for description of flow simulation model and also helps robust streamline tracing because the format of simulation output files is always fixed.

A.1.2.1. Geometry Data Input

For the purpose of tracing streamline, we need two of necessary information; one is geometry data and the other is flux or velocity data. After flow simulation, simulator generates the grid file (*.GRID*) with general corner point geometry system. DESTINY scans the grid file to extract geometry information automatically.

A.1.2.2. Schedule Data Input

Schedule data includes two of important information in view of streamline tracing. One is the completion data and the other is observed history for history matching application. The completion data is a kind of dynamic information, in other words, it can change during full simulation time because of infill drilling, re-completion and switching from producer to injector etc. The restart files of simulator (*.X0001, *.X0001* etc.) contain the completion information. They also include well type and well status (*OPEN/SHUT*). DESTINY scans these data and decides starting and ending location of streamlines.

A.1.2.3. Well Performance Data

In order to integrate production data to flow simulation model via history matching, we need to compute the difference of observed history and simulated result. These information is available in the summary files (*.S0001, *.S0002 etc). When we describe the field history in flow simulation model, the keyword of *WCONHIST* will be used typically. In this case, DESTINY can scan observed history from the summary files. Then, it calculates the discrepancy of the observed history and simulated result.

A.1.2.4. Robust Streamline Tracing under Non-Neighbor Connection

There was a technical issue of tracing streamline in faulted geometry, what is called, non-neighbor connection (NNC). By design, ECLIPSE does not report the natural indexing NNC. The meaning of the natural indexing NNC is that two grid blocks with consecutive indexes are adjacent to each other but they are in NNC. To trace streamlines in faulted geometry, all of NNC information including natural indexing NNC and NNC flux are required. The natural indexing NNC is detected and recognized from geometry data, specifically, from the discrepancy of z-coordinate value of each grid.

A.1.2.5. Object-Oriented Programming

For the management and the future development of DESTINY, it has been re-organized to be more object-oriented. With this feature, we can add the new functionality or interface to other type of finite simulator easily. It helps also clear the memory leakage problem which will be discussed next section.

A.1.2.6. Memory Leakage Issue

Though it is quite related to programming not to reservoir engineering, when the huge field case is applied, it needs to be considered. Now DESTINY is improved in this regard by object-orientation modulation and by using built-in standard library in C++ complier.

A.1.3. Important Items Regarding Setting up ECLIPSE Deck for DESTINY

Several items which user needs to keep in mind will be listed up first. Details of setting up DESTINY will be discussed later.

A.1.3.1. Specification of Summary Files

Typically, commercial or in-house simulator has the option for specifying the summer information. The summary data consist of well performance such as the total production amount, production rate of each phase and fractional flow etc. In ECLIPSE case, user can specify the output data in *SUMMARY* section in the input deck. Since DESTINY extracts the list of all well name from the summary specification file, **.SMSPEC*, user needs to specify more than one output at least. For instance, user has to specify in the input deck as following

```
SUMMARY
WWCT /
WWCTH /
```

If the history matching module (i.e. GTT inversion) is applied as described later, it is highly recommended to use *WCONHIST* instead of *WCONPROD* in the *SCHEDULE* section. Then, DESTINY will extract the observed well production history

from *SUMMARY* file automatically. In this specific case, user is advised to include *WWCTH* also in *SUMMARY* specification as shown the example above.

A.1.3.2. Setting up the Reporting *SUMMARY/RESTART* Output Files

Since tracing streamline relies fully on the output of the external finite difference simulator, user needs to set the option of reporting output in the input deck correctly. At the current version, DESTINY expects the output files such as **.S0001, *.X0002*, in the binary format at each simulation time step and these files should be separate not unified (i.e. **.UNSMRY, *.UNRST*). Here are the key specifications of the output files from simulator.

- **Binary Format Not Ascii Format**
- **Separates File Not Unified File**
- **Report at Each Simulation Time Step**

Destiny reads the restart files to allocate the fluxes needed to trace the streamlines. User can specify these conditions with the following setting.

```
RPTSOL
RESTART=2 /

RPTRST
'BASIC=3' FREQ=1 FLOWS PRESSURE ALLPROPS /
```

'BASIC=3': restart files are created every nth report time with frequency "FREQ=n"

FREQ=1

FLOWS: Output of inter-block flows

PRESSURE: Output of grid block pressures

ALLPROPS: output includes fluid densities, viscosities, formation volume factors, and phase relative permeabilities

A.1.3.3. What User Needs to Avoid in ECLIPSE

Since commercial simulator has tremendous flexibility to describe all kinds of field situations, several options in ECLIPSE are not acceptable and causes failure in tracing streamlines. Those are listed up below

- **Local Grid Refinement**
- **Well Located in Non-Neighbor Connection**

Unfortunately, the current version of DESTINY is not able to handle those condition, so user needs to make sure to avoid them.

A.2. Compilation and Running of DESTINY

A.2.1. Creating a DESTINY Workspace

The DESTINY distribution consists of a C++ source code (*.h and *.cpp files) and two synthetic decks to run the application using ECLIPSE as forward simulator. After unzipping the distribution a folder called *..DESTINY/* should be available. There will be two sub-folders *..DESTINY\APPLICATIONS* and *..DESTINY\DESTINYS*, which contains the input decks and source code to run the application. The compiler used for DESTINY development is Microsoft Visual Studio 2005 in WINDOWS system. However, different compiler and operating system such as g++ in LINUX system was tested successfully with minor changes. The default environment of compiler and system is Microsoft Visual Studio 2005 in WINDOWS

The first step is to create a workspace under your C++ compiler. Go to *File→New→Project* provide *DESTINYM* as project name and select the parameters as shown in the following screen,
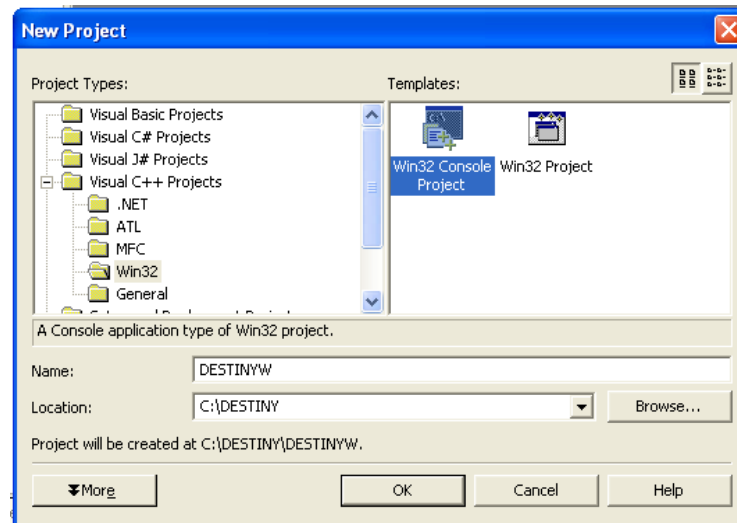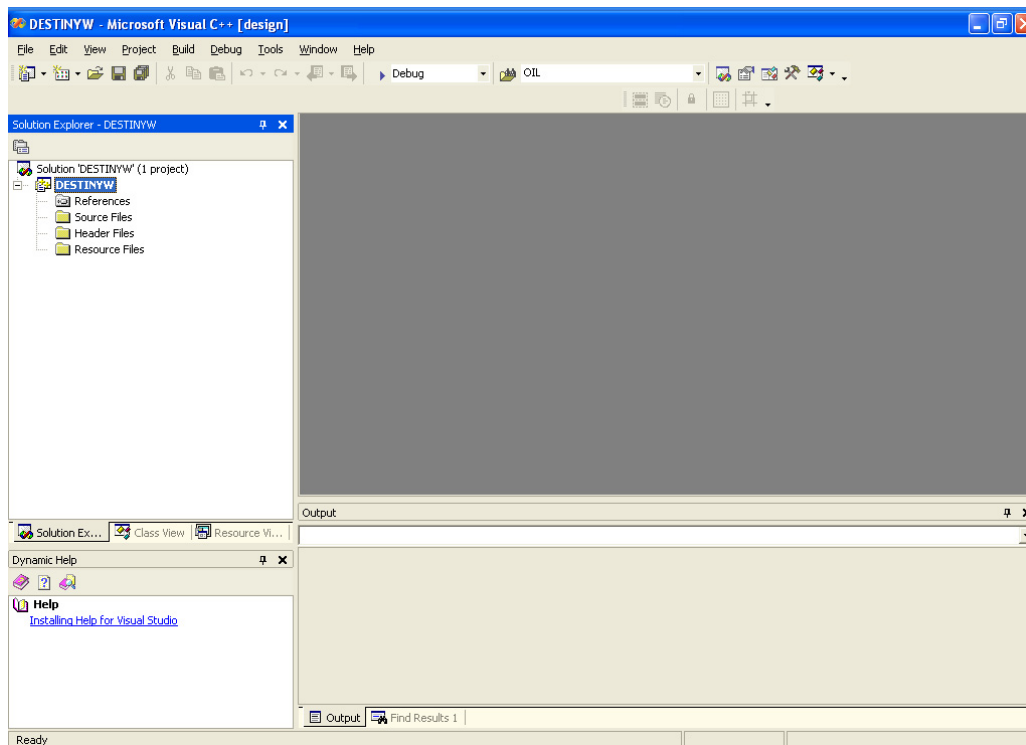

Fig. A.2 New Project on Visual Studio

After pressing *OK* the *Win32 Application Wizard* panel will appear, click on *Application Settings* and select the settings as shown in the following screen,
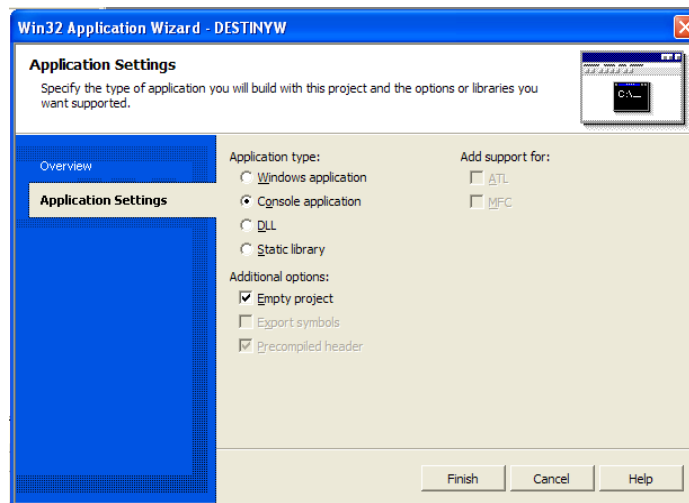
Fig. A.3 Application Settings Visual Studio

After pressing *Finish* you should have an empty workspace that should look like,

Fig. A.4 Empty Workspace in Visual Studio

Go to *Project→Add existing Items* and from *..DESTINY\DESTINYS* add all source files. From the *Solution Explorer* double click the file *DESTINY3.cpp*; this is the main program file where all input objects/data are loaded to DESTINY. You are now in position to build the entire DESTINY workspace; go to *Build→Build DESTINYW* and the compiler will generate the executable and all **.obj* files.

A.2.2. Running DESTINY

There are several ways to run DESTINY; the simplest one is just copying the executable *../DESTINY/DESTINYW/DEBUG/DESTINYW.exe* to the folder where the *DESTINY* input deck lives. However, sometimes it will be required to run the application from the compiler or the command line in order to check the performance of the tracing

and inversion. This could the case if an error on the input is detected, or an unexpected tracing/inversion error occurs.

By default DESTINY reports results on execution sequences after each major operation is done. The user will always get comments whether the operations are successful or unsuccessful. These comments are vital to solve any execution error and the user should always have them available. If the user is running DESTINY for the first time and he/she is not familiar with C++ compilers, it is recommended to follow the guidelines under command line execution. C++ users could report the specific functions, classes, stack status or any reporting features available while debugging.

A.2.2.1. Running from the Command Line.

This is a very helpful and easy way of running DESTINY; in this running mode a log file will be created to track the application execution sequence. Open a command prompt window and go the folder where the *DESTINY* input deck lives. Make sure you have the executable under the same folder and on the command line write *DESTINYW.exe -> DESTINY.LOG* (as shown on the snapshot). This system call will create a file with the entire DESTINY command line output.

Fig. A.5 Running DESTINY on command line

A.2.2.2. Running from compiler.

The first thing to do is ensuring that your compiler working directory is set to the same folder where the *DESTINY* input deck lives. Go to *Project→DESTINYW Properties* and under the *Debugging* panel choose the proper working directory (as shown in the following snapshot)
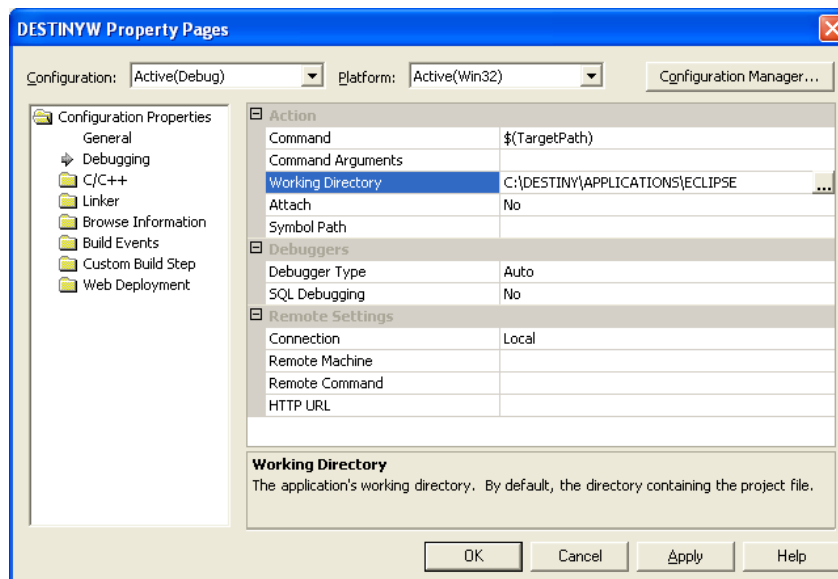
Fig. A.6 Running DESTINY from the Debug Mode Visual Studio

You can now go to *Debug→Start* and use the compiler to track the details of *DESTINY* execution.

A.3. DESTINY Input Deck

Basically, any DESTINY input deck requires the following information:

- Grid Properties
- Simulator Settings
- Tracing and Inversion Settings

The previous information must be defined in a single file called *DESTINY.DIP*. All input is handled via keywords that will call specific DESTINY scanning functions. These readers will open the simulator input deck files and will scan and feed *DESTINY* objects with all required information. When providing filenames and directory paths, avoid using special characters (i.e., ! @ # $ % ^ .); this will create reading errors while opening files. The details and a brief description of all these keyword will be presented next.

A.3.1. DIP_DATA_FILE
File with general model information

ALL Users: This keyword defines the file holding the main ECLIPSE input deck. This file will be used to make the system call to run ECLIPSE in batch mode and should have the full ECLIPSE input data structure. DESTINY will look inside this file to read saturation and fluid functions. It will also extract the regions used to associate each PVT and Saturation table for each cell. The following is a list of recognized keywords,

Saturation functions: *SGFN, SGOF, SOF2, SOF3, SWFN* and *SWOF*
PVT functions: *PVCDO, PVCO, PVDG, PVDO, PVTO* and *PVTW*

C++ users: All these properties will be stored under the *CDIPRockFluid* and *CDIPReservoir* class. These properties are required to define mobility and several displacement properties required for tracing and inversion procedures.

Example: *DIP_DATA_FILE*
         C:\DESTINY\APPLICATIONS\ECLIPSE\ECLIPSE.DATA

A.3.2. DIP_PROP_FILE #INT

Files with reservoir grid properties

All Users: This keyword defines the files that hold the reservoir grid properties. The keyword is followed by an integer (*#INT*) on the same line. This integer defines the number of subsequent property files names to be stored. For each property file there must be a preceding line defining the selected simulator property convention (*SCALAR_ECLIPSE_TYPE*). These file names will be used to overwrite the updated grid properties during inversion process. DESTINY will scan the grid property from **.INIT* file not from these files directly. The only required properties under this record are porosity and permeability. Porosity will be used in time of flight calculations and permeability on the inversion updates.

C++ users: All defined static properties will be stored under the *m_vStatic* member of the *CDIPGridCPG* class. Any grid associated property can be defined with these set of keywords and used in any part of the code.

> *Example: DIP_PROP_FILES 2*
>   *SCALAR_ECLIPSE_TYPE*
>   *C:\DESTINY\APPLICATIONS\ECLIPSE\PERMX.GRDECL*
>   *SCALAR_ECLIPSE_TYPE*
>   *C:\DESTINY\APPLICATIONS\ECLIPSE\PORO.GRDECL*

A.3.3. General DESTINY Settings

A.3.3.1. DIP_STREAMLINE_NUM
Number of Streamlines and output

All Users: The keyword is followed by a line with two records. The records are defined as follows,

1st INTEGER	Number of Streamlines to be used
2nd BOOLEAN	Defines if output files with streamlines is desired. The default streamline output in DESTINY satisfies binary FLOVIZ/PETREL formats

> *Example:*   *DIP_STREAMLINE_NUM*
>   *500*   *TRUE*

A.3.3.2. DIP_FORWARD_SIMULATOR
Defines simulator to be used

All Users: The keyword is followed by a line with three records. The records are defined as follows,

1st STRING	Defines which simulator is to be used for tracing and inversion. DESTINY is interfaced to work with *ECLIPSE/VIP/FRONTSIM* (Use simulator name to select the proper system calls)
2nd BOOLEAN	Defines if utility/debug files are required (*TRUE*:: REMOVE || *FALSE*::KEEP). It is recommended to leave this record as *FALSE*
3rd STRING	Defines which format is used for Summary / Restart files from simulator (*BINARY / ASCII*). Default is *BINARY*.

Example: *DIP_FORWARD_SIMULATOR*
    ECLIPSE   FALSE   BINARY

A.3.3.3. DIP_TRACING_SETTING
Defines setting for tracing

All Users: The keyword is followed by a line with nine records. The records are defined as follows,

1st *STRING*	Phases involved in forward model. This will set DESTINY readers to scan phase fluxes as reported by the selected simulator. Use mnemonics *OIL*, *WAT* and *GAS* in any order followed by *PHASE*
2nd *STRING*	Phases involved in tracing. This will set DESTINY to perform tracing based on single/multi phases. Use mnemonics *OIL*, *WAT* and *GAS* in any order followed by *PROD* if streamlines are starting from producers only. Use mnemonics *OIL*, *WAT* and *GAS* in any order followed by *SINK* if streamlines are starting from any cell.
3rd *STRING*	Defines if we want to *RUN* the forward simulator or not. If *STOP* is selected there must be an available set of restart files following *ECLIPSE* formatting.
4th *STRING*	Defines if tracing is to be done at *(ALL)* schedule dates or at a *(SINGLE)* date.
5th *FLOAT*	If *SINGLE* date tracing is selected in 4th argument, this record sets the schedule date in which tracing is to be done.
6th *STRING*	Sets a flag to request *(ASCII/BINARY)* output from streamlines. No action will be taken when *BINARY* is selected.

7th STRING   Defines if the number of streamlines per completion is defined based on flux *(STCFLUX)* or should be uniformly *(STCUNI)* distributed. Default is defined based on fluxes, even if the keyword is not included in DIP file.

8th STRING   Defines the type tracing to tackle faults and NNC connections. The default in DESTINY for inversion purposes is POLLOCK's construction (POLLOCK/ MODPOLLOCK/LBLJIMENEZ)

9th STRING   Defines the type discretization for tracing. The default in DESTINY is HORIZONTAL. (HORIZONTAL/ VERTICAL/ SQUARE)

10th BOOLEAN   Defines if inversion process is applied (*TRUE*: TRACING ONLY || *FALSE*: INVERSION APPLIED). It is recommended to leave this record as *FALSE*

By default DESTINY considers the total velocity to start tracing streamlines from producers until any source is reached. It is also possible to generate single-phase based streamlines which can either start from the producers or from any cell with a phase fractional flow greater than zero (*SINK* suffix in 2nd keyword). If the *SINK* option is selected an additional set of output files will be generated containing such streamlines. However, history matching module, i.e. GTT, is not available with sink tracing.

By setting the 3rd keyword to *STOP,* DESTINY will not make the system call to run the simulator. This running option is quite handy after running a forward model and generating single/multi phase streamlines is desired.

Example 1:   Two phase model with total flux tracing done from producers, simulator is run and ascii files are generated. The output streamlines will be based in the total flux field
    DIP_TRACING_SETTING

OILWATPHASE   OILWATPROD   RUN   ALL   0   ASCII   STCFLUX
POLLACK   HORIZONTAL   TRUE

Example 2:   *Three phase model with water tracing done only from producers,*
                simulator is not run. The output streamlines will be based only on
                water at producers
        DIP_TRACING_SETTING
        OILGASWATPHASE   WATPROD   STOP   ALL   0   BINARY
STCFLUX LBLJIMENEZ   SQUARE   TRUE

Example 2:   *Three phase model with water tracing done from producers and*
                cells with fractional flow greater than zero. The output will be in
                two files, one containing the streamlines only from the producer;
                the other file will have the streamlines starting from any cell
        DIP_TRACING_SETTING
        OILWATGASPHASE   WATSINK   STOP   ALL   0   BINARY
STCUNI POLLACK   HORIZONTAL   TRUE

A.3.3.4. DIP_SENS_TUNING
Defines setting for sensitivity tuning

All Users: The keyword is followed by four lines with three records on each line. The
records are defined as follows,

1st STRING   When set to *TRUE* sensitivity normalization for
                        equalization of the sensitivities is applied. The normali-
                        zation facilitates the inversion algorithm based on data
                        misfit.

2th STRING   When set to *PERCCUTOFF*, a percentile based cutoff will
                        be applied to *WWCT* sensitivities on a well-basis. It is used

to reduce unusual high and low sensitivity values. Default record is *NONE*

3*th* FLOAT   Defines the lower percentile for the WWCT sensitivity cut-off.

4*th* FLOAT   Defines the upper percentile for the WWCT sensitivity cut-off.

5*th* STRING   When set to *TOFCUTOFF*, a time of flight based cutoff will be applied to *WWCT* sensitivities on a well-basis. Used to eliminate the sensitivities in stagnation region which may cause distort inversion performance. Default record is *NONE*

6*th* FLOAT   Defines the threshold of the time of flight for the WWCT sensitivity cut-off.

Example: *DIP_SENS_TUNING*
        SENSNORM PERCCUTOFF 0.05 0.95 TOFCUTOFF 2000

A.3.3.5. DIP_DATA_MISFIT
Defines misfit tolerance to stop inversion

All Users: The keyword is followed by a line with two records. The records are defined as follows,

1*st* FLOAT   Overall travel time misfit defined along all wells
2*nd* FLOAT   Overall amplitude misfit defined along all wells

These values will be used to stop the inversion whenever the specified tolerance is satisfied.

Example: *DIP_DATA_MISFIT*

-- TIMETOL   WWCTTOL
10.0   0.5

A.3.3.6. DIP_INV_TUNNING

Defines tuning parameters for running LSQR minimization

All Users: The keyword is followed by a line with four records. The records are defined as follows,

1st FLOAT	Number of LSQR iterations
2nd FLOAT	Decrease factor to be applied over the norm and smoothing constraints through iterations.
3rd FLOAT	Maximum weight given to permeability changes at each iteration.
4th FLOAT	Minimum weight given to permeability changes at each iteration.

Example: DIP_INV_TUNNING
30.0   1.0   1.0   1.0

A.3.3.7. DIP_INV_CONSTRAINTS

Defines norm and smoothing constraints to minimize objective function

All Users: The keyword is followed by three lines with three records on each line. The records are defined as follows,

1st FLOAT FLOAT FLOAT	Norm constraint
2nd FLOAT FLOAT *FLOAT*	Horizontal smoothing constraint
3rd FLOAT FLOAT FLOAT	Vertical smoothing constraint

The inversion constraints on this version of *DESTINY* are only meant to update permeability. Only the first values on each line will be considered during the minimization of the objective function. The other values are reserved for further development when integrating additional reservoir parameters.

> *Example:*   *DIP_INV_CONSTRAINTS*
>> *-- DAMPING1 DAMPING2 DAMPING3*
>>> *1.0   0.0   0.0*
>> *-- HSMOOTH1 HSMOOTH2 HSMOOTH3*
>>> *0.8   0.0   0.0*
>> *-- VSMOOTH1 VSMOOTH2 VSMOOTH3*
>>> *0.0   0.0   0.0*

A.3.3.8. DIP_INV_INTEGRATION #INT
Defines type of production data integration

All Users: The keyword is followed by an integer (*#INT*). This integer defines the number of subsequent lines to be scanned. The records are defined as follows,

    1st STRING   String to integrate production water-cut (WWCT)

This version of *DESTINY* is enabled to integrate production water-cut. The gas oil ratio integration is under current development. The new development will be able to perform either single or joint production integration.

> *Example:*   *DIP_INV_INTEGRATION 1*
>> *WWCT*

A.3.3.9. DIP_INV_SETTING
Defines setting for inversion

All Users: The keyword is followed by a line with ten records. The records are defined as follows,

1st *INTEGER* — Number of single travel time iterations. Whenever this number is greater than zero the 4rd record must be set to *TRUE*

2nd *INTEGER* — Number of generalized travel time iterations. By default single travel time iterations will be run first.

3rd *INTEGER* — Number of amplitude history match iterations.

4th *BOOLEAN* — Boolean to enable single travel time sensitivity calculations. Must be set to TRUE whenever 1st record is greater than zero.

5th *FLOAT* — This is the *WWCT* value selected for single travel time misfit evaluation. At every producing well, whenever the *WWCT* reaches this value both simulated and observed times will be extracted and used for misfit and sensitivity calculations.

6th *BOOLEAN* — This Boolean sets a flag for printing ASCII files with every cell streamline-based sensitivity.

7th *BOOLEAN* — Reserved keyword always set this record to *TRUE*.

8th *STRING* — *PERM*_RANGE enables user to set permeability range during history match. By default, initial permeability field range is used. (*NONE*)

9th *FLOAT* — Minimum permeability during history match.

10th *FLOAT* — Maximum permeability during history match.

By setting the 1st , 2nd and 3rd records to zero DESTINY will run under tracing mode only. The production sensitivities and misfit at the wells could be generated and reported to ASCII files. This running mode could be easily interfaced to any other

streamline-based history matched workflow (i.e., assisted history match, Ensemble Kalman Filtering, etc.). If the inversion module is applied, in other words, setting the 1st, 2nd and 3rd records to non-zero at least one of them, 10th item in *DIP_TRACING_SETTING* should be *FALSE*.

> *Example 1:*   *Only tracing will be performed, by default GTT sensitivities will be calculated and printed out*
>
>   *DIP_INV_SETTINGS*
>
>   *0   0   0   FALSE   0.2   TRUE   TRUE   NONE   0.001*

80000

> *Example 1:*   *GTT history matching will be performed by 9 iterations sensitivities will be calculated and printed out*
>
>   *DIP_INV_SETTINGS*
>
>   *0   9   0   FALSE   0.2   TRUE   TRUE   NONE   0.001*

80000

A.3.3.10. DIP_INV_UPSCALE_SETTING
Defines setting for inversion

All Users: The keyword is followed by a line with ten records. The records are defined as follows,

1st BOOLEAN	Flag for Dual scale inversion option (*TRUE / FALSE*). If *FALSE* is used, following records will be ignored.
2nd STRING	*PERCCUTOFFUPSCALE* enables user to set percentile cutoff of coarse-scale sensitivity. Default is *NONE*.
3th FLOAT	Defines the lower percentile for the WWCT coarse- scale sensitivity cut-off.

4th FLOAT Defines the upper percentile for the WWCT coarse- scale sensitivity cut-off.

Example: *DIP_INV_UPSCALE_SETTINGS*
TRUE *PERCCUTOFFUPSCALE* *0.1* *0.9*

A.4. DESTINY Output

DESTINY provides a lot of output which is very useful to monitor the performance of both tracing and inversion. The streamline output is compatible with a wide range of commercial visualization packages. DESTINY generates streamline files which can be loaded to *FLOVIZ*, *PETREL*, *TECPLOT*. The modularity and structure of the code would allow a fairly simple implementation satisfying any required specifications in both *ASCII* and binary format.

The inversion output offers enough information to know the status of the history matching performance at any iteration. DESTINY has implemented functions to monitor the permeability changes during the inversions iterations. Descriptive statistics can be generated to monitor the moment's behavior on field-wide or on a facie-based basis if available.

A.4.1. Streamline Output

A brief summary of the streamline tracing output is presented next. For more details refer to the tracing tutorial (*Section 5*)

- **SLNXXX Files**: When the binary output is selected, DESTINY will generate **.sln* files for every simulation time step. *ECLIPSE* users can use the restart files and the **.sln* files to load the entire simulation workspace to *FLOVIZ* or *PETREL*.

- **TECPLOT Files**: These files are available when the *ASCII* option is selected under *DIP_TRACING_SETTING*. A whole new group of output files will have the suffix *_TECPLOT* added. The *ASCII* file will follow the *TECPLOT* polyline free-format with an associated property. The defaulted property is the time of flight from the producers. However, the writing functions can be easily modified to print out any trajectory based property.

- **DYNAMIC GRAPHICS Files**: These files are available when the *ASCII* option is selected under *DIP_TRACING_SETTING*. A whole new group of output files will have the suffix *_COVIZ* added. The *ASCII* file will follow the *DYNAMIC GRAPHICS* free-format structure. Similar to *TECPLOT*, the writing functions can be easily modified to print out any trajectory based property.

A.4.2. Inversion Output

- **Updated permeability files**: When loading the initial simulation deck, DESTINY will store the permeability file defined under *DIP_PROP_FILE*. After running the first inversion iteration this file will be modified and by the end of each iteration, the updated permeability will be written out (the file will have a suffix with the iteration number in which the permeability was updated).

- **resinv.obj**: This file has the objective function behavior through all iterations. It has two columns representing the travel time and amplitude misfit defined at all producing wells included in the data integration

- **resInv.wwctX**: It contains the simulated and observed production water-cut for all wells included in the project. At the header of each well the travel time misfit will be written out. This file is generated at the end of each iteration.

- ***dynamic.bin***: Binary file containing the production sensitivities. This file is used by LSQR to perform the objective function minimization.

- ***dynamic.ascii***: ASCII file containing the production sensitivities. This file is provided for history matching applications where streamline-based sensitivities are used as complementary information.

A.5. Streamline Tracing Examples

In this section a 5-spot synthetic (**Fig. A.7**) model will be used to illustrate how *DESTINY* generates streamlines using *ECLIPSE*. We will show how to generate streamlines based on the total velocity and also based on single phase fluxes. Visualization output using *FLOVIZ/PETREL/TECPLOT* will be presented for all cases.
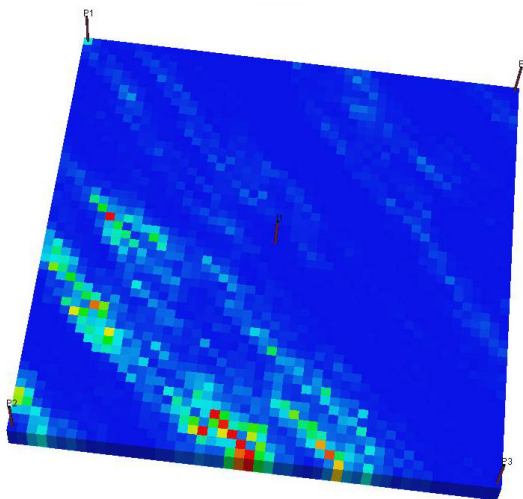
Fig. A.7 Five spot synthetic example

After receiving your *DESTINY* distribution, the input deck for this example is under *..\DESTINY\APPLICATIONS\ECL\INPUT*. The input files consist of the following files:

ECLIPSE.DATA

ECLSCHEDULE.DATA

DESTINY.DIP

ECLIPSEGRID.GRDECL

PERMX.GRDECL

PORO.GRDECL

Copy all these files under *..\DESTINY\APPLICATIONS\ECL_SYN*. This will be your working space if you are running the application from the compiler. For this particular example we will use the executable generated under the *../DESTINYW/Debug/* (make sure you copy the executable to the working directory).

A.5.1. Total Flux Tracing (FLOVIZ Binary Files)

We will start by running the tracing using the total velocity field. The setting under *DIP_TRACING_SETTING* and *DIP_INV_SETTINGS* inside the *DESTINY.DIP* file must be as follows. Since we are only doing tracing the inversion setting parameters can be defaulted to what appears on the file

DIP_TRACING_SETTING

OILWATPHASE   OILWATPROD   RUN   ALL   0   BINARY   STCFLUX POLLOCK   HORIZONTAL   TRUE

DIP_INV_SETTINGS

0   0   0   FALSE   0.2   FALSE   TRUE   NONE 0.1   80000

After running the executable, you should see the command prompt window with the execution comments. *ECLIPSE* will run first and then the streamlines will be

generated. At the end of the execution *sln* files will be available and you should be able to visualize streamlines. (**Fig. A.8**) shows the streamlines and oil saturation using *FLOVIZ* at all schedule dates.
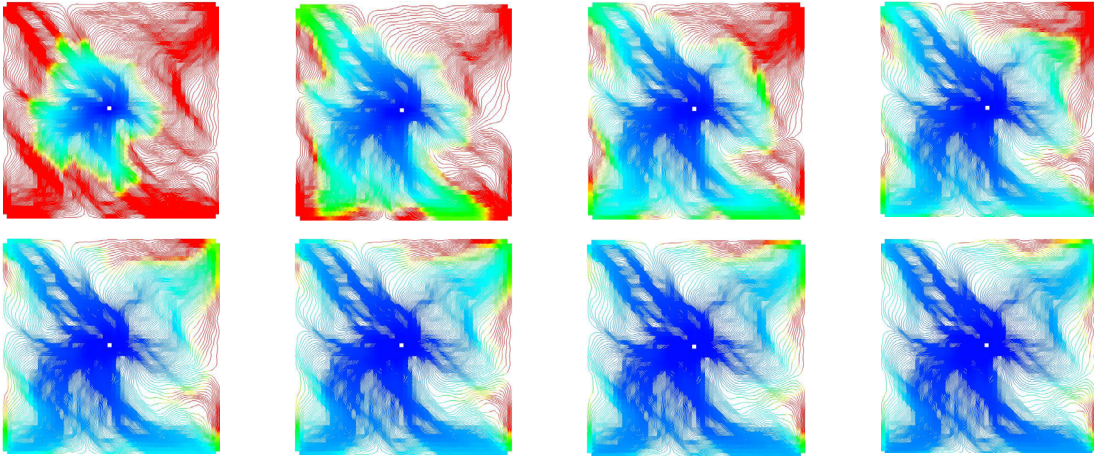

**Fig. A.8 Streamline Trajectory (Color represents water saturation)**

A.5.2. Total Flux Tracing (ASCII Files)

Ascii files can be obtained to visualize in *TECPLOT* or *DYNAMIC GRAPHICS* by changing the *DIP_TRACING_SETTING*. Note that there is no need to run the simulator again since the flux files are already available. Change the tracing setting inside *DESTINY. DIP* to

DIP_TRACING_SETTING
OILWATPHASE   OILWATPROD   STOP   ALL   0   ASCII   STCFLUX POLLOCK   HORIZONTAL   TRUE
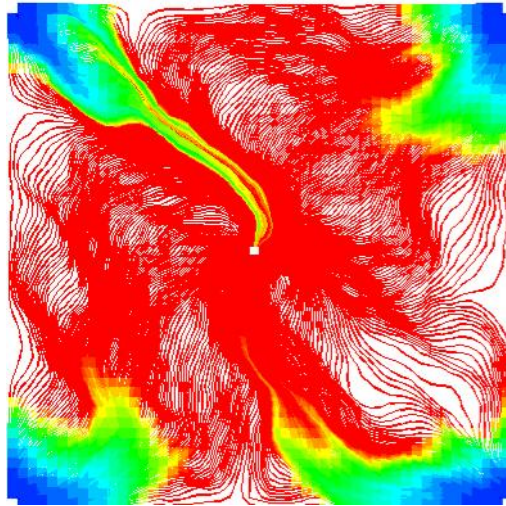
Fig. A.9 Time of flight from the producers

After running the executable again, a new group of files with the suffix *_TECPLOT* and *_COVIZ* will be available. (**Fig. A.9**) shows the streamlines and time of flight from producers using *TECPLOT* at the first schedule date

A.5.3. Water Phase Tracing (FLOVIZ binary files)

Let's generate streamlines based only on the water velocity. Let's first generate streamlines starting from the producer only. Again, there is no need to run the simulator since the restart files are available, change the tracing setting as follows

> *DIP_TRACING_SETTING*
> *OILWATPHASE   WATPROD   STOP   ALL   0   BINARY   STCFLUX*
> *POLLOCK   HORIZONTAL   TRUE*

Run the executable again and load the streamlines to FLOVIZ. (**Fig. A.10**) shows the water streamlines starting only form the producers. This set of streamlines is only for

visualization purposes. Note that the water front is not fully defined with these streamlines; however, the snapshots show how the water is breaking through in the producers.
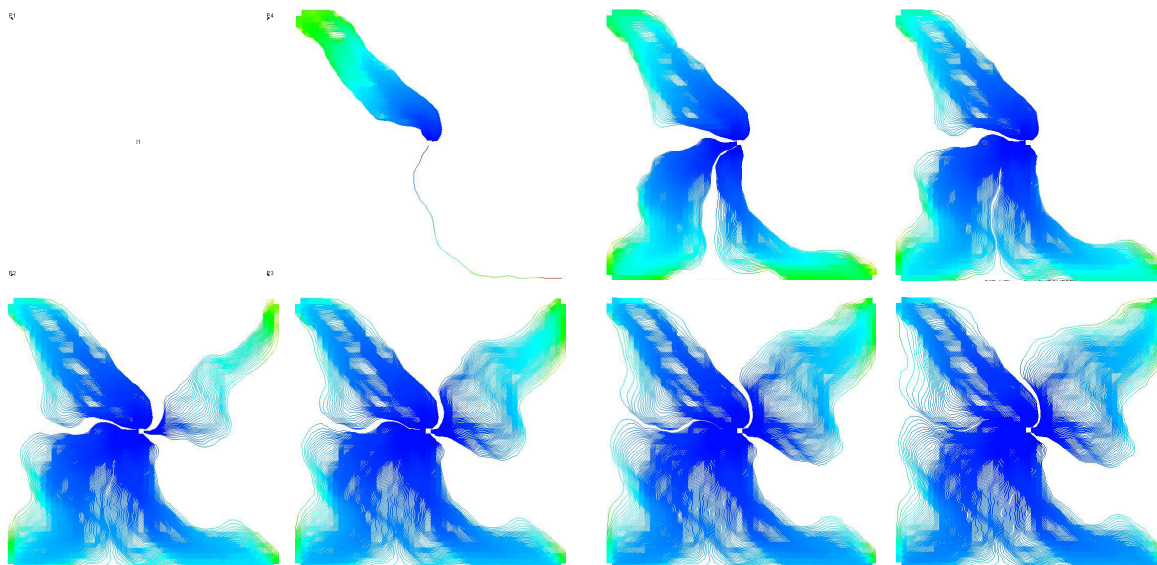
Fig. A.10 Water Phase Streamlines (Color represents water saturation)

The second phase-tracing alternative is considering all cells as potential sinks. In this example all cells with a water fractional flow greater than zero will be used as starting points for tracing. In big models, considering all cells will lead to huge files depending on the size of the grid. These starting points can be modified only inside the code; C++ users can go to *CDIPStreamCalc::streamLineTraceSinkCenter* and modify the fractional flow condition to define a cell as a starting point.

Continuining with the example, change the tracing setting as follows

DIP_TRACING_SETTING
OILWATPHASE   WATSINK   STOP   ALL   0   BINARY   STCFLUX POLLOCK   HORIZONTAL   TRUE

This will enable the tracing stating from the cell centers and will create an additional set of *.sln files with the suffix *SINK*. After loading the streamlines to *FLOVIZ* they should look like (**Fig. A.11**),
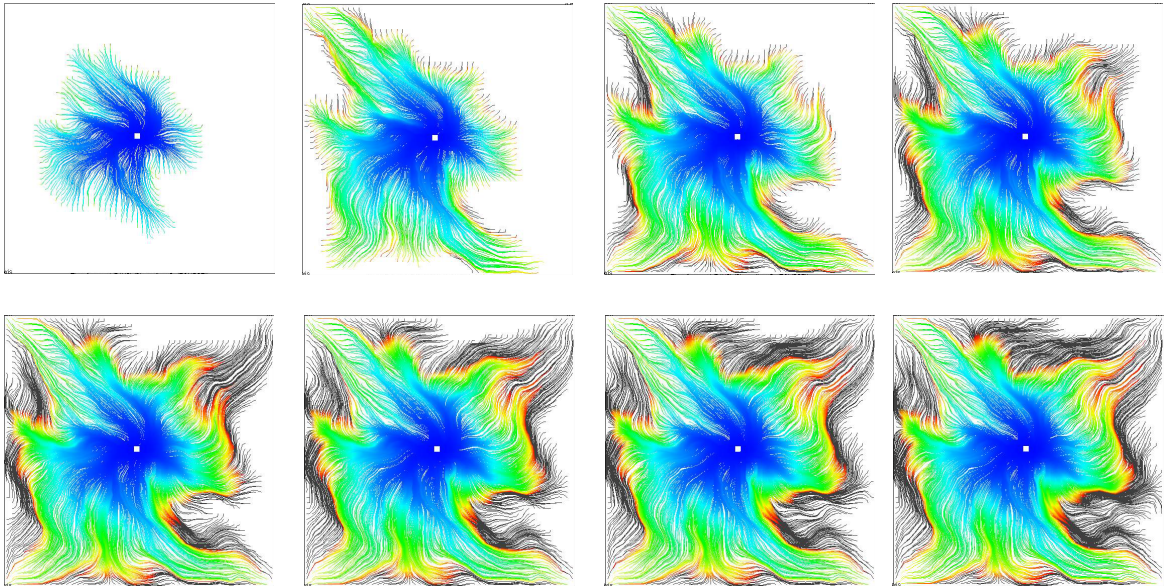

Fig. A.11 Water streamlines traveled from the middle of the cells (Color represent time of flight from Injector)

A.6. Inversion Example

In this section we will use the 5-spot synthetic model used on the tracing section to illustrate how *DESTINY* integrates production water-cut using *ECLIPSE*.

The input deck for this example is the same as for the tracing example. Clean your working folder *..\DESTINY\APPLICATIONS\ECL_SYN* and copy the input files again. Inside *DESTINY.DIP* set the following settings,

DIP_TRACING_SETTING
OILWATPHASE   OILWATPROD   RUN   ALL   0   BINARY   STCFLUX POLLOCK   HORIZONTAL   FALSE

DIP_INV_SETTINGS

0   9   0   FALSE   0.2   TRUE   TRUE   NONE   0.001
80000

It is important to set the tracing to the default option considering total flux and streamlines starting from producers. For this example nine GTT iterations will be executed. Note that *ASCII* output is requested for the well sensitivities.

After running *ECLIPSE* the file *resinv.obj* shows the initial prior model misfit. The travel time misfit is 538 days and the amplitude misfit is 22.248. The model was initialized enumerating pressure and water saturation to constant values. All producers were constrained by liquid rate (600 STB/D) and the injector by water rate (2400 STB/D).The details of the forward run can be found in ..*APPLICATIONS\ECL_SYN*

The file *resInv.wwct0* shows the initial production water-cut performance in all wells; this is shown in **Fig A.12**. The prior model is not able to fully represent the observed water breakthrough. The production data integration will be accomplished after decomposing the underlying fluid flow domain and define streamline-based sensitivities.

Fig A.13 shows the streamline-derived sensitivity of each well at the first iteration. The color code represents the sensitivity magnitude for each cell. The red color represents high sensitivity values and the blue represents small values. Please note that these particular plots come from *ASCII* files named after each producer well name.

After calculating the sensitivities the algorithm will perform an LSQR optimization and will update the permeability field. The main LSQR output is a deviation array that must be added to the current permeability model. The deviation is under the file *resinv.deviation*
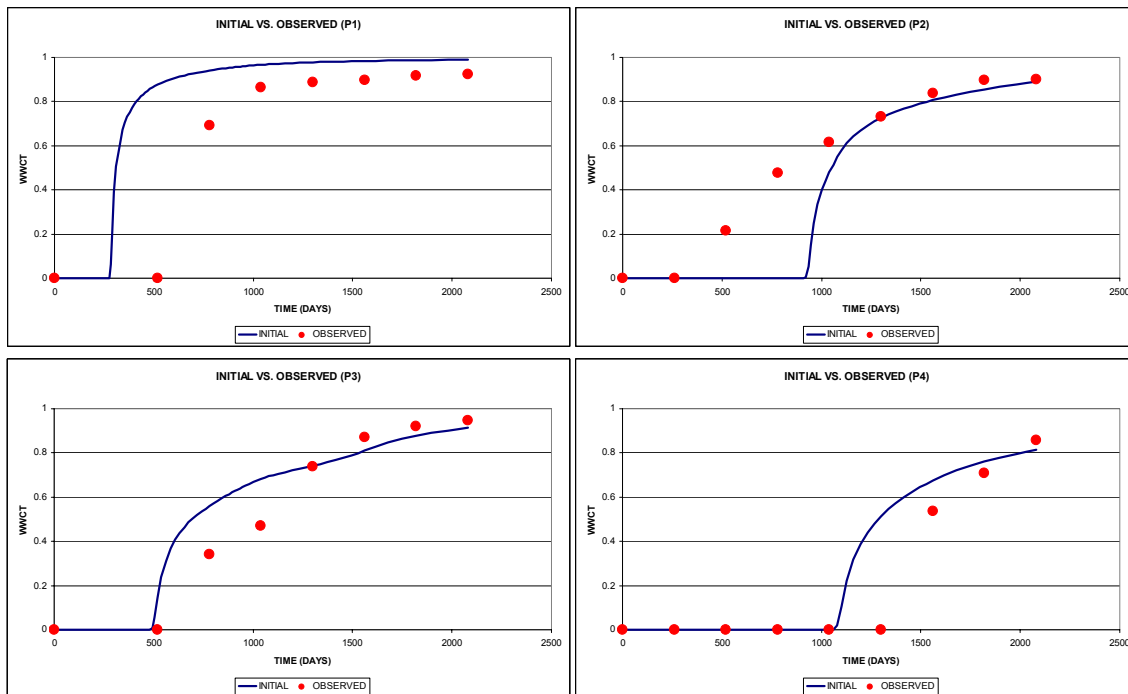
Fig. A.12 Initial well water-cut match for heterogeneous five spot example

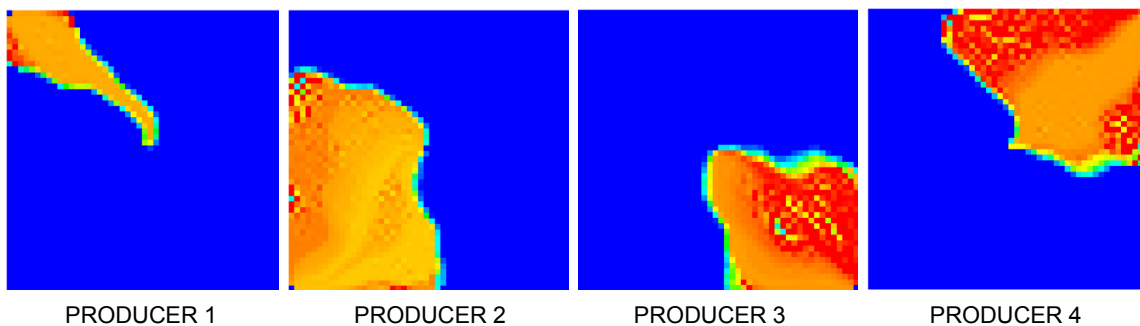PRODUCER 1   PRODUCER 2   PRODUCER 3   PRODUCER 4

Fig. A.13 Producer sensitivities for heterogeneous five spot example, 1st iteration

As soon as the permeability is updated, a new system call to *ECLIPSE* will be done and the new restart files will be used for both tracing and check for misfit convergence. **Fig. A.15** shows how the permeability is changing through all iterations. After each iteration is finished a set of permeability files will be generated (*PERMX.GRDECL1, PERMX.GRDECL2*, etc) as shown Fig. A.14.
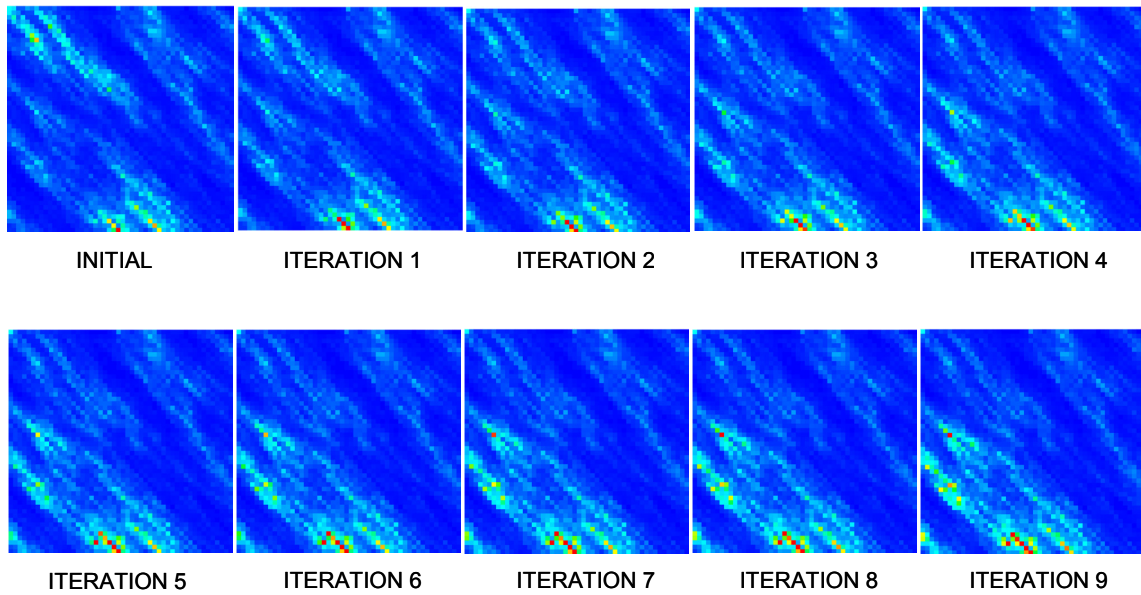
Fig. A.14 Permeability field through iterations for heterogeneous five spot example
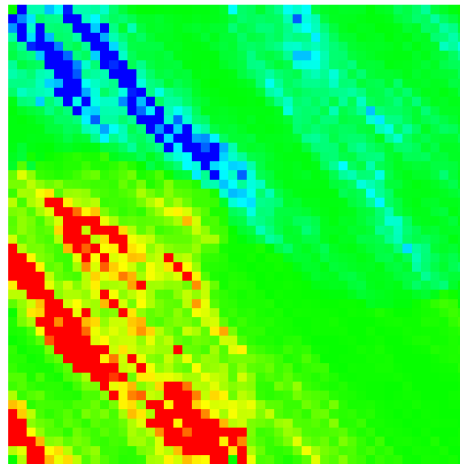
Fig.A.15 Model changes after nine iterations

Fig. A.15 shows the difference between the final and initial permeability. This picture is an excellent diagnostic indicator when addressing the presence or absence of barriers, fractures or even faults.

An important validation step for the new permeability is checking the moment's behavior. **Fig. A.16** shows the histogram for the permeability before and after the inversion. Clearly we can see that we're preserving the first and second moments of the prior permeability. This is a crucial indicator towards reconciling water-cut and the geologic model.
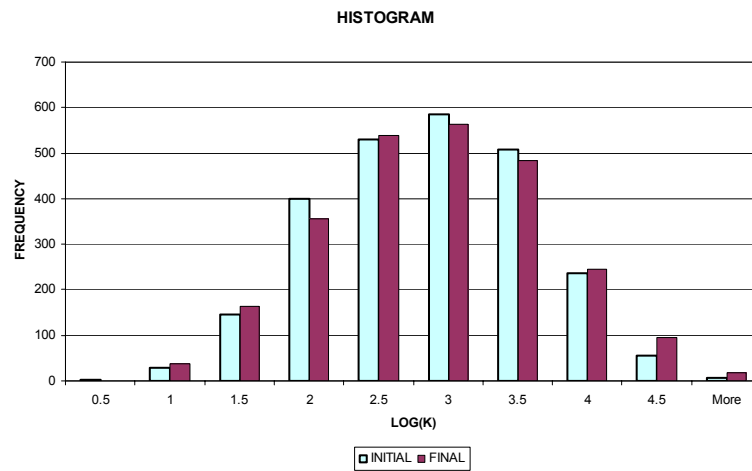
Fig. A.16 Histogram comparison between final and initial permeability for heterogeneous five spot example.

Fig. A.17 shows the water-cut match in all wells before and after the inversion. The initial water-cut is under the file *resInv.wwct0* and the history matched is under *resInv.wwct9*. The travel time misfit was reduced from 538 days to 98 (that is an order of magnitude) and the amplitude misfit was reduced from 22.25 to 4.94 (more than an order of magnitude).
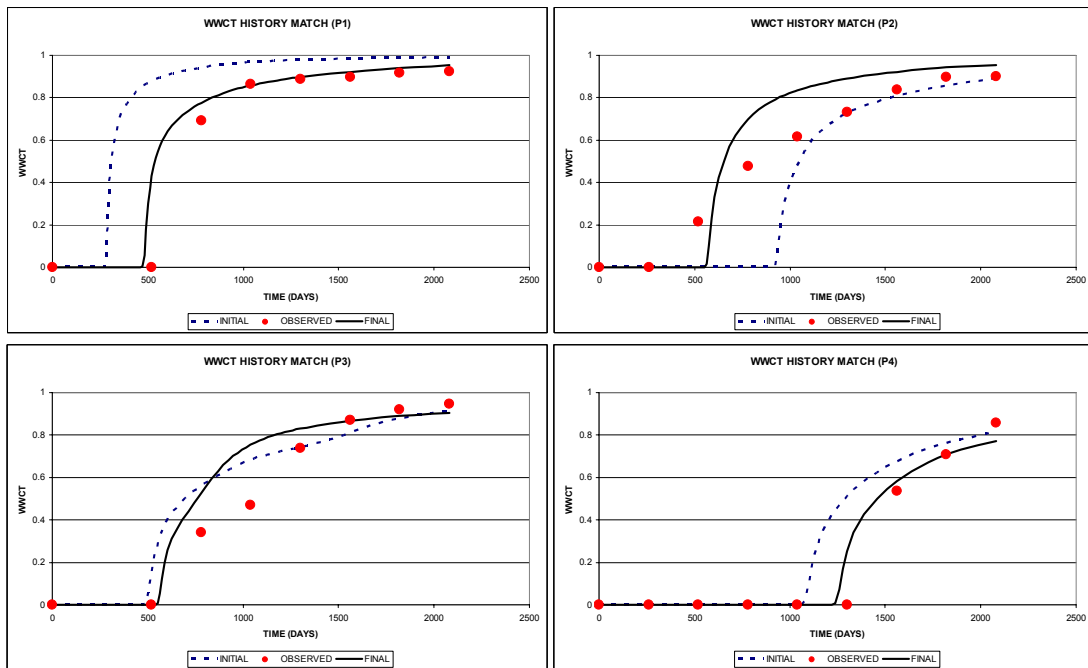
Fig. A.17 Water-cut history match before and after inversion for heterogeneous five spot example.

Both travel time and water-cut misfit are presented in **Fig. A.18**. The objective function behavior is reported in file *resinv.obj*.
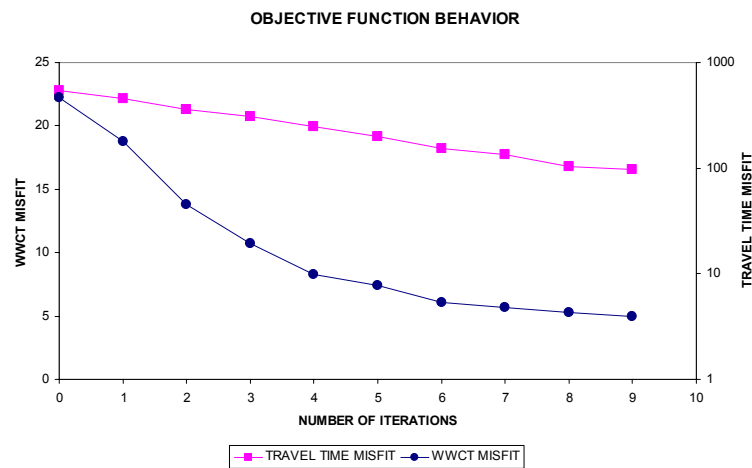

Fig. A.18 Objective function behavior for heterogeneous five spot example

APPENDIX B

COMPUTATION OF TRAJECTORY FROM NUMERICAL GRADIENTS (HEUN'S METHOD)

In chapter 3, the computation of the pressure front trajectory is critical because the asymptotic solution in Eq. 3.3 to the diffusivity equation is defined along the trajectory. In this appendix, we revisit Heun's method (Kreyszig, 1993) and demonstrate the procedure of calculation the trajectory.

Heun's Method. First-order initial value problem such as Eq. 3.12 consists of a differential equation and a condition the solution must satisfy. For simple demonstration, let

$$y' = f(x, y), \qquad y(x_0) = y_0 \tag{B.1}$$

assuming f to be such that the problem has a unique solution on some interval containing x_0. Because we have the diffusive time of flight from numerical simulation result, we shall discuss 'step-by-step methods', that is, we start from the given $y_0 = y(x_0)$ and proceed stepwise.

$$x_1 = x_0 + h, \quad x_2 = x_0 + 2h, \quad x_3 = x_0 + 3h, \quad \cdots \tag{B.2}$$

where the step size h is a fix value. The computation in each step is done by the same formula. Such formulas are suggested by the Taylor series

$$y(x + h) = y(x) + hy'(x) + \frac{h^2}{2}y''(x) + \cdots \tag{B.3}$$

Now for a small value of h, the higher powers h^2, h^3,$\cdots$ are very small. This suggests the crude approximation

$$y(x+h) \approx y(x) + hy'(x) = y(x) + hf(x,y) \tag{B.4}$$

and we conclude the following approximation in general.

$$y_{n+1} = y_n + hf(x_n, y_n) \tag{B.5}$$

This is called the Euler-Cauchy method.

By taking more terms in Eq. B.3 into account we obtain numerical methods of higher order and precision. But there is a practical problem. If we substitute $y' = f(x, y(x))$ into Eq. B.3, we have

$$y(x+h) = y(x) + hf + \frac{h^2}{2} f' + \frac{h^3}{6} f'' + \cdots \tag{B.6}$$

Instead of computing cumbersome f'', f''', we replace it by computing f for one or several suitably chosen auxiliary values of (x,y). One of these method is the so-called 'Heun's method' or 'improved Euler-Cauchy method'. In each step, we compute the auxiliary value first

$$y_{n+1}^* = y_n + hf(x_n, y_n) \tag{B.7}$$

and then the next value is

$$y_n = y_n + \frac{h}{2}\left[f(x_n, y_n) + f(x_{n+1}, y_{n+1}^*)\right] \tag{B.8}$$

In fact, we may say that in the interval from x_n to $x_n + h/2$ we approximate the solution y by the straight line with slope $f(x_n, y_n)$, and then we continue along the straight line with slope $f(x_{n+1}, y_{n+1}^*)$ until x reaches x_{n+1}. The Heun's method is a predictor-corrector method because in each step we first predict a value by Eq. B.7 and then correct it by Eq. B.8.

Pressure Front Trajectory Tracing Procedure. In the section 3.2.2, we adopt the Heun's method to compute the trajectory, ψ, which is the solution to the following differential equation (Vasco and Finsterle, 2004),

$$\frac{d\psi}{d\zeta} = \nabla \tau(\mathbf{x}) \tag{B.9}$$

where the term ζ indicates the distance along the trajectory ψ. The gradient of diffusive time of flight, $\nabla \tau$ can be obtained from numerical simulation.

As mentioned before, this type of numerical calculation requires the predefined step size or 'marching length' in this problem. We use $\Delta\zeta$ as marching length. Supposing 2-dimensional domain, we calculate the auxiliary point from (x_i, y_i) with $\Delta\zeta$

$$
\begin{aligned}
x_{i+1}^* &= x_i - \frac{\nabla\tau(x_i, y_i) \cdot \nabla_x\tau(x_i, y_i)}{\left\|\nabla\tau(x_i, y_i)\right\|\left\|\nabla_x\tau(x_i, y_i)\right\|}\Delta\zeta \\
y_{i+1}^* &= y_i - \frac{\nabla\tau(x_i, y_i) \cdot \nabla_y\tau(x_i, y_i)}{\left\|\nabla\tau(x_i, y_i)\right\|\left\|\nabla_y\tau(x_i, y_i)\right\|}\Delta\zeta
\end{aligned}
\tag{B.10}
$$

where x_i, y_i are x and y coordinates of ψ_i respectively and x_{i+1}^*, y_{i+1}^* are x and y coordinates of the auxiliary point, ψ_{i+1}^*. Also ∇_x, ∇_y denote the x-direction an y-

direction gradients. Finally, the $(i+1)$-th step point is further refined using the gradient at ψ^*_{i+1} (corrector step)

$$x_{i+1} = x_i - \frac{\Delta\varsigma}{2}\left[\frac{\nabla\tau(x_i,y_i)\cdot\nabla_x\tau(x_i,y_i)}{\left|\nabla\tau(x_i,y_i)\right|\left|\nabla_x\tau(x_i,y_i)\right|} + \frac{\nabla\tau(x^*_{i+1},y^*_{i+1})\cdot\nabla_x\tau(x^*_{i+1},y^*_{i+1})}{\left|\nabla\tau(x^*_{i+1},y^*_{i+1})\right|\left|\nabla_x\tau(x^*_{i+1},y^*_{i+1})\right|}\right]$$

$$y_{i+1} = y_i - \frac{\Delta\varsigma}{2}\left[\frac{\nabla\tau(x_i,y_i)\cdot\nabla_y\tau(x_i,y_i)}{\left|\nabla\tau(x_i,y_i)\right|\left|\nabla_y\tau(x_i,y_i)\right|} + \frac{\nabla\tau(x^*_{i+1},y^*_{i+1})\cdot\nabla_y\tau(x^*_{i+1},y^*_{i+1})}{\left|\nabla\tau(x^*_{i+1},y^*_{i+1})\right|\left|\nabla_y\tau(x^*_{i+1},y^*_{i+1})\right|}\right]$$

(B.11)

APPENDIX C

VERIFICATION OF THE PRESERVATION OF THE TOTAL HETEROGENEITY

In chapter 2, we discussed an 'optimal' coarsening algorithm for the coarse-scale inversion. One of the characteristics of this method is preservation of the total heterogeneity. This is expressed in Eq. 2.5. The derivation presented here follows that of King et al. (2005)

Consider two vertically adjacent coarsened grids, *a* and *b*, at any intermediate coarsening step. P^C, the property of the next step coarsened grid is given by

$$P^C = \frac{n_a P_a^C + n_b P_b^C}{n_a + n_b} \tag{C.1}$$

where, n_a, n_b and P_a^C, P_b^C are the weights and the properties of *a* and *b* (**Fig. C.1**).
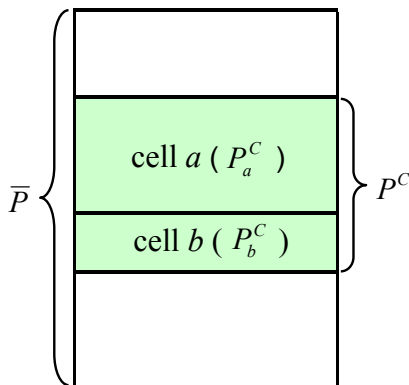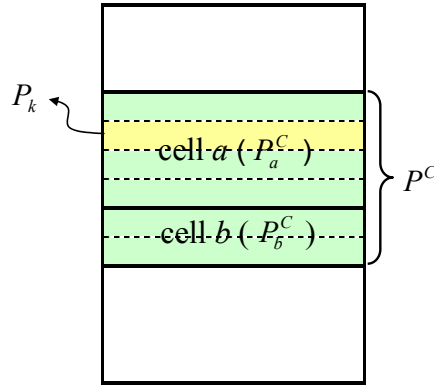

Fig. C.1 Diagram for decrease of *B* during coarsening

In order to verify the preservation of the total heterogeneity, we will calculate the difference (decrease) of B in Eq. 2.3, δB.

$$
\begin{aligned}
\delta B &= \left(n_a + n_b\right)\left(P^C - \overline{P}\right)^2 - n_a\left(P_a^C - \overline{P}\right)^2 - n_b\left(P_b^C - \overline{P}\right)^2 \\
&= \left[\frac{\left(n_a P_a^C + n_b P_b^C\right)^2}{n_a + n_b} - 2\left(n_a P_a^C + n_b P_b^C\right)\overline{P}\right] \\
&\quad - \left[n_a\left(P_a^C\right)^2 + n_b\left(P_b^C\right)^2 - 2n_a P_a^C \overline{P} + 2n_b P_b^C \overline{P}\right] \\
&= -\frac{n_a n_b}{n_a + n_b}\left(P_a^C - P_b^C\right)^2
\end{aligned}
$$

(C.2)

where, $\overline{P}$ is the average property of each column.

Fig. C.2 Diagram for increase of W during coarsening

Now, we will calculate W in Eq. 2.1 of coarsened grid with a and b. (**Fig. C.2**)

$$
\begin{aligned}
W &= \sum_k^M n_k\left(P_k - P^C\right)^2 + \sum_k^N n_k\left(P_k - P^C\right)^2 \\
&= \sum_k^M n_k\left(P_k - P_a^C\right)^2 + \sum_k^N n_k\left(P_k - P_b^C\right)^2 + \delta W \\
&= W_a + W_b + \delta W
\end{aligned}
$$

(C.3)

In this manipulation, $\sum\limits_{k}^{M}$ represent the summation of the fine grids properties within the

intermediate coarse grid a and, similarly, $\sum\limits_{k}^{N}$, $\sum\limits_{k}^{M+N}$ represent the summation of the fine

grids properties within the intermediate coarse grid b and the coarsened grid with a and b respectively. Then, δW is given by

$$
\begin{aligned}
\delta W \\
&= \sum_{k}^{M} n_{k}\left[2P_{k}P_{a}^{C} - \left(P_{a}^{C}\right)^{2} - 2P_{k}P^{C} + \left(P^{C}\right)^{2}\right] \\
&+ \sum_{k}^{N} n_{k}\left[2P_{k}P_{b}^{C} - \left(P_{b}^{C}\right)^{2} - 2P_{k}P^{C} + \left(P^{C}\right)^{2}\right] \\
&= \sum_{k}^{M} n_{k}\left[2P_{k}P_{a}^{C} - \left(P_{a}^{C}\right)^{2}\right] + \sum_{k}^{N} n_{k}\left[2P_{k}P_{b}^{C} - \left(P_{b}^{C}\right)^{2}\right] \\
&+ \sum_{k}^{M+N} n_{k}\left[\left(P^{C}\right)^{2} - 2P_{k}P^{C}\right] \\
&= n_{a}\left(P_{a}^{C}\right)^{2} + n_{b}\left(P_{b}^{C}\right)^{2} - \left(n_{a} + n_{b}\right)\left(P^{C}\right)^{2} \\
&= n_{a}\left(P_{a}^{C}\right)^{2} + n_{b}\left(P_{b}^{C}\right)^{2} - \frac{\left(n_{a}P_{a}^{C} + n_{b}P_{b}^{C}\right)^{2}}{\left(n_{a} + n_{b}\right)} \\
&= \frac{n_{a}n_{b}}{n_{a} + n_{b}}\left(P_{a}^{C} - P_{b}^{C}\right)^{2}
\end{aligned}
\tag{C.4}
$$

Thus, at any stage of sequential coarsening, the increase of W is always same as the decrease of B resulting from the coarsening. Before starting 'optimal' coarsening, B of the initial fine-scale geologic model is the same as the total variation, H. Thus, the total variation is preserved during sequential coarsening.

VITA

Name:

Jong Uk Kim

Address:

Petroleum Engineering Department

3116 TAMU

College Station, TX USA 77843

Email Address:

jukimb@gmail.com

Education:

Ph.D.: Petroleum Engineering, Texas A&M University, 2009

M.S.: Energy Resources Engineering, Seoul National University, 2002

B.S.: Energy Resources Engineering, Seoul National University, 1998